A prelude to cleavage: Orchestrating cytokinesis onset in mammalian cells • IE Adriaans 2020

A prelude to cleavage: Orchestrating cytokinesis onset in mammalian cells

Ingrid Elisabeth Adriaans

A prelude to cleavage:

Orchestrating cytokinesis onset in mammalian cells

Ingrid Elisabeth Adriaans

ISBN: 978-90-393-7246-3

Print: Proefschriftmaken

Cover and artwork: Pieter W. Adriaans

Graphical support: Cootje Mombers

A prelude to cleavage:
Orchestrating cytokinesis onset in mammalian cells

Een prelude van deling:
Het dirigeren van cytokinese in zoogdiercellen

(met een samenvatting in het Nederlands)

Proefschrift

ter verkrijging van de graad van doctor aan de
Universiteit Utrecht
op gezag van de
rector magnificus, prof.dr. H.R.B.M. Kummeling,
ingevolge het besluit van het college voor promoties
in het openbaar te verdedigen op

donderdag 6 februari 2020 des ochtends te 10.30 uur

door

Ingrid Elisabeth Adriaans

geboren op 24 september 1984
te Dordrecht

Promotor:

Prof. dr. Susanne M.A. Lens

Dit proefschrift werd (mede) mogelijk gemaakt met financiële steun van Oncode Institute dat deels financieel gesteund wordt door KWF Kankerbestrijding, en de Nederlandse Organisatie voor Wetenschappelijk Onderzoek (NWO-Vici 91812610 naar S.M.A. Lens).

Table of contents

List of abbreviations

APC/C	Anaphase Promoting Complex/Cyclosome
Cdk1	Cyclin dependent kinase
CPC	Chromosomal Passenger Complex
EB1	End-Binding protein 1
ECT2	Epithelial Cell Transforming 2
EQ	Equatorial
FL	Full Length
GAP	GTPase Activating Protein
GEF	Guanine nucleotide Exchange Factor
GFP	Green Fluorescent Protein
G1/2	Gap phase 1/2
IF	Immunofluorescence
INCENP	INner CEntromere Protein
IP	Immunoprecipitation
KD	Knockdown
KIF	Kinesin Family Member
KO	Knockout
M phase	Mitosis phase
MAP	Microtubule Associated Proteins
MKLP1	Mitotic Kinesin-Like Protein 1
MKLP2	Mitotic Kinesin-Like Protein 2
eMLC	essential Myosin II Light Chain
rMLC	regulatory Myosin II Light Chain
MT	Microtubules
NEB	Nuclear Envelope Breakdown
NL	Neck Linker
PLK1	Polo-Like Kinase 1
PP1	Protein Phosphatase 1
PRC1	Protein Regulator of Cytokinesis 1
RACGAP1	Rac GTPase Activating Protein 1
RFP	Red Fluorescent Protein
RhoA	Ras homolog gene family A
ROCK	Rho-associated, Coiled-coil-containing Protein Kinase
S phase	Synthesis phase

Chapter 1

General Introduction

Ingrid E. Adriaans

Cell division

An adult human body is made out of roughly $3.72*10^{13}$ cells (Bianconi et al., 2013), all originating from one fertilized oocyte. This single cell has thus produced at least more than 45 generations of daughter cells through cell division. During life, cell division is needed to renew or repair (damaged) tissues and to expand the army of antigen-specific lymphocytes that protect the body against the invasion of bacteria and viruses. Cell division, which can be seen with a light microscope as one cell splitting into two, is in fact the final phase of the cell cycle.

The cell cycle

The cell cycle can be considered the life cycle of a cell. It consists of two main phases: S (Synthesis) phase and M (Mitosis) phase, and in most mammalian cells the S and M phases are separated by two interval or GAP (G) phases (G1 between M and S phase, and G2 between S and M phase). During S phase the genome, partitioned into 46 chromosomes in humans, is entirely copied, and in M phase, the two identical copies of the chromosomes (now called sister chromatids) are equally segregated and subsequently transmitted into two daughter cells when the mother cell physically splits into two. Thus, M phase consists of a nuclear division (mitosis), and a cytoplasmic division (cytokinesis, Figure 1) and will be discussed in more detail later. During the two GAP phases, G1 and G2, cells mostly grow by synthesizing proteins, organelles, membranes and other constituents that form the bulk of the cell mass. Without growth, the daughter cells would be half the size of their mother with each division (Lubischer, 2007).

S and M phase need to be executed and coordinated with great precision to secure the integrity of our genome. The core driving factors of the cell cycle are the Cyclin-dependent kinases (Cdks), and the tight control of Cdk activity ensures proper timing and coordination of cell cycle events. Binding of specific Cyclins to these kinases is required for kinase activation and substrate specificity. Cyclin levels rise and fall throughout the cell cycle at specific times through a combination of transcriptional regulation and selective proteolysis, thereby timing the activation and inactivation of Cdks. Cdk activity is further regulated by reversible phosphorylation of Cdks, subcellular localization of the Cyclins, and by Cdk inhibitors (CKIs, such as p21, p27 and members of the INK4 family) that bind and inactivate specific Cyclin-Cdk complexes (Harper et al., 1995; Xiong et al., 1993; Sherr and Roberts, 1999; Morgan, 1995, 1997). In the unicellular organism, budding yeast (*S. cerevisiae)*, only one Cdk (Cdc28) regulates the entire cell cycle (Mendenhall and Hodge, 1998; Coudreuse and Nurse, 2010). In mammalian cells, however, multiple Cdks and Cyclins control cell cycle progression: Cyclin D-Cdk4/6 are active in G1, and Cyclin E-Cdk2 drive cells into S phase where Cyclin A-Cdk2 takes over to guide DNA replication. In G2, Cyclin A levels remain high and binds both Cdk2 and Cdk1. The latter Cyclin A complex together with Cyclin B-Cdk1 triggers the G2 – M transition. Cyclin A is subsequently destroyed in early mitosis, making mitosis fully dependent on Cyclin B-Cdk1. The degradation of Cyclin B and the consequent inactivation of Cdk1 mediate the exit from mitosis and entry into G1.

M phase: Nuclear division

When a cell enters M phase, the cytoskeleton and nucleus are dramatically reorganized. This reorganization is mainly orchestrated by Cyclin B-Cdk1 which phosphorylates a large number of

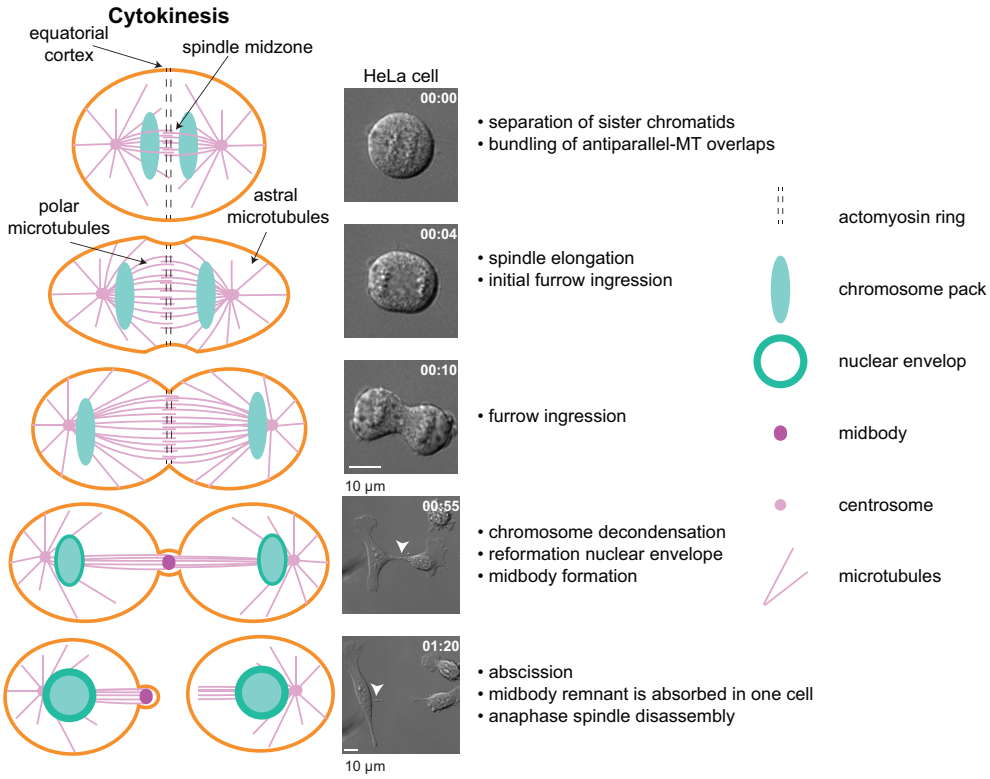

Figure 1: Anaphase and cytokinesis
Schematic representation of the stages of and structures involved in cytokinesis. Cytokinesis starts at anaphase onset. Representative stills of HeLa cells in corresponding stages of cytokinesis are shown in the middle panel. Scale bar = 10 µm

proteins in the nucleus, nuclear envelope and of the cytoskeleton (Özlü et al., 2010; Blethrow et al., 2008). In **prophase**, the chromatin starts to condense and becomes visible as individual chromosomes. The interphase microtubule network is destabilized and new microtubules begin to grow from the two centrosomes and eventually form the mitotic spindle (Prosser and Pelletier, 2017; Meraldi and Nigg, 2002; Gallaud et al., 2014). Through the action of motor proteins, such as kinesin-5 and dynein, the two centrosomes are pushed and pulled towards opposite poles of the cell (Ferenz et al., 2010; Raaijmakers et al., 2012).The nuclear envelope breaks down (NEB) and completion of NEB marks the onset of **prometaphase**. NEB enables the 'search and capture' of sister chromatids at their kinetochores, multiprotein structures that assemble on the centromeres of chromosomes, by microtubules of the mitotic spindle. Moreover, the mitotic spindle is further organized. Where microtubules from opposing spindle poles meet (polar microtubules), antiparallel microtubule overlaps are formed by the action of motor proteins and Microtubule Associated Proteins (MAPS) (Glotzer, 2009). Moreover, microtubules that grow from the centrosomes towards the cell cortex (astral microtubules), secure the spindle in place. When all the chromosomes are aligned in the middle of the cell, **metaphase** is reached. The sister chromatids now bi-orient

on the mitotic spindle, meaning that each pair of sister chromatids becomes connected to microtubules emanating from opposite spindle poles, whilst the sisters are still kept together by a ring-shaped protein complex called, cohesin (Peters et al., 2008; Nasmyth, 2011; Tanaka, 2005). When all sister chromatid pairs are correctly attached to the mitotic spindle, the Anaphase Promoting Complex/Cyclosome (APC/C) bound to CDC20 is activated resulting in the ubiquitination of Cyclin B and securin, and their subsequent proteolysis by the proteasome (Primorac and Musacchio, 2013). The breakdown of securin frees the protease separase that cleaves cohesin, releasing the sister chromatids. The breakdown of Cyclin B leads to the inactivation of Cdk1 and the subsequent gradual reversal of the mitotic phosphorylations by PP1 and PP2A phosphatases (Meadows and Millar, 2015). **Anaphase A** starts with the separation of the sister chromatids caused by the cleavage of cohesin. In addition, microtubules attached to kinetochores depolymerize and pull the sisters towards the opposite spindle poles (Asbury, 2017). Moreover, the mitotic spindle reorganizes and microtubules from the opposing poles become extensively bundled at the antiparallel overlaps in the middle of the spindle. This is called the central spindle or spindle midzone (Figure 1). Motor proteins accumulating on the spindle midzone generate forces that push the centrosomes further apart and together with cortical pulling forces acting on the astral microtubules, the anaphase spindle is elongated allowing further separation of the chromosomes (**anaphase B**) (Glotzer, 2009). Nuclear division is completed in **telophase**. During this phase, the separated chromosomes decondense, the nuclear membrane reassembles around the chromosomes forming a new nucleus, and the anaphase spindle is disassembled.

M phase: Cytoplasmic division

Nuclear division is coordinated with cytoplasmic division (cytokinesis). Cytokinesis starts in anaphase with ingression of the cell membrane, referred to as the cleavage or cytokinetic furrow (Figure 1). The plane of division is perpendicular to the pole-to-pole axis of the mitotic spindle and determined by the position of the spindle in the cell (discussed later)(Morin and Bellaïche, 2011). In case of symmetric cell divisions, which give rise to two daughter cells of identical size and properties, and the focus of this thesis, the furrow ingresses in the cell equator. As the furrow constricts, the anaphase spindle elongates and the spindle midzone is compacted by the ingressing furrow and through microtubule bundling (Hu et al., 2012a). Furrow constriction proceeds until an intercellular bridge, with a microtubule- and protein dense structure in the middle called the midbody, connects the two daughter cells (Hu et al., 2012a; D'Avino and Capalbo, 2016; Skop et al., 2004). This bridge can persist for hours until a process called abscission severs it and the two daughter cells are released (Figure 1) (Steigemann and Gerlich, 2009). Of note, the spatiotemporal regulation of cytokinesis is important for genome stability. If cytokinesis begins before the sister chromatids are well separated, the ingressing furrow can either physically damage the chromosomes or give rise to a deviant number of whole chromosomes in the daughter cells (aneuploidy) when cytokinesis is completed (Janssen et al., 2011; Potapova and Gorbsky, 2017; Norden et al., 2006; Li and Zhang, 2009). Moreover, a cell can faithfully conduct nuclear division but if cytokinesis fails, the cell enters G1 with twice the number of chromosomes (tetraploidy) and centrosomes. In most cases the excess number centrosomes is 'sensed' in G1 and will cause a cell cycle arrest (Lens and Medema, 2019; Andreassen et al., 2001; Margolis et al., 2003; Ganem et al., 2014). However, in some cases the

tetraploid cell continues to cycle. In the following S phase both the chromosomes and centrosomes are duplicated and the cell enters M phase with four centrosomes instead of two. This frequently results in the formation of a multipolar spindle on which the sister chromatids cannot properly bi-orient. Cells then either undergo a multipolar division with an increased incidence of mis-segregating chromosomes, giving rise to near-diploid aneuploidies in the daughter cells, or the spindle poles cluster and the cell undergoes a pseudo-bipolar anaphase with mis-segregating chromosomes resulting in near-tetraploid aneuploidies (Storchova and Pellman, 2004; Ganem et al., 2009; Silkworth et al., 2009). Both near-diploid and near-tetraploid aneuploidies are frequently observed in cancer (Shackney et al., 1989; Galipeau et al., 1996; Ganem et al., 2007; Storchova and Kuffer, 2008; Lens and Medema, 2019; Weaver and Cleveland, 2006; Duijf et al., 2013; Taylor et al., 2018).

Formation of the actomyosin ring

Cleavage furrow ingression is mediated by a structure called the actomyosin ring (Figure 1) (Mangione and Gould, 2019). This ring is connected to the cell membrane and consists of F-actin filaments, nonmuscle-myosin II and other cytoskeletal proteins, such as formins, profilins and Anillin, that affect F-actin organization (Mangione and Gould, 2019). Actin filaments form a disordered meshwork just below the cell membrane, but in anaphase these actin filaments start to align in an anti-parallel manner along the equatorial cortex (Yu et al., 2006; Spira et al., 2017). Nonmuscle-myosin II is a motor protein consisting of multiple subunits: myosin II heavy chain, essential myosin II light chain (eMLC) and regulatory myosin II light chain (rMLC). Two heavy chain molecules form a coiled coil structure with two globular ATP-binding motor domains at their N-terminus. Each motor domain associates with one eMLC and one rMLC, and large numbers of myosin II molecules subsequently form thick higher order filaments with motor domains positioned at each site of the filament. The opposite motor domains bind two anti-parallel actin filaments and constriction occurs when myosin II moves along these actin filaments in opposite direction, pulling the actin filaments and the cell membrane to which F-actin is attached inward, highly similar to a string pulling on a purse (Ma et al., 2012; Shutova and Svitkina, 2018; Matsumura, 2005). As the ring constricts, F-actin disassembly balances actin polymerization through the actin filament severing activity of cofilin and the ATPase activity of myosin II (Wiggan et al., 2012; Xue and Sokac, 2016; Leite et al., 2019). In fact, F-actin disassembly is equally important for furrow ingression as F-actin polymerization (Mendes Pinto et al., 2012).

Actomyosin ring formation and contraction depends on the activation of the small GTPase, RhoA (Basant and Glotzer, 2018) (Figure 2). In anaphase, RhoA shuttles between an active GTP-bound state and an inactive GDP-bound state, through the activities of the Guanine nucleotide Exchange Factor (GEF), ECT2, and a GTPase Activating Protein (GAP), most likely RhoGAP35 (aka p190RhoGAP-A) in human cells (Somers and Saint, 2003; Yüce et al., 2005; Nishimura, 2006; Kamijo et al., 2006; Li et al., 2010; Manukyan et al., 2015). Optogenetic experiments in human cells revealed that the acute recruitment of a constitutive active RhoA GEF (in this study the GEF domain of Leukemia-Associated RhoGEF (LARG) was used) to any location on the cell cortex induces local furrow ingression even when cells are not in anaphase (Wagner and Glotzer, 2016; Jaiswal et al., 2011). This demonstrates that local RhoA activation

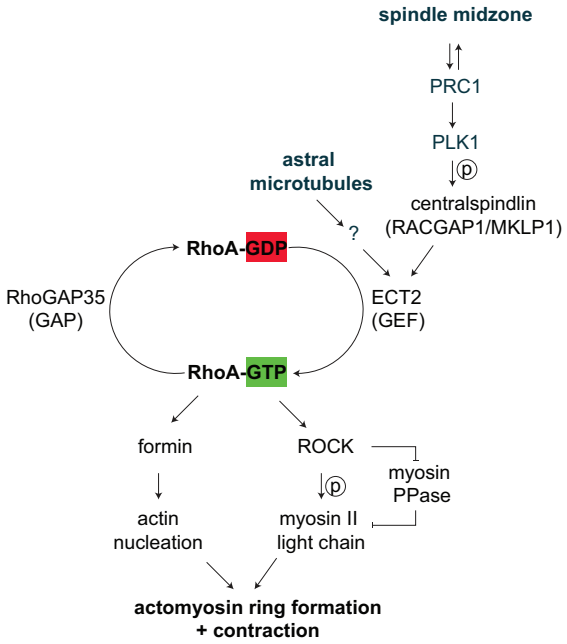

Figure 2: Schematic for the pathway activating RhoA and the formation and contraction of the actomyosin ring. PRC1 is located on the spindle midzone were it bundles microtubules and recruits PLK1. PLK1 phosphorylates RACGAP1 in centralspindlin, which creates a binding site for ECT2 and activates ECT2. ECT2 activates RhoA by the exchange of GDP for GTP. RhoA-GTP binds ROCK and formin. Formin nucleates and ROCK activates myosin II by directly and indirectly promoting the phosphorylation of the myosin II light chain. Together, this leads the formation and the contraction of the actomyosin ring. ECT2 and RhoA activation can also be stimulated by astral microtubules through a mechanism that is not yet clear.

is sufficient to initiate cytokinesis. In contrast, optogenetic manipulation of ECT2, only resulted in RhoA activation and furrow ingression when ECT2 was placed at the equatorial cortex in anaphase. ECT2 placement outside the equatorial cortex failed to induce ectopic furrow ingression (Kotýnková et al., 2016; Wagner and Glotzer, 2016), which implies that localized furrow ingression comes down to how ECT2 gets activated and localized at the equatorial cortex (discussed below).

Once RhoA is activated in the equatorial cell membrane, it has at least three main targets involved in actomyosin ring formation and contraction. First, RhoA-GTP binds to formins such as mDia1 and mDia2, and this binding stimulates their ability to nucleate the assembly of new actin filaments (Figure 2) (Kühn and Geyer, 2014; Watanabe et al., 2008, 2010; Lammers et al., 2008). Profilin increases the elongation rate of formin-assembled actin filaments (Romero et al., 2004; Kovar et al., 2006). Second, RhoA-GTP interacts with Rho-associated, coiled-coil-containing protein kinase (ROCK). When bound and activated by RhoA-GTP, ROCK activates myosin II in two ways; it directly phosphorylates rMLC, and it phosphorylates and inhibits myosin phosphatase thereby indirectly promoting rMCL phosphorylation (Amano et al., 1996, 2010; Kimura et al., 1996; Totsukawa et al., 2000). Phosphorylation of rMLC stimulates myosin II motor activity, filament formation and myosin II recruitment to the equatorial cortex (Dean and Spudich, 2006; Totsukawa et al., 2000). Third, RhoA-GTP recruits Anillin to the equatorial cortex, most likely through direct association (Piekny and Glotzer, 2008). Since Anillin also directly binds myosin II, F-actin, ECT2 and other proteins, it appears to act as a scaffolding protein that brings together many factors at the equatorial cortex involved in furrow ingression (Piekny and Glotzer, 2008; Straight et al., 2005; Kotýnková et al., 2016; Piekny and Maddox, 2010). Moreover, Anillin was recently shown to inhibit the cortical dissociation of active RhoA, thereby increasing its dwell time near its effectors in the

equatorial cortex (Budnar et al., 2019).

When constriction of the actomyosin ring is complete and the midbody is formed, proteins present on the midbody, such as MKLP1, Arf6, RACGAP1 and Anillin, link the cell membrane to the midbody ensuring the furrow does not regress when the actomyosin ring is disassembled (Hu et al., 2012a; Lekomtsev et al., 2012; Makyio et al., 2012; Joseph et al., 2012). Finally, at the intracellular bridge, next to the midbody, abscission takes place by the ESCRT-III complex which mediates membrane constriction and recruits factors that disassemble midbody microtubules and catalyzes the scission of membrane structures (Mierzwa and Gerlich, 2014; Wollert et al., 2009).

Spatial regulation of the division site

The spatiotemporal regulation of cytokinesis initiation has intrigued scientist since the nineteenth century, and many theories were posed to explain it. For example, in 1876, Bütschli thought that astral microtubules were channels creating a current of fluids away from the astral center. Because the two spindles asters meet in the midzone, the increase in current would be additive there, increasing the tension specifically in the midzone causing cell elongation and eventually furrow ingression (Rappaport, 1996). In 1948, Jean Clark Dan, a marine biologist, wrote the following about cell division: ”…. One of the most spectacular of biological phenomena, its apparent simplicity captures the imagination and baffles it; the tremendous range of variations in this process challenges and, at the same time, discourages the investigator” (Dan, 1948). This statement still holds true, the process is visually elegant and seemingly simplistic, but the molecular mechanisms underlying the process appear complex and involve redundancy at various levels. With the advances in microscopy and molecular biology, many theories have proven incorrect, but some of them have stood the test of time. Pivotal experiments performed by Rappaport *et al*. in sand dollar eggs, demonstrated that the anaphase spindle dictates the site of the cytokinetic furrow (Rappaport, 1961). In these experiments, sand dollar eggs were pressed into all kinds of shapes by a glass rod, and revealed that wherever the spindle went, the cleavage furrow would always occur perpendicular to and in the middle of the spindle. How the anaphase spindle signals to the cell cortex to initiate cytokinesis is discussed below.

Spindle midzone stimulation

In 1974 Rappaport reported that, in sand dollar and sea urchin (echinoderm) eggs, and newt kidney epithelial cells, cleavage was initiated when the cell cortex was in close proximity of the surface of the spindle midzone (Rappaport and Rappaport, 1974; Rappaport, 1996). Subsequent experiments in grasshopper neuroblasts showed that when the spindle was bent into an arc shape, with the spindle poles on one side and the spindle midzone on the other, the cleavage furrow would form on the side of the spindle midzone, and not on the side of the spindle poles (Kawamura, 1977). Moreover, perforations made adjacent to the spindle midzone in rat kidney epithelial cells, specifically blocked furrow ingression on the perforated side of the cell, indicating some sort of communication between the spindle midzone and the cell cortex (Cao and Wang, 1996). Collectively, these results have led the hypothesis that the antiparallel overlapping microtubules of the spindle midzone serve as a landing platform for proteins

which signal to the equatorial cortex to initiate cytokinesis (figure 3).

The spindle midzone is formed in part by the microtubule bundling protein, Protein Regulator of Cytokinesis 1 (PRC1), which binds to the antiparallel microtubule overlaps of the anaphase spindle(Subramanian et al., 2010). Before anaphase, PRC1 is inactivated through Cyclin B-Cdk1 dependent phosphorylation (Neef et al., 2007). However, at anaphase onset, PRC1 starts to extensively bundle the spindle midzone microtubules together with the kinesin-6 motor proteins, Mitotic Kinesin-Like Protein 1 (MKLP1, KIF23, hsZEN4) and Mitotic Kinesin-Like Protein 2 (MKLP2, KIF20A) (Glotzer, 2009; Mollinari et al., 2002; Neef et al., 2003; Kitagawa et al., 2014; Mishima et al., 2002; Zhu et al., 2006). Moreover, PRC1 forms a complex with the motor protein KIF4A which controls the length of the antiparallel microtubule overlaps by inhibition of microtubule growth (Kurasawa et al., 2004; Zhu and Jiang, 2004; Subramanian et al., 2013; Wijeratne and Subramanian, 2018; Hu et al., 2011; Bieling et al., 2010; Hannabuss et al., 2019).

MKLP1 is a subunit of the heterotetrametric centralspindlin protein complex, which consists of two MKLP1 and two RACGAP1 (mgcRACGAP, hsCYK4) molecules (White and Glotzer, 2012; Basant et al., 2015). Centralspindlin is considered the activator of ECT2, the GEF that activates RhoA in anaphase (Somers and Saint, 2003; Yüce et al., 2005; Nishimura, 2006; Mishima, 2016; Basant and Glotzer, 2018). ECT2 exists in an inactive conformation due to an intramolecular interaction between its N- and C-terminal domain. Autoinhibition is relieved when phosphorylated RACGAP1 in centralspindlin binds to the ECT2 N-terminus (Yüce et al., 2005; Zou et al., 2014). As such, RACGAP1, which functions as a canonical GAP (and thus inactivator) of the small GTP-ase RAC1, functions as an activator of RhoA in anaphase (Zhang and Glotzer, 2015; Bastos et al., 2013). RACGAP1 is phosphorylated by Polo-Like Kinase 1 (PLK1) on the spindle midzone resulting in the recruitment and activation of ECT2 at this location (Brennan et al., 2007; Burkard et al., 2009; Petronczki et al., 2007). However, an ECT2 mutant lacking its C-terminal Pleckstrin Homology (PH) domain and polybasic cluster, which are required for its localization to the equatorial membrane, fails to initiate cytokinesis (Kotýnková et al., 2016), suggesting that active ECT2 needs to translocate from the spindle midzone to the equatorial cell membrane to locally activate RhoA (Wolfe et al., 2009).

However, in some cells such as zygotes, the distance between the cell cortex and the spindle midzone is substantial and it is unclear how ECT2 could span this distance and specify the equatorial cortex with such precision. Yet, cleavage furrow ingression is initiated and completed in these cells (Rappaport and Rappaport, 1974; Rappaport, 1971; Wühr et al., 2010). Moreover, depletion of PRC1 in mammalian cells, which disrupts spindle midzone formation and PLK1 and centralspindlin localization on the spindle midzone, does not affect the initiation of cytokinesis. This suggests that the anaphase spindle also generates midzone-independent signals that activate RhoA in the (equatorial) cell membrane (Jiang et al., 1998; Mollinari et al., 2005; Zhu et al., 2006; Zhu and Jiang, 2004; Verbrugghe and White, 2004)

Astral microtubule stimulation

These alternative RhoA stimulatory signals from the anaphase spindle might be delivered by the astral

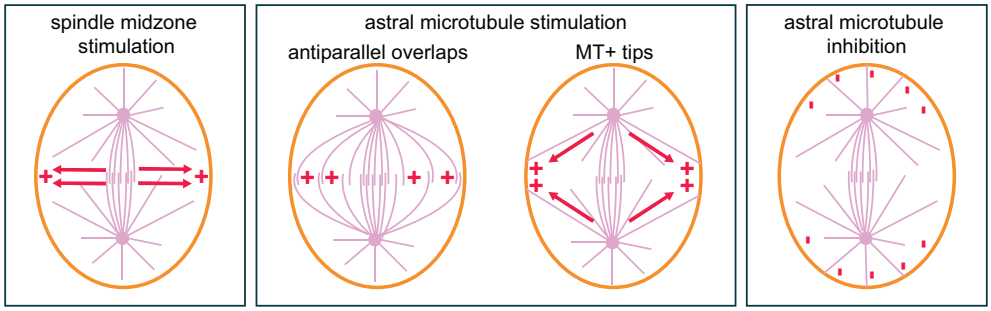

Figure 3: Four models explaining the spatial regulation of the division site in mammalian cells.
The spindle midzone model proposes that signals from the spindle midzone stimulate the adjacent cortex to initiate cytokinesis. The astral stimulation model suggests that signals from the astral microtubules (MTs) stimulate furrow ingression. Either by forming anti-parallel overlaps or by direct contacts between the MT plus-ends and the cortex. The astral inhibition model proposes that astral microtubules inhibit cortical contractility near the spindle poles.

microtubules (Devore et al., 1989). Evidence for astral microtubule stimulation again came from classical experiments by Rappaport *et al*. (Rappaport, 1961) (Figure 4). Sand dollar eggs were pressed with a glass rod in the middle of the cell into a doughnut shape, which caused the spindle to be pushed to one side. Furrow ingression only took place on the side of the doughnut where the spindle was positioned leading to a torus-shaped cell. The subsequent division was striking because in addition to the cleavage furrow that formed between the separating sister chromatids, an additional furrow was formed between the neighboring asters of two independent spindles. This kind of furrow is now called the “Rappaport furrow” and has led to the theory that astral microtubules can stimulate furrow ingression. In line with this, in 1971 Hiramoto *et al.* subsequently demonstrated that in blastomeres of sea urchin eggs, single spindle asters could also induce cleavage furrow ingression (Hiramoto, 1971). Similarly, cytokinesis also occurs in mammalian somatic cells with monopolar spindles (Canman et al., 2003), leading to the hypothesis that contraction of the cell cortex can be induced by ‘a substance or substances released at the tips of the astral arrays’ (Hiramoto, 1971).

How astral microtubules activate furrow ingression is still unclear. One theory is that the astral microtubules from opposing spindle poles meet near the equatorial cortex creating antiparallel microtubule overlaps and thus form “mini-spindle midzones” (Motegi et al., 2006; Devore et al., 1989). In line with this, a recent study showed that astral microtubules growing from artificial centrosomes in a cell-free cytoplasmic extract from Xenopus eggs can form antiparallel overlaps when the microtubules from different centrosomes meet. These overlaps recruit PRC1, centralspindlin and the Chromosomal Passenger Complex (CPC) (Nguyen et al., 2014). This model suggests that the molecular mechanism by which astral microtubules stimulate furrow ingression are very similar to the way the spindle midzone induces furrow ingression. However, it does not explain cytokinesis in cells with monopolar spindles, nor the observation that furrow ingression occurs in the absence of PRC1, which disturbs spindle midzone formation in cells with a bipolar spindle (Canman et al., 2003; Hu et al., 2008; Jiang et al., 1998; Mollinari et al., 2005; Zhu and Jiang, 2004; Zhu et al., 2006). In these cells, furrow ingression occurs at sites where the plus-ends of a subset of stable astral

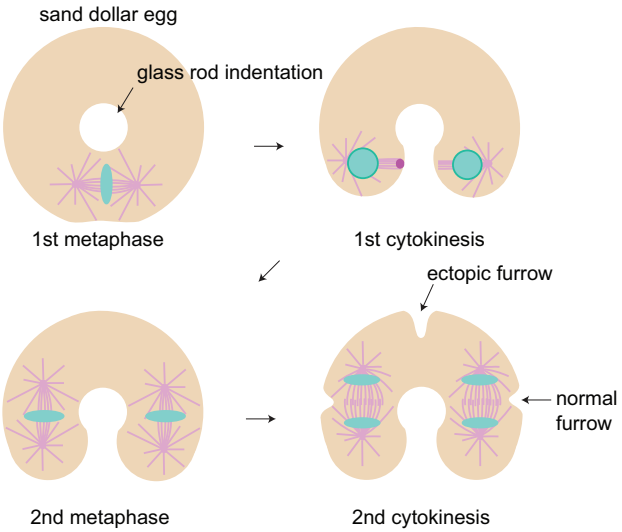

Figure 4: Rappaport's torus experiment
Sand dollar eggs were pressed with a glass rod in the middle of the cell into a doughnut shape, which caused the spindle to be pushed to one side. Cytokinesis of this cell leads to a torus-shaped cell. The next division leads to an extra ectopic furrow that forms between the neighboring asters of two independent spindles. This kind of furrow is called the "Rappaport furrow".

microtubules interact with the cortex (Foe and Von Dassow, 2008; Canman et al., 2003). Interestingly, more recently a study in Drosophila melanogaster S2 cells revealed that centralspindlin localizes to the plus tips of astral microtubules and that ECT2 was recruited to, and RhoA activated at, the cortical sites contacted by these microtubule plus-tips. In early anaphases these contacts were made in the entire cortex resulting in local patches of active RhoA all over the cortex. However, minutes later these active RhoA patches were no longer observed near the spindle poles but were retained in the equatorial cortex (Verma and Maresca, 2019). How these microtubule plus-ends are directed towards the equatorial cortex is unclear.

Thus, although astral microtubules can stimulate cytokinesis initiation in the cell equator, the biochemical signal these astral microtubules convey is still incompletely understood. The Chromosomal Passenger Complex (CPC) and MKLP2 are potential candidates since they localize at the equatorial cortex in anaphase and this localization requires the presence of astral microtubules (O'Connell and Wang, 2000; Murata-Hori and Wang, 2002; Théry et al., 2005; Mishima, 2016). The CPC consists of INCENP, Borealin, Survivin and Aurora B kinase, and prior to anaphase the complex is localized at the centromeres of the chromosomes and promotes faithful chromosome segregation (Van Der Horst and Lens, 2014). In early anaphase, the CPC translocates from the centromeres to the anti-parallel microtubule overlaps of the spindle midzone and to the equatorial cortex. The translocation and anaphase localization of the CPC is dependent on the presence of MKLP2 (Cesario et al., 2006; Gruneberg et al., 2004; Kitagawa et al., 2014, 2013; Nguyen et al., 2014). In anaphase, the enzymatic subunit of the CPC, Aurora B, phosphorylates MKLP1 in centralspindlin. This disrupts the interaction between MKLP1 and its inhibitor 14-3-3 and results in the subsequent oligomerization of centralspindlin (Guse et al., 2005; Douglas et al., 2010; Basant et al., 2015). Interestingly, in C. elegans embryos, the oligomerization of centralspindlin, initiated by the CPC, was shown to promote RhoA activation in the equatorial cortex (Basant et al., 2015). Although centralspindlin has been observed at the equatorial cortex and at microtubule plus-ends during anaphase

in mammalian cells (Vale et al., 2009; Nishimura, 2006; Breznau et al., 2017; Verma and Maresca, 2019), inhibition of Aurora B kinase just before anaphase onset, or knock-down of MKLP2 in human cells does not interfere with furrow ingression, suggesting this potential astral microtubule stimulatory route to cytokinesis initiation does either not exist in human cells or is masked as a consequence of redundancy (see chapter 2) (Guse et al., 2005; Ahonen et al., 2009; Steigemann and Gerlich, 2009; Davies et al., 2014).

Astral microtubule relaxation

Studies in which microtubules were depolymerized during anaphase described the formation of multiple ingression furrows all over the cortex (Werner et al., 2007; Tse et al., 2011; Basant et al., 2015; Foe and Von Dassow, 2008; Mangal et al., 2018; Murthy and Wadsworth, 2008; Canman et al., 2000). These findings resulted in the idea that cells in late mitosis experience a global contraction signal spanning the cortex, which is inhibited at the poles by astral microtubules. The inhibitory signal of astral microtubules would by the strongest near the centrosomes, most likely because of the high density of astral microtubules, and therefore cause the polar cortex to relax. Further away, at the equatorial cortex, the density of astral microtubules is way less, and hence the relaxation signal weaker, causing the cell membrane to ingress at the equator (Dechant and Glotzer, 2003). The biochemical properties of this inhibitory signal conveyed by the astral microtubules is unknown. The observation that placement of ECT2 near the spindle poles did not induce furrow ingression whilst the placement of a constitutive active GEF domain did, might indicate that the regulation is at the level of ECT2 (Jaiswal et al., 2011; Wagner and Glotzer, 2016; Kotýnková et al., 2016). Alternatively, the inhibitory effect of the astral microtubules near the poles might be indirect. Recent work suggested that protein phosphatase 1 (PP1) localized on chromosomes via its association with SDS22, could cause cortical relaxation near the poles. As the sister chromatids were pulled towards the opposite spindle poles, this phosphatase was able to dephosphorylate and inactivate the ezrin/radixin/moesin proteins at pole cortex. This softened the cortex near the spindle poles enabling spindle and cell elongation (Rodrigues et al., 2015). In this scenario, astral inhibition seems an indirect consequence of the role of these microtubules in spindle elongation and chromosome segregation.

In summary, the anaphase spindle is key in the spatiotemporal control of cytokinesis initiation. The signals from the anaphase spindle are either delivered to the cortex by the spindle midzone or by the astral microtubules. And astral microtubules can convey both inhibitory and stimulatory signals to the cell cortex. The different spindle-derived signals that mediate furrow ingression may all be operational during cytokinesis, and cause redundancy. Alternatively, some of these routes to furrow ingression may be more important or dominant in some cells than in others. For example, experiments in large cells, mostly zygotes, suggest an important role for astral microtubules in the initiation of cytokinesis (Su et al., 2014; Mishima, 2016), while experiments in smaller cells, such as mammalian somatic cells, indicated a more prominent role for the spindle midzone (Cao and Wang, 1996).

Thesis outline

The molecular mechanisms underlying cytokinesis appear complex and involve redundancy at various levels. Signals from the anaphase spindle define where and when cytokinesis is initiated but the biochemical nature of these signals is still unclear (reviewed in **chapter 1**). Whilst the spindle midzone was considered the main determinant of cytokinesis initiation in small mammalian cells, we disagreed with this notion based on the observation that small human cells lacking an organized spindle midzone could still initiate cytokinesis (Mollinari et al., 2005; Zhu et al., 2006). This suggested alternative routes to furrow ingression in human cells. In **chapter 2,** we studied the regulation of spindle midzone-independent cytokinesis initiation by knockdown of PRC1. We found that cytokinesis initiation in these cells could occur in the absence of PLK1 activity. Instead, we found it required a pool of Aurora B kinase localized at the equatorial cortex.

Uncovering a role for cortical-associated Aurora B in cytokinesis initiation led us to question how Aurora B reaches the equatorial cortex in anaphase. Since this localization required the presence of the kinesin-6 motor MKLP2 and astral microtubules, we tested the hypothesis that Aurora B, as part of the CPC, is transported to the cortex by MKLP2 in **chapter 3**. Using microscopy-based *in vitro* reconstitution assays with purified proteins and live cell imaging, we provide evidence that supports this hypothesis.

Mass Spectrometric analysis of MKLP2 purified from human cells identified MAP7 (Microtubule Associated Protein 7, Ensconsin) and MAP7D2 as interactors of MKLP2. In **chapter 4**, we demonstrate that MAP7 is required for the proper localization of MKLP2 and the CPC in anaphase. Without MAP7, MKLP2 and the CPC appear as foci resembling liquid condensates between the segregating chromosomes in anaphase.

Finally, in **chapter 5** we discuss these new findings and how they fit in the previously discussed mechanistic models of cytokinesis initiation.

Chapter 2

PLK1 plays dual roles in centralspindlin regulation during cytokinesis

Ingrid E. Adriaans[1,2], Angika Basant[3,4], Bas Ponsioen[1,2], Michael Glotzer[3], Susanne M. A. Lens[1,2*]

[1]Oncode Institute and [2]Center for Molecular Medicine, University Medical Center Utrecht, Utrecht University, Utrecht, The Netherlands. [3]Department of Molecular Genetics and Cell Biology, University of Chicago, Chicago, USA. [4]Current address: Cellular Signalling and Cytoskeletal Function Lab, The Francis Crick Institute, London NW1 1AT, United Kingdom.

Published in Journal of Cell Biology, 6 February, 2019

Summary

Adriaans *et al*. provide evidence for the existence of two molecular pathways that can initiate cytokinesis in human cells. One depending on PLK1 and originating at the spindle midzone, and the other depending on Aurora B activity at the equatorial cortex.

Abstract

Cytokinesis begins upon anaphase onset. An early step involves local activation of the small GTPase RhoA which triggers assembly of an actomyosin-based contractile ring at the equatorial cortex. Here we delineated the contributions of PLK1 and Aurora B to RhoA activation and cytokinesis initiation in human cells. Knock-down of PRC1, which disrupts the spindle midzone, revealed the existence of two pathways that can initiate cleavage furrow ingression. One pathway depends on a well-organized spindle midzone and PLK1, while the other depends on Aurora B activity and centralspindlin at the equatorial cortex and can operate independently of PLK1. We further show that PLK1 inhibition sequesters centralspindlin onto the spindle midzone making it unavailable for Aurora B at the equatorial cortex. We propose that PLK1 activity promotes the release of centralspindlin from the spindle midzone through inhibition of PRC1, allowing centralspindlin to function as a regulator of spindle midzone formation and as an activator of RhoA at the equatorial cortex.

Introduction

Cytokinesis drives the physical separation of daughter cells at the end of mitosis. Failure to complete cytokinesis gives rise to tetraploid cells with supernumerary centrosomes. Depending on the cell type and cellular context, cytokinesis failure can either result in a G1 arrest, or allow cell cycle progression of the tetraploid cells into the next mitosis (Uetake and Sluder, 2004; Andreassen et al., 2001). These dividing tetraploid cells are at risk of becoming aneuploid, owing to, for example, the extra number of centrosomes that can cause the missegregation of chromosomes during mitosis (Ganem et al., 2009; Tanaka et al., 2015; Silkworth et al., 2009). Hence proper execution and completion of cytokinesis is essential for genomic stability.

In animal cells, cytokinesis starts in anaphase with the formation of an actomyosin-based contractile ring at the equatorial cortex that drives ingression of the cleavage furrow. Prior to membrane furrowing interpolar microtubules are bundled between the separating sister chromatids to form the spindle midzone (also referred to as central spindle). As the furrow ingresses, these microtubule bundles are compacted into a cytoplasmic bridge, with the midbody in its center. The midbody attaches the ingressed cell membrane to the intercellular bridge and promotes the final phase of cytokinesis, known as abscission (Lekomtsev et al., 2012; D'Avino and Capalbo, 2016; Steigemann and Gerlich, 2009; Hu et al., 2012b). Formation of the contractile ring requires activation of the small GTPase RhoA by the Guanine Nucleotide Exchange Factor (GEF), ECT2 (Basant and Glotzer, 2018). Active, GTP-bound RhoA activates components of the actomyosin-based ring, such as diaphanous-related formin that facilitates the assembly of actin filaments (Otomo et al., 2005; Watanabe et al., 2008; Piekny et al., 2005; Chen et al., 2017), and Rho-Kinase (ROCK), which activates nonmuscle myosin II to power ring constriction (Kosako et al., 2000; Amano et al., 1996). Optogenetic manipulation of RhoA activity showed that local activation of RhoA on the cell

membrane is sufficient to drive cleavage furrow initiation independent of cell cycle stage (Wagner and Glotzer, 2016). Hence, strict spatial and temporal regulation of RhoA activity is essential to coordinate the onset of cytokinesis with nuclear division.

Current models for local RhoA activation and cleavage furrow initiation describe at least two anaphase spindle-derived stimulatory signals: one originating from the spindle midzone and another derived from astral microtubules that end at the equatorial cortex (Mishima, 2016). Experiments in large echinoderm embryos suggest a stimulatory role of astral microtubules in the initiation of cleavage furrow ingression (Mishima, 2016; Su et al., 2014), whilst data in smaller (mostly mammalian) cells emphasized a role for the spindle midzone (Cao and Wang, 1996). The overlapping antiparallel microtubules of the spindle midzone serve as a platform for the localization of a variety of proteins that promote RhoA activation and cleavage furrow ingression directly parallel to the microtubule overlap. In addition, astral microtubules convey inhibitory signals at cell poles (Mangal et al., 2018; Werner et al., 2007; Wagner and Glotzer, 2016).

Protein Regulator of Cytokinesis 1 (PRC1) is essential for the assembly of a fully functional spindle midzone (Zhu et al., 2006; Mollinari et al., 2005, 2002). PRC1 is a homodimeric microtubule binding protein that is directly involved in bundling antiparallel microtubules (Li et al., 2018). Its microtubule bundling activity is required for spindle midzone formation, thereby indirectly contributing to the recruitment of other spindle midzone-localized proteins, such as centralspindlin and the Chromosomal Passenger Complex (CPC) (Zhu et al., 2006; Mollinari et al., 2005). Furthermore, through interaction with the kinesin KIF4A and Polo-like kinase 1 (PLK1) (Zhu and Jiang, 2004; Kurasawa et al., 2004), PRC1 also directly recruits regulatory proteins to the spindle midzone.

Centralspindlin is a heterotetramer consisting of two molecules of the kinesin-6 MKLP1 (KIF23) and two molecules of RACGAP1 (hsCyk4, MgcRacGAP) (Basant and Glotzer, 2018). Oligomerization of the complex is needed to bundle microtubules and organize the spindle midzone (Hutterer et al., 2009). In addition to microtubule bundling, centralspindlin promotes RhoA activation and cleavage furrow initiation (Somers and Saint, 2003; Yüce et al., 2005; Nishimura, 2006). This latter function of centralspindlin appears to rely on PLK1-dependent binding of RACGAP1 to ECT2 (Petronczki et al., 2007; Burkard et al., 2009; Wolfe et al., 2009). Mutation of PLK1 phosphorylation sites in the non-catalytic N-terminus of RACGAP1 disrupts its interaction with the N-terminal BRCT domain in ECT2 and disturbs the initiation of cytokinesis (Burkard et al., 2009; Wolfe et al., 2009). In line, inhibition of PLK1 activity at anaphase onset prevents RhoA activation at the equatorial cortex and cleavage furrow ingression (Petronczki et al., 2007; Brennan et al., 2007). Because inhibition of PLK1 activity or expression of a RACGAP1 PLK1-phosphorylation site mutant disrupt the spindle midzone localization of ECT2, it was proposed that the spindle midzone localization of ECT2 is a determining factor for the spatial activation of RhoA at the equatorial cortex (Burkard et al., 2009; Wolfe et al., 2009).

The Chromosomal Passenger Complex (CPC), consisting of inner centromere protein (INCENP), Survivin, Borealin and Aurora B kinase, relocates from chromosomes to the spindle midzone and equatorial

cortex at anaphase onset in an MKLP2 (KIF20A)-dependent manner (Gruneberg et al., 2004; Hümmer and Mayer, 2009; Kitagawa et al., 2013, 2014). One of the spindle midzone targets of Aurora B is the centralspindlin subunit MKLP1 (Guse et al., 2005; Neef et al., 2006). Phosphorylation of S708 of MKLP1 disrupts the interaction between MKLP1 and 14-3-3 proteins, permitting centralspindlin oligomerization (Guse et al., 2005; Douglas et al., 2010; Basant et al., 2015). In *C. elegans* embryos, Aurora B-induced oligomerization of centralspindlin promotes RhoA activation and cleavage furrow ingression and Aurora B activity is largely dispensable when centralspindlin constitutively oligomerizes (Basant et al., 2015). However, in mammalian cells, inhibition of Aurora B kinase activity at anaphase onset does not prevent initiation of cytokinesis, though it does prevent completion of cytokinesis (Guse et al., 2005; Ahonen et al., 2009). This suggests that RhoA activation can occur in the absence of Aurora B activity in mammalian cells, and that in these cells Aurora B activity appears to be more relevant at later stages of cytokinesis most likely by promoting the formation of the spindle midzone and midbody (D'Avino and Capalbo, 2016).

Whilst the spindle midzone is considered to provide important cues for RhoA activation at the equatorial cortex in mammalian cells (Yüce et al., 2005; Nishimura, 2006; Petronczki et al., 2007; Burkard et al., 2009; Wolfe et al., 2009), knock-down of PRC1, which clearly disrupts the spindle midzone, does not impair RhoA activation and cleavage furrow ingression (Jiang et al., 1998; Mollinari et al., 2005; Zhu and Jiang, 2004; Zhu et al., 2006). This implies that spindle midzone-independent cues can also locally activate RhoA in small, mammalian cells. Here we demonstrate that in the absence of PRC1, RhoA is activated at the equatorial cortex, at least in part, through centralspindlin oligomerization induced by cortical Aurora B activity. Remarkably, we find that in PRC1-deficient cells, cytokinesis initiation can occur in the absence of PLK1 activity. This alternative PLK1-independent route to RhoA activation has been overlooked because of an unrecognized inhibitory effect of PLK1 on PRC1 in anaphase. Specifically, we propose that PLK1 activity limits PRC1-dependent hyper-bundling of spindle midzone microtubules, and reduces centralspindlin sequestration at the spindle midzone, making it available for Aurora B to activate RhoA at the equatorial cortex.

Results

Disruption of the spindle midzone allows PLK1-independent RhoA activation and furrow ingression.

In human cells lacking PRC1, cleavage furrow ingression takes place despite the absence of a well-organized spindle midzone that concentrates cytokinetic regulators (Mollinari et al., 2005; Zhu et al., 2006). This suggests the existence of spindle midzone-independent cues in human cells that contribute to the local concentration of active RhoA. To delineate this spindle midzone-independent pathway, we analyzed the contribution of key cytokinesis regulators to cytokinesis initiation in a PRC1 knock-down background. We first confirmed that after PRC1 knock-down the spindle midzone was severely disrupted, as shown by the disorganized appearance of midzone microtubules (Fig. 1A, B). In addition, live cell imaging of anaphase cells depleted of PRC1 reveals that most cells exhibit full cleavage furrow ingression followed by cleavage furrow regression (Fig. 1C, D). The frequency and extent of furrow ingression was assessed and a distinction was made between no furrow ingression and minimal furrow ingression (Fig. 1D and Fig. S1A).

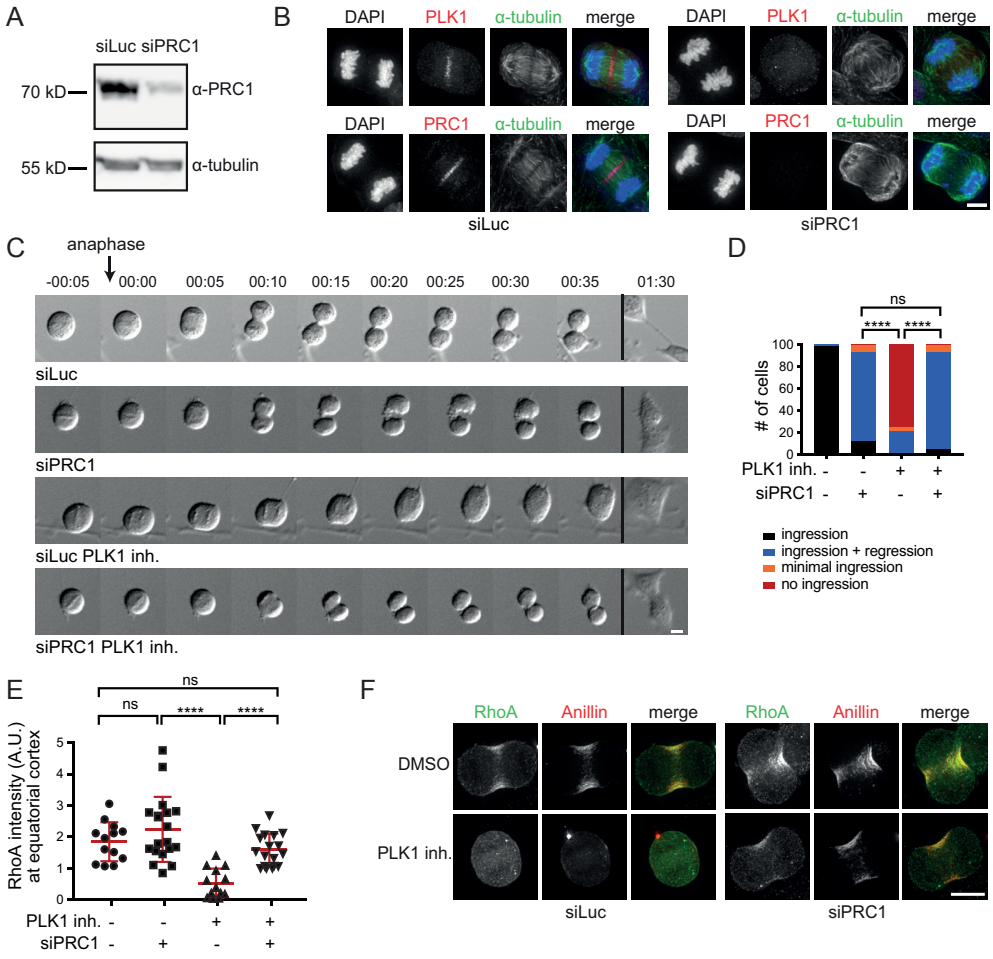

Figure 1: PRC1 depletion reveals PLK1-independent RhoA activation and furrow ingression.
(A) Western blot of HeLa cells transfected with control siRNA (siLuc) or siRNA specific for PRC1. The Western blot was probed with an anti-PRC1 antibody. α-Tubulin is shown as loading control. (B) IF for PLK1, PRC1 and α-tubulin of HeLa cells transfected with siLuc or siPRC1. DNA was visualized using DAPI. Scale bar indicates 5 μm. (C) DIC stills of a live cell imaging experiment of HeLa cells transfected with either siLuc or siPRC1 plus or minus addition of BI2536 (100 nM) prior to anaphase onset. Scale bar indicates 10 μm. Timepoint 00:00 (hours:minutes) refers to the first frame where we observed separating sisters. Stills of more time frames are shown in Fig. S1B. (D) Percentage of cells showing either complete furrow ingression, full furrow ingression followed by furrow regression, visible but minimal furrow ingression or no furrow ingression (n = 100 cells imaged per condition). **** = $p < 0.0001$; Chi-squared test for comparison of the indicated conditions, ns = not significant. One representative experiment out of 2 is shown. (E) Quantification of fluorescence intensity levels of RhoA at the equatorial cortex in anaphase as shown in (F). Each dot represents an individual cell. Error bars depict the standard deviation (SD) of the mean. **** = $p < 0.0001$; Student's t-test for comparison of the indicated conditions, ns = not significant. (F) IF for RhoA and Anillin of HeLa cells in anaphase transfected with the indicated siRNAs and treated plus or minus BI2536 (100 nM). Scale bar indicates 10 μm.

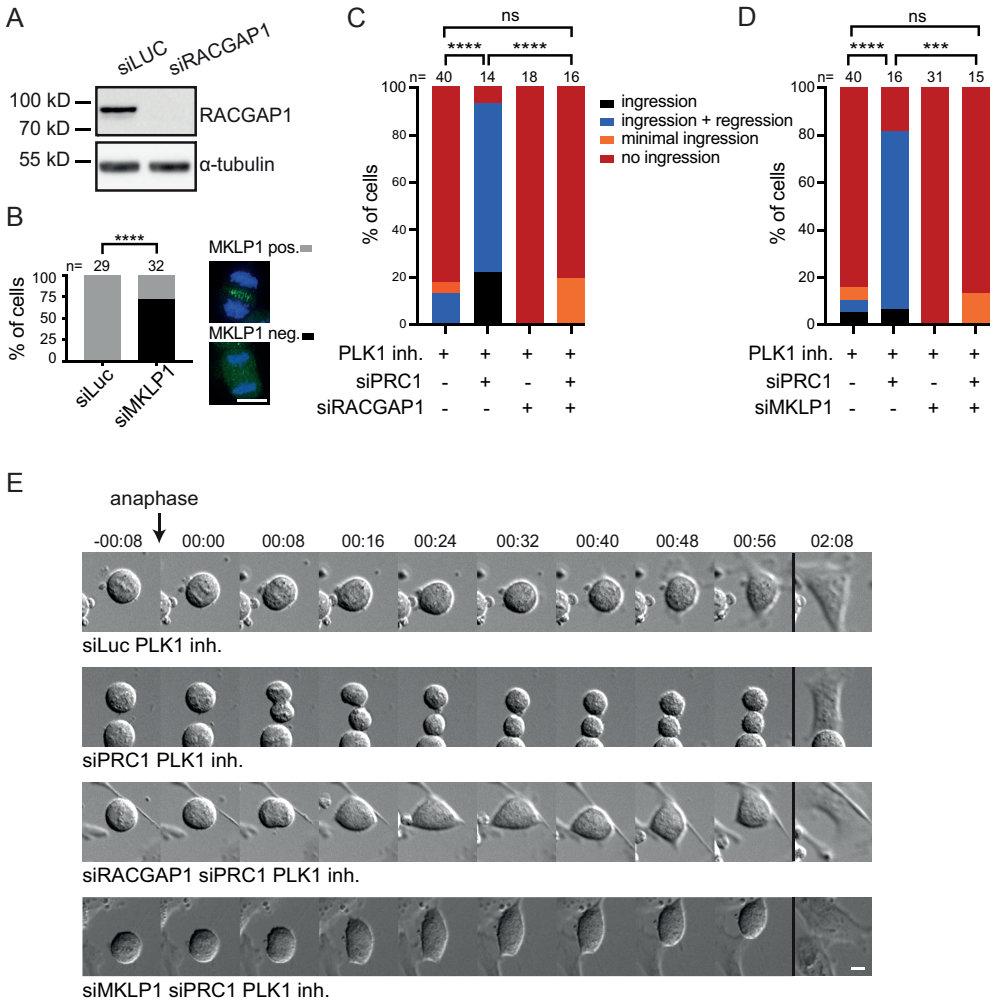

Figure 2: PLK1-independent furrow ingression requires centralspindlin.
(A) Western blot of samples derived from HeLa cells transfected with either siLuc or siRACGAP1. The Western blot was probed with an anti-RACGAP1 antibody. α-Tubulin is shown as loading control. (B) HeLa cells were transfected with siLuc or siMKLP1 and processed for IF (right panel). The percentage of cells with detectable MKLP1 in anaphase was scored and used as a measure for knock-down efficiency (left panel). The number of cells that were scored per condition is indicated (n). One representative experiment out of 2 is shown. **** = $p < 0.0001$; Chi squared test for comparison of the indicated conditions. (C, D) HeLa cells transfected with the indicated siRNAs were imaged live. PLK1 was inhibited by addition of BI2536 (100 nM) prior to anaphase onset (PLK1 inh.). The number of cells showing complete furrow ingression, full furrow ingression followed by furrow regression, visible but minimal furrow ingression or no furrow ingression was scored. The number of cells analyzed per condition is indicated (n). One representative experiment out of 2 is shown. **** = $p < 0.0001$, *** = $p < 0.001$; Chi squared test for comparison of the indicated conditions, ns = not significant. (E) DIC stills of HeLa cells transfected with the indicated siRNAs plus or minus addition of BI2536 (100 nM) prior to anaphase onset. Scale bar indicates 10 μm. Stills of more time frames are shown in Fig. S1D.

Because PLK1 is a critical regulator of RhoA activation and cleavage furrow ingression (Burkard et al., 2009; Petronczki et al., 2007), we tested its involvement in spindle midzone-independent cytokinesis initiation. PLK1 activity was inhibited in metaphase, prior to anaphase onset, by addition of the small molecule inhibitor BI2536 (Steegmaier et al., 2007). Remarkably, while PLK1 inhibition alone completely prevented furrow ingression in ~80% of control transfected cells, PLK1 inhibition allowed full furrow ingression in PRC1 knockdown cells (Fig. 1C, D, Fig. S1B), after a ± 5 min. delay in the onset of furrow ingression (Fig. S1C). PRC1 depletion restored RhoA and Anillin localization to the equatorial zone in PLK1 inhibited cells (Fig. 1E, F). Thus, although PLK1 activity is critical for RhoA activation and initiation of cytokinesis in cells containing PRC1, it is dispensable when PRC1 is absent and the spindle midzone is disrupted. This suggests that PRC1 can function both as an activator and as an inhibitor of RhoA activation.

PLK1-independent furrow ingression relies on the centralspindlin complex.

The centralspindlin complex is an important target of PLK1 and is involved in the activation of the RhoA GEF, ECT2 (Burkard et al., 2009; Wolfe et al., 2009; Brennan et al., 2007; Santamaria et al., 2007). We therefore tested whether centralspindlin is required for furrow ingression in cells depleted of PRC1 and treated with an inhibitor of PLK1, by depleting the two components of centralspindlin, RACGAP1 and MKLP1. Following RACGAP1 knock-down the protein was indeed no longer detectable on Western blot (Fig. 2A). MKLP1 knockdown was confirmed by immunofluorescence (IF) as the antibody failed to detect the protein on Western blot. The frequency of cells with undetectable MKLP1 localization in the anaphase midzone was used as a proxy for knockdown efficiency (Fig. 2B). We combined PLK1 inhibition with knockdown of either PRC1, RACGAP1 or MKLP1, or with co-depletion of PRC1 and RACGAP1, or of PRC1 and MKLP1 (Fig. 2C-E, Fig. S1D). Approximately 80% of the siPRC1 transfected cells, initiated cytokinesis when PLK1 was inhibited (Fig. 1D and Fig. 2C,D). However, cytokinesis initiation was almost completely blocked when RACGAP1 or MKLP1 was also depleted (Fig. 2C-E and Fig. S1D). This demonstrates that whilst spindle midzone-independent furrow ingression does not require PLK1 activity, it does require centralspindlin. In *C. elegans* embryos, disruption of the spindle midzone by SPD-1 (the *C. elegans* ortholog of PRC1) depletion does not block furrowing (Verbrugghe and White, 2004; Lee et al., 2015). However, these earlier experiments were performed in the presence of NOP-1, a nematode-specific ECT2 activator (Tse et al., 2011). Therefore, we tested whether RhoA activation and furrowing can occur in embryos deficient in both SPD-1 and NOP-1. All such embryos initiated furrow formation, though ~50% of embryos did not complete furrow ingression. Furrow ingression was slower in the embryos depleted of SPD-1, but furrow initiation occurred more quickly following anaphase onset (Fig. S2A). The more rapid initiation of furrowing may be a consequence of the more rapid and extensive spindle elongation (Fig. S2B). In 5/8 embryos, RACGAP1 (CYK-4) was readily detected on the membrane during furrowing (Fig. S2C). These results indicate conservation of a spindle midzone-independent, and centralspindlin-dependent pathway for RhoA activation.

Aurora B activity at the equatorial cortex is required for spindle midzone-independent furrow ingression.

By depleting PRC1, we uncovered a PLK1-independent, but centralspindlin-dependent pathway for localized RhoA activation and furrow ingression. We hypothesized that another kinase might regulate

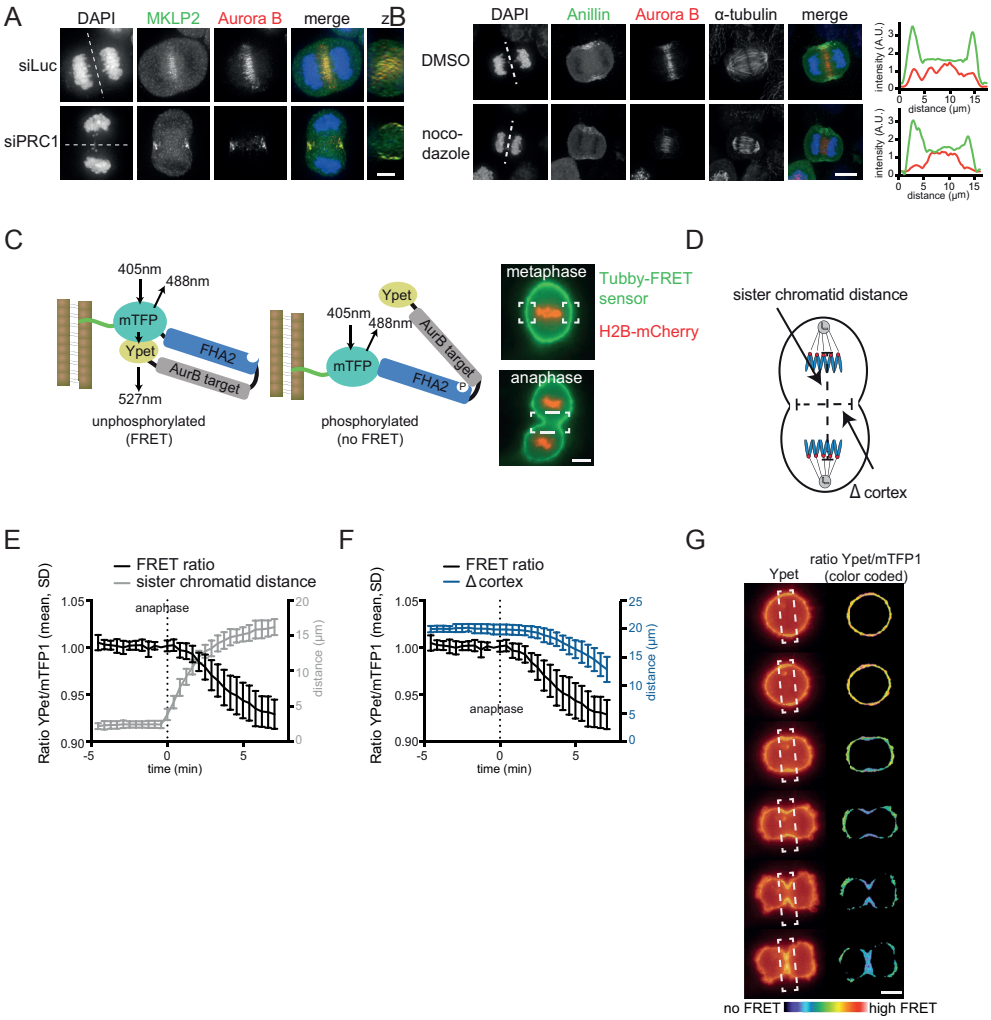

Figure 3: Aurora B localization and activity at the equatorial cortex.
(A) IF for MKLP2 and Aurora B in HeLa cells transfected with siLuc or siPRC1. Dotted line indicates z-plane for z-axis view. Scale bar indicates 5 μm. (B) IF for Anillin and Aurora B in anaphase cells treated with 83 nM nocodazole to depolymerize microtubules that are not part of the spindle midzone. Scale bar indicates 5 μm. Dotted line indicates z-plane for line plot analysis of Anillin (green) and Aurora B (red) intensity (far right). (C) Left: Scheme of the FRET-based Aurora B biosensor fused to Tubby protein (green line). Right: HeLa Flp-In T-Rex cells stably expressing Tubby-Aurora B FRET sensor (green) and H2B-mCherry (red). White boxes indicate the areas where FRET was measured. Scale bar = 10 μm. (D) Measurement of distance between the separating sister chromatids and the width of the ingressing furrow (Δ cortex). (E, F) HeLa cells stably expressing the Tubby-Aurora B FRET sensor and H2B-mCherry were synchronized in G2 by treatment with the CDK1 inhibitor RO3306 and imaged live after release from the G2 block. The emission ratio at the equatorial cortex was calculated for each timepoint (interval = 25 sec., mean ± SD of 10 cells) and plotted with the distance between the separating sister chromatids (E) or with the width of the ingressing furrow (F). (G) Color-coded images of the YPet/mTFP1 emission ratios. Scale bar = 10 μm.

centralspindlin-dependent RhoA activation and considered Aurora B kinase a likely candidate. Aurora B is located at the equatorial cortex in anaphase, and this localization becomes even more apparent after PRC1 depletion (Fig. 3A) (Earnshaw and Cooke, 1991; Murata-Hori and Wang, 2002; Mollinari et al., 2005). In both wild-type and PRC1-deficient cells, MKLP2 is required to relocalize the kinase from the chromosomes to the equatorial cortex (Fig. S3A, B) (Gruneberg et al., 2004; Hümmer and Mayer, 2009; Kitagawa et al., 2013). Moreover, we confirmed that this cortical localization of Aurora B was largely dependent on non-spindle midzone microtubules, because a concentration of nocodazole (83 nM) that did not depolymerize the stable spindle midzone microtubules but removed microtubules outside the spindle midzone, reduced the localization of Aurora B at the equatorial cortex (Fig. 3B, Fig. S3C)(Théry et al., 2005; Murata-Hori and Wang, 2002; O'Connell and Wang, 2000; Mishima, 2016; Tame et al., 2014). We next assessed the catalytic activity of this cortical pool of Aurora B. We fused a Förster Resonance Energy Transfer (FRET)-based Aurora B phosphorylation sensor to the c-terminal (aa 243-505) Tubby

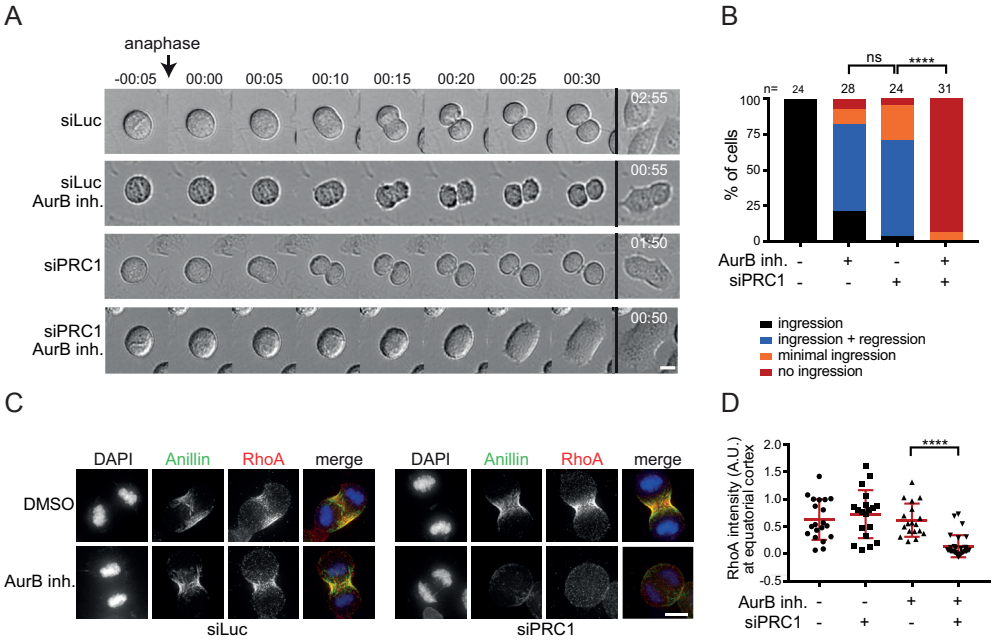

Figure 4: Aurora B activity at the equatorial cortex is required for spindle midzone-independent furrow ingression.

(A) Representative brightfield stills of a live cell imaging experiment with HeLa cells transfected with the indicated siRNAs and treated with (AurB inh.) or without the Aurora B inhibitor ZM447439 (2 μM) prior to anaphase onset. Scale bar indicates 10 μm. (B) Cells were treated and imaged as in (A), and the percentage of cells showing either stable furrow ingression, furrow ingression followed by furrow regression, minimal furrow ingression, no furrow ingression was scored. The number of cells analyzed per condition is indicated (n). One representative experiment out of 2 is shown. **** = $p < 0.0001$; Chi squared test for comparison of the indicated conditions, ns = not significant. (C) IF for Anillin and RhoA. DNA was visualized using DAPI. Scale bar = 5 μm. (D) Quantification of the fluorescence intensity levels of RhoA at the equatorial cortex in anaphase. Each dot represents an individual cell. Error bars depict the standard deviation (SD) of the mean. **** = $p < 0.0001$; Student's t-test for comparison of the indicated conditions.

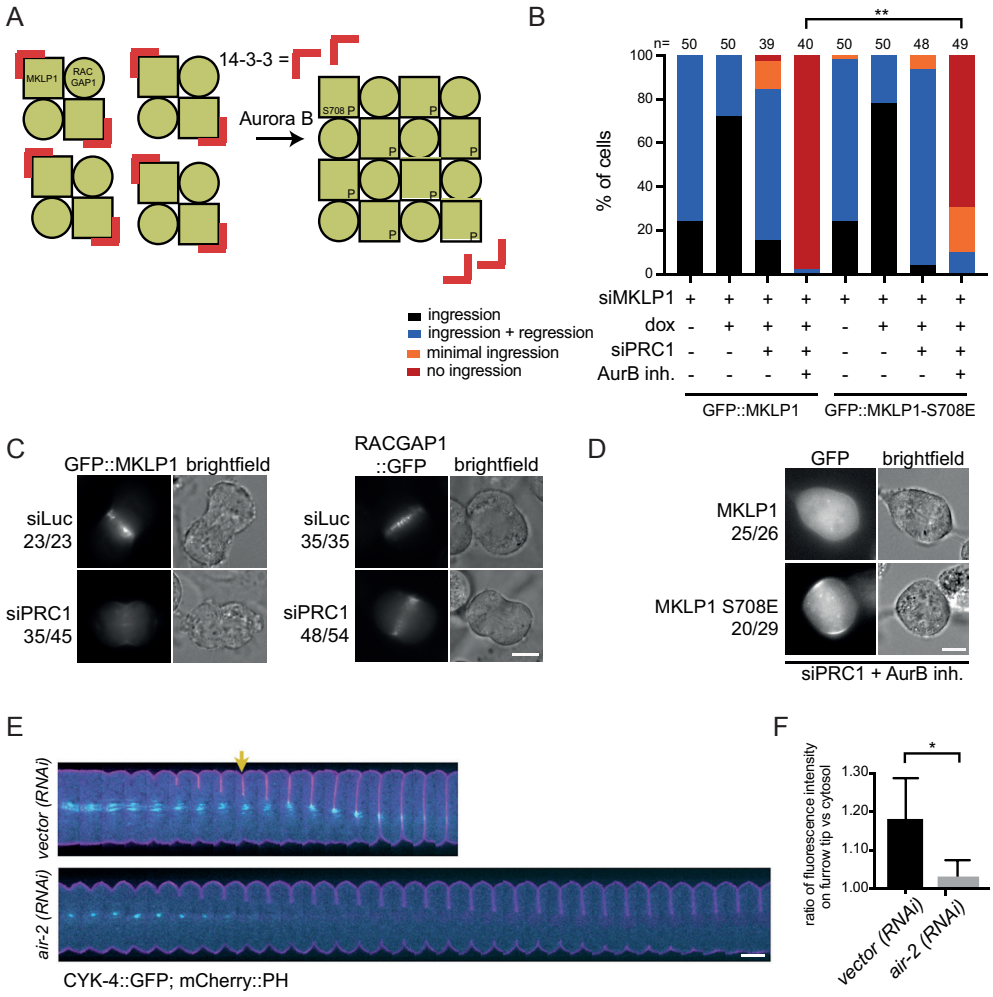

Figure 5: Aurora B-dependent centralspindlin oligomerization contributes to spindle midzone-independent furrow ingression.

(A) Scheme explaining how oligomerization of centralspindlin is induced by Aurora B dependent phosphorylation of MKLP1. (B) HeLa cell lines with stable inducible expression of GFP::MKLP1 and GFP::MKLP1-S708E were transfected with the indicated siRNAs, treated with or without ZM447439 before anaphase, and imaged live. The number of cells showing stable furrow regression, full furrow regression followed by furrow regression, visible but minimal furrow ingression or no furrow ingression was scored. The number of cells analyzed per condition is indicated. One representative experiment out of 3 is shown. ** = $p < 0.01$; Chi-squared test for comparison of the indicated conditions. (C) Representative stills of HeLa cells in anaphase with stable inducible expression of GFP::MKLP1 and RACGAP1::GFP and transfected with the indicated siRNAs. Scale bar = 10 μm. Numbers indicate the number of times the depicted localization was observed / total number of cells that was imaged live. (D) Representative stills of HeLa cells in anaphase with stable inducible expression of GFP::MKLP1 and GFP::MKLP1-S708E and transfected with siPRC1 and treated with the Aurora B inhibitor ZM447439 (2 μM) prior to anaphase onset. Scale bar = 10 μm. (E) *C. elegans* embryos expressing a mCherry::PH membrane marker (pink) with a CYK-4::GFP transgene (cyan) were depleted of endogenous Aurora B (AIR-2) by RNAi. These embryos were filmed starting at metaphase in the first division cycle. Shown are montages of the equatorial region as the cell divides (n≥5). The arrow indicates the appearance of cortical CYK-4::GFP under wild-type conditions. Scale bar indicates 10 μm. (F) Embryos expressing CYK-4::GFP were scored for the extent of recruitment of the GFP marker to the ingressing furrow tip during anaphase, relative to a cytosolic background (see methods). Error bars represent ± SD, * = $p < 0.05$, Student's t-test, n≥5.

domain of mouse Tubby protein, which binds phosphatidylinositol 4,5-biphosphate (PtdIns $(4,5)P_2$) (Szentpetery et al., 2009; Santagata et al., 2001; Fuller et al., 2008) (Fig. 3C). The Tubby-FRET sensor was detected at the cell membrane before and during anaphase (Fig. 3C). Although chromosome-bound Aurora B is active during (pro)metaphase (Fuller et al., 2008), we did not detect phosphorylation of the membrane-localized sensor in early mitosis (Fig. S3D). Phosphorylation of the membrane-localized sensor becomes detectable at anaphase onset, prior to visible membrane ingression, and was most prominent at the equatorial cortex (Fig. 3D-G). Depletion of MKLP2 or inhibition of Aurora B with ZM447439 before anaphase onset, prevented the generation of the signal from the FRET probe (Fig. 3E, F).

Thus, an active pool of Aurora B kinase resides at the equatorial cortex at anaphase onset. To test the function of this pool of Aurora B, we inhibited Aurora B in both PRC1-proficient and PRC1-deficient cells. Inhibition of Aurora B activity in the presence of PRC1 did not prevent RhoA localization and Anillin accumulation at the equatorial cortex, and did not block cleavage furrow ingression (Fig. 4A-D, Videos 1, 2). In line with previous studies, only the later stages of cytokinesis were impaired after Aurora B inhibition, as cleavage furrows eventually regressed (Fig. 4A, B, Videos 1, 2) (Guse et al., 2005; Steigemann and Gerlich, 2009). However, in the absence of PRC1, cleavage furrow ingression and RhoA localization was fully dependent on Aurora B activity (Fig. 4A-D, Videos 3, 4). In addition, knock-down of MKLP2, which prevents the accumulation of Aurora B at the equatorial cortex (Fig. S3A), also impaired furrow ingression in PRC1-depleted cells (Fig. S3B). This suggests a pivotal role for localized Aurora B in stimulating RhoA activity at the equatorial cortex when the spindle midzone is disrupted (Fig. 4A-D). Of note, knockdown of PRC1 did not enhance Aurora B activity at the equatorial cortex (Fig. S3G). This suggests that in the absence of PRC1, the spindle midzone-associated pool of Aurora B does not relocalize to the equatorial cortex to result in increased kinase activity. Thus, Aurora B activity is not critical for cytokinesis initiation in PRC1-proficient cells, but becomes essential for cleavage furrow ingression, after PRC1 depletion, when the spindle midzone is disrupted.

Aurora B-dependent centralspindlin localization and oligomerization contributes to spindle midzone-independent furrow ingression.

MKLP1 is an established substrate of Aurora B (Guse et al., 2005), and phosphorylation of S708 in MKLP1 by Aurora B disrupts the binding of 14-3-3 proteins to MKLP1 (Douglas et al., 2010). Dissociation of 14-3-3 from MKLP1 promotes centralspindlin oligomerization, which supports spindle midzone formation in human cells (Hutterer et al., 2009), and cortical contractility in *C. elegans* embryos (Basant et al., 2015) (Fig. 5A). To test whether Aurora B-mediated centralspindlin oligomerization was responsible for spindle midzone-independent cytokinesis initiation in human cells, we generated a cell line stably expressing a phosphomimetic MKLP1-S708E variant (Fig. 5B-D and Fig. S4A, B). Both GFP::MKLP1 and GFP::MKLP1 S708E localized to the midzone in anaphase and were capable of restoring RACGAP1 localization in a MKLP1 knock-down add-back experiment (Fig. S4B). In otherwise wild-type cells, MKLP1 knockdown causes furrow regression after initial ingression, similar to what has been reported by others (Yüce et al., 2005; Nishimura, 2006; Zhao and Fang, 2005; Kamijo et al., 2006; Nguyen et al., 2014) (Fig. 5B). Expression of siRNA-resistant GFP::MKLP1 or GFP::MKLP1-S708E prevented furrow regression in the vast majority of the cells (Fig. 5B), confirming the functionality of the siRNA-resistant-GFP tagged

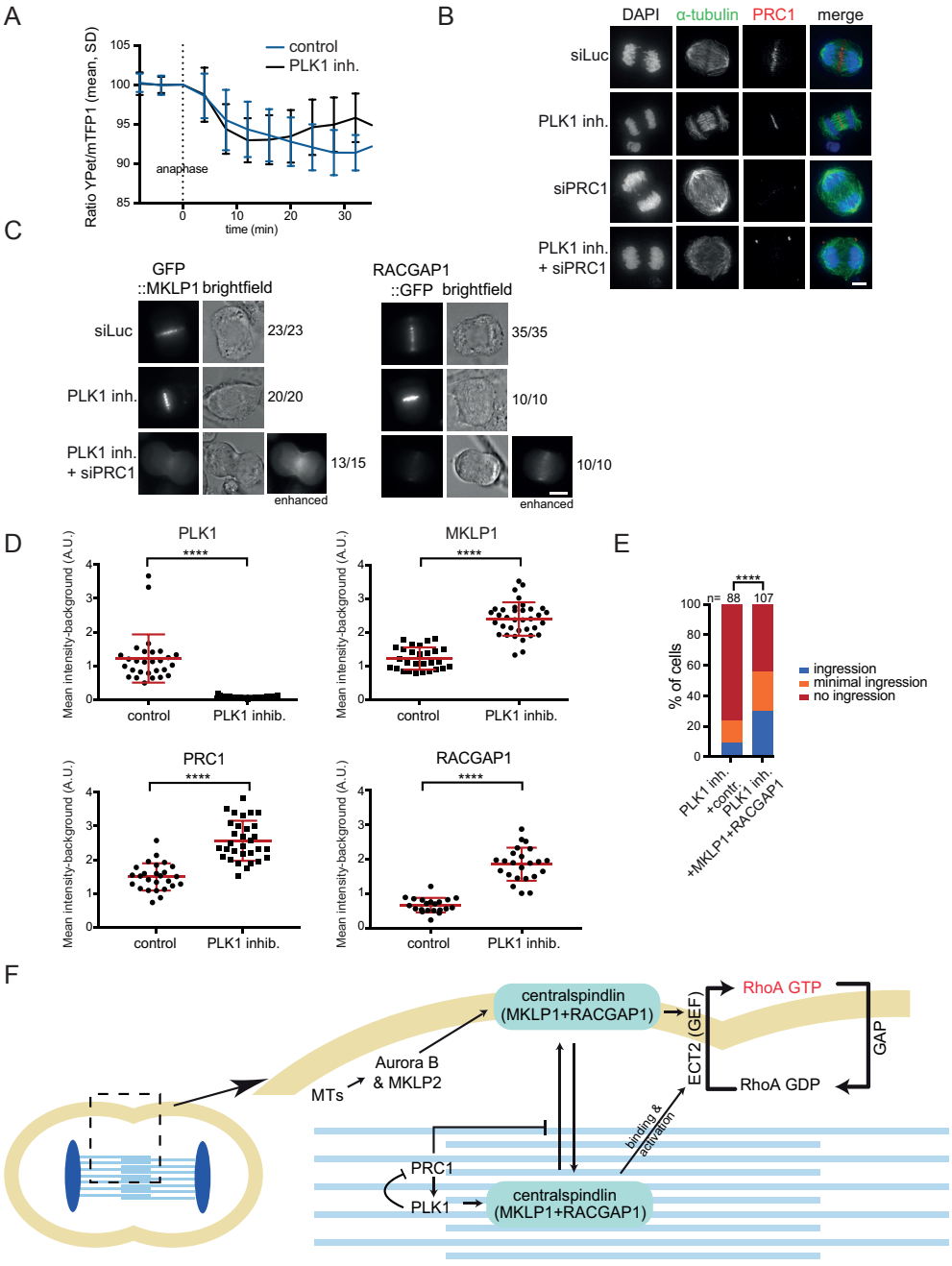

Figure 6: PLK1 suppresses PRC1 to allow dynamic exchange of centralspindlin between the spindle midzone and cell cortex.

(A) HeLa cells stably expressing the Tubby-Aurora B FRET sensor and H2B-mCherry were synchronized in G2 using RO3306 and imaged live after release from the Cdk1 inhibitor. 35 minutes after release BI2536 (100 nM) was added. The emission ratio at the equatorial cortex was calculated for each time point (interval = 5 min). Mean ± SD of 11 cells is shown. (B) IF for α-tubulin and PRC1 of HeLa cells in anaphase transfected with the indicated siRNAs and treated with

or without BI2536. Scale bar indicates 5 μm. (C) Representative stills of HeLa cells in anaphase with stable inducible expression of GFP::MKLP1 and RACGAP1::GFP and transfected with the indicated siRNAs and treated with or without BI2536 (100 nM). Scale bar = 10 μm. Numbers indicate the number of times the depicted localization was observed / total number of cells that was imaged live. See also Fig. S5A. (D) Quantification of the immunofluorescence (IF) intensity levels of PLK1, MKLP1, PRC1 and RACGAP1 at the spindle midzone in anaphase (see also Fig. S5B). Each dot represents an individual cell. One representative experiment out of 3 is shown. Error bars depict standard deviations of the mean. ** = $p < 0.01$; *** = $p < 0.001$, **** $p < 0.0001$ (Student's t-test). (E) HeLa cells were infected with control GFP virus or with lentiviruses expressing GFP::MKLP1 and RACGAP1::GFP and were treated with BI2536 (100 nM) before anaphase onset, and imaged live. The number of cells showing full furrow ingression, visible but minimal furrow ingression or no furrow ingression was scored. The number of cells analyzed per condition is indicated (n). **** = $p < 0.0001$; Chi- squared test for comparison of the indicated conditions. (F) Model explaining how PLK1 and Aurora B activate centralspindlin and RhoA at the equatorial cortex. The phosphorylation of RACGAP1 by PLK1 promotes centralspindlin binding and activation of ECT2, while Aurora B most likely promotes ECT2 activation via oligomerization of centralspindlin after phosphorylation of MKLP1. PLK1 also exerts an inhibitory effect on PRC1 which promotes the release of a fraction of centralspindlin from the spindle midzone. MTs = microtubules.

MKLP1 proteins. Importantly, MKLP1-S708E rescued the initiation of cleavage furrow ingression in a fraction of cells double depleted of PRC1 and MKLP1 and treated with the inhibitor of Aurora B (Fig. 5B). Collectively, this suggests that in PRC1 knockdown cells, Aurora B induces local clustering of centralspindlin that contributes to RhoA activation and implies that at least some centralspindlin resides at the equatorial cortex. To test the latter, we performed live cell imaging experiments with GFP::MKLP1 and RACGAP1::GFP in PRC1-depleted cells. After PRC1 knock-down, GFP::MKLP1 and RACGAP1::GFP no longer localized to microtubules in the midzone region (Fig. 5C) (Mollinari et al., 2005), but were detected at the equatorial cortex (Fig. 5C). Of note, we failed to detect MKLP1 at the equatorial cortex and only infrequently detected RACGAP1 at this site when we performed IF on fixed cells (data not shown), implying that these proteins are weakly bound to the cortex and most likely were lost during fixation. Furthermore, GFP::MKLP1 was no longer detected at the equatorial cortex in PRC1-depleted cells when Aurora B kinase activity was inhibited, while GFP::MKLP1-S708E was (Fig. 5D). Similarly, in 21 out of 32 cells analyzed, RACGAP1::GFP was also no longer detected at the equatorial cortex in PRC1-depleted cells when Aurora B kinase activity was inhibited (Fig. S4C). This implies that cortical Aurora B activity contributes to the recruitment or accumulation of centralspindlin to the equatorial cortex, most likely through phosphorylation of S708 in MKLP1.

In line with the findings in human cells, in *C. elegans* embryos, the homolog of RACGAP1 (CYK4) can be detected on the equatorial plasma membrane as the furrow ingresses (Fig. 5E, F and Video 5). Depletion of Aurora B (AIR-2) in these cells results in a measurable loss of membrane accumulation of centralspindlin (Fig. 5E, F and Video 6). Based on these collective findings, we propose that in human cells a small, or a highly dynamic pool of centralspindlin at the equatorial cortex is sufficient to drive initiation of cytokinesis.

PLK1 suppresses PRC1 to limit sequestration of centralspindlin on the spindle midzone

Our findings suggest that RhoA activation at the equatorial cortex can occur by both PLK1-dependent and -independent cues, and that PLK1-independent RhoA activation requires Aurora B. If these cytokinesis initiation-routes act strictly in parallel, inhibition of one pathway would still allow the other pathway to operate. This is indeed observed after Aurora B inhibition, but not after PLK1 inhibition. Why does furrow ingression fail when PLK1 is inhibited in PRC1-proficient cells, when, according to our model, Aurora B

should suffice to activate RhoA? One explanation could be that PLK1 inhibits cortical Aurora B activity when PRC1 is present. To test this possibility, we used the membrane-localized FRET-based Aurora B biosensor and found that Aurora B was equally active at the equatorial cortex in PLK1 inhibited cells as in cells with active PLK1 in which the furrow ingressed (Fig. 6A). We then asked whether PLK1 inhibition affects availability of Aurora B substrates at the cortex. PLK1 activity has been shown to limit the extent of PRC1-dependent microtubule bundling and centralspindlin recruitment to the mitotic spindle in metaphase (Hu et al., 2012b). This prompted us to investigate whether PLK1 also limits PRC1 activity at the spindle midzone in anaphase. Indeed, spindle midzone microtubules appeared more bundled in PLK1-inhibited anaphase cells and this was diminished after PRC1 depletion (Fig. 6B). Moreover, quantification of the levels of MKLP1, RACGAP1 and PRC1 at the spindle midzone revealed that the levels of these proteins increased when PLK1 is inhibited (Fig. 6C, D, Fig. S5A, B). Moreover, PRC1 knock-down in PLK1 inhibited cells allowed localization of centralspindlin at the equatorial cortex (Fig. 6C). Based on this, we hypothesized that PLK1 limits the extent of PRC1-mediated microtubule bunding and spindle midzone recruitment of centralspindlin in anaphase. As a corollary, we hypothesized that PRC1 promotes excessive recruitment of centralspindlin to the spindle midzone when PLK1 is inhibited, thereby sequestering it away from the equatorial cortex. PRC1 depletion in PLK1-inhibited cells, would release centralspindlin from the spindle midzone allowing it to become activated by Aurora B at the equatorial cortex (Fig. 6F). Based on this model, we reasoned that by overexpressing centralspindlin (via co-overexpression of GFP::MKLP1 and RACGAP1::GFP, Fig. S5C), we could “saturate” the PRC1-dependent sequestering of centralspindlin to the spindle midzone after PLK1 inhibition and that some of the overexpressed centralspindlin would be available to mediate RhoA activation at the equatorial cortex and induce furrow ingression. Indeed, we found that centralspindlin overexpression promoted the initiation of cleavage furrow ingression in a substantial fraction of PLK1 inhibited, PRC1-proficient cells (Fig. 6E).

Discussion

In this study we uncovered a PLK1-independent, Aurora B-dependent route to RhoA activation and cytokinesis initiation in human cells through knock-down of the microtubule bundling protein PRC1. This PLK1-independent route to cytokinesis initiation has been missed, due to an unrecognized inhibitory effect of PLK1 on PRC1 in anaphase. We demonstrate that PLK1 constrains PRC1 in anaphase which serves two purposes; it limits PRC1’s microtubule bundling activity and second it promotes the release of a (small) pool of centralspindlin from the spindle midzone. We argue that this allows centralspindlin to function both as a regulator of spindle midzone formation and as an activator of RhoA at the equatorial cortex. How PLK1 constrains PRC1 remains to be fully determined. PRC1 is a direct substrate of PLK1, and its phosphorylation by PLK1 is needed to bind PLK1 and to localize the kinase on the spindle midzone (Neef et al., 2007; Hu et al., 2012a). This makes it inherently difficult to discriminate how PLK1 affects PRC1 function in anaphase, because mutation of the PLK1 phosphosites in PRC1 impairs PLK1 recruitment to the spindle midzone (Neef et al., 2007). PRC1 may directly sequester centralspindlin on the spindle midzone after PLK1 inhibition, as RACGAP1 can interact with PRC1 (Lee et al., 2015; Ban et al., 2004), or it may do so indirectly by creating hyper-bundled microtubules in the midzone. Distinguishing these possibilities through structure-function analysis of PRC1 is also challenging because its overexpression results in precocious spindle binding during metaphase (Mollinari et al., 2005; Hu et

al., 2012b and our own unpublished observations).

An important implication from our work is that ECT2 and RhoA activation can occur in the absence of PLK1 activity. PLK1 was shown to activate the RhoA GEF, ECT2, through phosphorylation of RACGAP1 which promotes RACGAP1 binding to the auto-inhibitory N-terminus of ECT2. This relieves the intramolecular inhibition on the ECT2 GEF domain (Wolfe et al., 2009; Burkard et al., 2009; Zhang and Glotzer, 2015). The N-terminus of RACGAP1 harbors 4 evolutionary conserved PLK1 phosphorylation sites and mutating these sites to alanine (RACGAP1-4A) attenuates complex formation between centralspindlin and ECT2, fails to activate RhoA, and leads to loss of ECT2 from the spindle midzone (Wolfe et al., 2009; Burkard et al., 2009). These results point to a crucial role for PLK1 in activating ECT2 and RhoA. How can ECT2 and RhoA become activated in PRC1-depleted cells when PLK1 is inhibited? Our results are complementary to recent work that demonstrates that mutations in the N-terminal BRCT domains of ECT2 that strongly reduce its binding to RACGAP1 and its localization to the spindle midzone, do not prevent equatorial RhoA activity and cleavage furrow ingression and supported cytokinesis (Kotýnková et al., 2016). Importantly, knockdown of RACGAP1 still impaired furrow ingression in cells reconstituted with the RACGAP1 binding-deficient ECT2 mutant (Kotýnková et al., 2016) as it does in PLK1-inhibited cells depleted of PRC1 (this study). Thus, RhoA activation during cytokinesis appears to be highly dependent on ECT2 activation by centralspindlin. Notably, the ECT2/RACGAP1 interaction is enhanced by, but does not require RACGAP1 phosphorylation by PLK1 (Somers and Saint, 2003; Yüce et al., 2005). RACGAP1 contains a C-terminal GAP domain that also interacts with ECT2 which may contribute to formation and function of this complex (Zhang and Glotzer, 2015). This mode of ECT2 activation (and thereby RhoA activation) might require, or be strongly promoted by, localized centralspindlin oligomerization at the equatorial cortex driven by Aurora B-dependent disengagement of 14-3-3 proteins from centralspindlin (Douglas et al., 2010; Basant et al., 2015).

This view is supported by optogenetic experiments with a C-terminally truncated ECT2 that only activates RhoA at the equator (Kotýnková et al., 2016), presumably due to the presence of centralspindlin at this site. Moreover, active Aurora B is present at the equatorial cortex in PRC1-depleted cells and may provide a local environment for centralspindlin oligomerization. Indeed, in *C. elegans*, centralspindlin oligomerization obviates the requirement for Aurora B activity (Basant et al., 2015). In cultured human cells, Aurora B activity is required for furrow ingression in PRC1-depleted cells and expression of MKLP1-S708E, mimicking Aurora B phosphorylation, partly restores ingression defects caused by Aurora B inhibition. This supports the idea that centralspindlin oligomerization can drive RhoA activation independent of PLK1. However, MKLP1-S708E, only rescues furrow ingression in a small fraction of the PRC1-depleted and Aurora B inhibited HeLa cells. This infers that Aurora B-dependent furrow ingression in PRC1-depleted cells is not solely explained by the phosphorylation of a single residue in a single Aurora B substrate (i.e. MKLP1-S708). In fact, Aurora B phosphorylates several other substrates during anaphase, such as RACGAP1, vimentin, SHCBP1 (SHC binding and spindle associated 1), and possibly myosin light chain and the myosin binding subunit of myosin phosphatase, which all contribute to furrow ingression and cytokinesis in human cells (Goto et al., 2003; Yokoyama et al., 2005; Asano et al., 2013; Hengeveld et al., 2012).

One could argue that the main role of PLK1 in cytokinesis initiation is to limit PRC1 activity to make centralspindlin available for Aurora B-dependent activation at the equatorial cortex. However, in such a scenario, inhibition of Aurora B would always impair cytokinesis initiation and this is not the case: in PRC1-proficient cells, furrow ingression takes place when Aurora B is inhibited. This implies that PLK1-dependent RACGAP1 phosphorylation and activation of ECT2 at the spindle midzone, and Aurora B at the equatorial cortex, can in principle function as two separate pathways to centralspindlin and RhoA activation, and cytokinesis initiation. We propose that in wild-type cells, the "PLK1-brake" on PRC1 will also support the release of PLK1-phosphorylated centralspindlin bound to ECT2, from the spindle midzone, allowing it to reach and activate RhoA at the equatorial cortex. Together, the PLK1- and Aurora B-dependent pathways to centralspindlin and RhoA activation may confer robustness to and proper timing of the processs of cleavage furrow ingression in mammalian cells.

In cells expressing the ECT2 binding-deficient RACGAP-4A mutant, PLK1 is active and expected to act on PRC1 allowing the release of a fraction of centralspindlin from the spindle midzone that can then become activated at the equatorial cortex. In other words, the Aurora B-dependent route to furrow ingression should be operational. However, cleavage furrow ingression does not take place in the RACGAP1-4A expressing cells (Wolfe et al., 2009). Interestingly, the RACGAP1-4A mutant appears more concentrated at the spindle midzone (Wolfe et al., 2009), similar to what is observed for endogenous RACGAP1 after PLK1 inhibition. This raises the question whether RACGAP1 phosphorylation by PLK1 might also promote the release of centralspindlin from the spindle midzone.

In conclusion, we provide evidence for the existence of two pathways resulting in centralspindlin and RhoA activation and cytokinesis initiation in human cells. One pathway depends on PLK1 and originates at the spindle midzone, and the other pathway depends on Aurora B activity at the equatorial cortex. We argue that this latter pathway has gone unnoticed due to an unrecognized inhibitory effect of PLK1 on PRC1 in anaphase. We propose that the PLK1-dependent "brake" on PRC1 is necessary to release a fraction of centralspindlin from the spindle midzone that can activate RhoA at the equatorial cortex. The finding that these two routes to centralspindlin and RhoA activation could operate independent from each other, highlights the robustness and plasticity of centralspindlin-induced cleavage furrow formation.

Materials and Methods

Cell culture

HeLa cells and HeLa Flp-In T-Rex cells were cultured in DMEM (Sigma-Aldrich) supplemented with 6% FCS (FBS, Sigma-Aldrich), 2 mM UltraGlutamine and 100 units/ml penicillin and 100 µg/ml streptomycin (Lonza). Culture medium of HeLa Flp-In T-Rex cells and of all HeLa Flp-In T-Rex derived cell lines (described below) was additionally supplemented with 4µg/ml Blasticidin (PAA Laboratories). All cell lines were cultured at 37°C with 5% CO_2.

Plasmids

cDNA encoding the membrane-binding Tubby domain of mouse Tubby protein (aa 243-505) (Szentpetery

et al., 2009) was obtained by PCR from a mouse brain cDNA library and was subsequently cloned into a pcDNA3 vector containing a mTFP1 and YPet FRET based sensor for Aurora B activity (Fuller et al., 2008; Wurzenberger et al., 2012). The CyPet donor of the original construct was replaced by mTFP1. Full length, wild-type MKLP1 was amplified by PCR from a human thymus cDNA library and cloned into a pEGFP-C1 vector (Clontech) and subsequently cloned into a pcDNA5™/FRT/TO vector (Invitrogen) in which the hygromycin B resistance cassette was replaced by a puromycin B resistance cassette (pcDNA5/FRT/TO-puro). Point mutations were introduced by site-directed mutagenesis. Full length, wild-type RACGAP1::GFP (Wolfe et al., 2009) was cloned into a pcDNA5™/FRT/TO-hygromycin B vector (Invitrogen). For lentiviral production, GFP::MKLP1 and RACGAP1::GFP were cloned in a pHAGE vector. As a control virus pHAGE-EFs-PCP-3xGFPnls (gift of Thoru Pederson, UMass Medical School, Worcester, MA, USA, addgene # 75385) (Ma et al., 2016) was used.

siRNA and plasmid transfection, viral production and transduction

HeLa cells were transfected with siLuc (Luciferase GL2 duplex; 5'-CGUACGCGGAAUACUUCGAdTdT-3'; Dharmacon/D-001100-01-20), siPRC1 (ON-TARGETplus SMARTpool; 5'-ACAAGAACUGAGGUGGUA-3', 5'-GCACGUAAGCUGAACACUA-3', 5'-CCGGAAAGCGCUGCAAUUA-3', 5'-UAAAUCACCUUCGGGAAAU-3'; L-019491-00-0005) siMKLP2 (ON-TARGETplus SMARTpool; 5'-ACACAGGCCUUGAUGAUGA-3', 5'-GGAACAUAGUCUUCAGGUA-3', 5'-GGUUAAAGCUAAAUUACAG-3', 5'-GAAACCAUUCCUUCGAAAU-3'; L-019491-00-0005), siMKLP1 (5'-CGACAUAACUUACGACAAAUU-3') or siRACGAP1 (Thermo Fischer, HSS120934 Stealth siRNA, 5'-GCCAAGAACUGAGACAGACAGUGUG-3') with HiPerfect Transfection Reagent (#301705; Qiagen). The final concentration of siRNAs was 20 nM for siLuc, siPRC1, RACGAP1 and MKLP2. The final concentration of siRNAs for siMKLP1 was 40 nM. Cells were analyzed 48 hours after siRNA transfection. A standard HiPerfect transfection protocol was used with a 3:1 ratio for siRNA:HiPerfect in Opti-MEM. Incubation of siRNA/HiPerfect mixture was done at 37 °C for 20 minutes. Transient transfection of plasmids was performed with X-tremeGENE™ 9 DNA Transfection Reagent according the manufacturers protocol (Roche). To generate stable cell lines with doxycyclin-inducible expression of GFP::MKLP1, GFP::MKLP1-S708E and RACGAP1::GFP, HeLa Flp-In T-Rex cells were co-transfected with pOG44 (Invitrogen) and pcDNA5/FRT/TO-puromycin plasmids encoding the indicated proteins. After transfection cells were selected in medium supplemented with 2 μg/ml puromycin and 4 μg/ml blasticidin (Invitrogen). To generate HeLa Flp-In T-Rex cells stably expressing the Tubby-Aurora B FRET sensor, cells were transfected with a pcDNA3 plasmid encoding Tubby-Aurora B FRET sensor and cells were selected and maintained in medium supplemented with 2 μg/ml puromycin (Sigma-Aldich) and 4 μg/ml blasticidin (Invitrogen). Finally, lentiviral particles were produced in HEK239T cells using third-generation packaging constructs (Dull et al., 1998). Supernatant containing viral particles was harvested 48 hours after transfection and passed through a 45-μm filter. HeLa cells were transduced overnight in the presence of 4 μg/ml polybrene (Sigma-Aldrich).

Cell synchronization and inhibitor treatment

For live cell imaging and immunofluorescence of anaphase cells, HeLa cells were plated in 2.5 mM thymidine (Sigma-Aldrich) for 24 hours and released into 5 μM RO3306 (Calbiochem) for 16 hours.

Where indicated, doxycycline (1 μg/ml, Sigma-Aldrich) was added together with RO3306 to induce protein expression. Cells were released from the RO3306 block by washing three times with medium. HeLa cells were either filmed immediately after release from RO3306 or fixed 60 minutes after RO3306 release. Where indicated BI2536 (100 nM final concentration, Selleck Chemicals) or ZM447439 (2 μM final concentration, Tocris Bioscience) was added 35 minutes after the RO3306 release. Alternatively, 83 nM DMSO or nocodazole (Sigma-Aldrich) was added 45 minutes after RO3306 release.

Western blot sample preparation, SDS-PAGE and Western blotting

HeLa cells were synchronized in G1/S phase by a 24 h incubation with thymidine. After release from the thymidine block, cells were accumulated in mitosis by addition of S-Trityl-L-Cysteine (STLC, 20 μM, Tocris Bioscience) for 16 hours. Mitotic enriched cells were collected and lysed in Laemmli buffer. Protein concentration was determined using a Lowry assay and protein samples were separated by SDS-PAGE and transferred to nitrocellulose membranes. Membranes were blocked in 4% milk in Tris-buffered Saline containing 0.5% Tween-20 (TBST) and subsequently incubated with the primary antibody for 2 hrs. Primary antibodies used were rabbit anti-PRC1 (Santa Cruz sc-8356), mouse anti-alpha tubulin (Sigma T5168), goat anti-RACGAP1 (Abcam ab2270) and mouse anti-GFP (Roche 11814460001). After washing the membranes with TBST, they were incubated with horseradish peroxidase (HRP)-conjugated secondary antibodies (Bio-Rad). An Enhanced Chemiluminescent (ECL) detection kit (GE Healthcare) was used to visualize the protein/antibody complex.

Immunofluorescence microscopy

Cells were grown in 24 well plates containing 12 mm High Precision coverslips (Superior-Marienfeld GmbH & Co). Cells were fixed with 4% PFA in PBS for 7 minutes and permeabilized in either methanol (-20°C) or in 0.25% Triton X-100 in PBS for 5 minutes (RACGAP1). Cells were blocked in PBS containing 3% BSA and 0.1% Tween-20. Primary antibodies used were rabbit anti-KIF20A/MKLP2 (Bethyl (ITK) A300-878A), rabbit anti-PRC1 (Santa Cruz sc-8356), mouse anti-Aurora B (BD Transduction labs 611083), rabbit anti-Anillin (Piekny and Glotzer, 2008), mouse anti-RhoA (Santa Cruz sc-418), rabbit anti-MKLP1 (Santa Cruz sc-867), rabbit anti-PLK1 (Santa Cruz sc-17783), rat anti-α-tubulin (Thermo Fisher MA1-80017), goat anti-RACGAP1 (Abcam ab2270). Secondary antibodies used were goat anti-mouse or goat anti-rabbit IgG-Alexa 488, goat anti-mouse or goat anti-rabbit IgG-Alexa 568 and goat anti-rat Alexa 647 (Invitrogen). In case of RACGAP1 staining, donkey anti-goat IgG-Alexa 568 was used in combination with chicken anti-mouse IgG-Alexa 488. For IF of RhoA, cells were fixed with 10% Trichloroacetic acid (TCA) in H_2O for 15 minutes on ice, washed 3 times with 30 mM glycine in PBS and permeabilized for 5 minutes at room temperature in 0.25% Triton-X 100 in PBS. Antibody dilutions and washes were done in 5% non-fat milk in PBS. 4',6-Diamidino-2-Phenylindole (DAPI) was used for DNA staining and coverslips were mounted using ProLong Antifade (Molecular Probes). Images were taken with a Personal DeltaVision system (Applied Precision) equipped with a 100x / NA 1.40 UPLS Apo-UIS2 objective (Olympus) and a CoolSNAP HQ CCD camera (Photometrics). Images were deconvolved in Softworx (Applied Precision). For each experiment all images were acquired with identical illumination settings. Images are projections of deconvolved Z-stacks, unless stated otherwise. For visualization of the transversal plane a 3D projection was made from a deconvolved Z-stack and an image of the indicated

viewpoint was used. Image analysis was performed with Fiji image processing software (ImageJ). To quantify and compare the mean fluorescence intensities (MFI) in spindle midzone and equatorial cortex, a ROI of similar size for either the midzone or the equatorial cortex was used for each image to determine the MFIs in that area. Where indicated, using the same ROI, MFI in a random region of the cytoplasm was obtained as background measurement.

Live cell microscopy

Cells were seeded in μ-Slides (4 or 24 well, ibiTreat, Ibidi), except for the experiments presented in Fig. 1D; Fig. 2C, D; Fig. 4A, B; Fig. 5B and Fig. S3B, where cells were seeded in Corning Costar 24 well plates (Corning Incorporated). Medium was changed to Leibovitz's medium (Sigma) supplemented with 10% FCS (FBS, Sigma-Aldrich), 2 mM UltraGlutamine and 100 units/ml penicillin and 100 µg/ml streptomycin (Lonza) prior to live cell imaging. FRET sensor imaging was performed on an inverted NIKON Ti microscope with a Perfect Focus System (PFS). Imaging was performed at 37°C using a Microscope Cage Incubator (OkoLab), with a 63x OIL NA 1.49, working distance (WD) 0.12 objective. The excitation filter, dichroic mirror and emission filter for mTFP1 were 430/24x, Z465LP and 480/40m. The excitation filter, dichroic mirror and emission filter for YFP were 500/20x, 89006bs and 535/30m (Chroma). The emissions from both fluorophores were collected simultaneously from a single Z plane using a TuCam beamsplitter and two Luca-EM-R-604 EMCCD cameras (Andor) controlled by company acquisition software (NIS Elements). Images were acquired using an Olympus IX-81 microscope with a 20X DIC UPLFLN NA 0.5 objective and a Hamamatsu ORCA-ER CCD Camera and a 37°C heated chamber, controlled by Cell-M software. Note that in case of seeding in Corning Costar plates we acquired brightfield images, while seeding in μ-Slides allowed us to acquire Differential Interference Contrast (DIC) images. Image analysis was performed with Fiji image processing software (ImageJ). Exception: The scoring of phenotypes in Figure 1D was done using a 10X CPLFLN NA0.3 objective to visualize more cells. The live cell images for GFP::MKLP1 and RACGAP1::GFP were acquired using an AxioImager Z1 (Zeiss) with a 63X long distance (LD) C-ApoChromat Korr water NA1.15 objective with an Orca Flash V4.0 sCMOS camera (Hamamatsu) and a 37°C heated chamber, controlled by ZEN Pro 2.3 software. Single timepoint images were taken of cells in anaphase. Z-stacks were made according to cell thickness with an optimal stepwidth of 0.27 μm. Image analysis was performed with Fiji image processing software (ImageJ). To quantify and compare the mean fluorescence intensities (MFI) in spindle midzone, a ROI of similar size for either the midzone or the equatorial cortex was used for each image to determine the MFIs in that area. Where indicated, using the same ROI, MFI in a random region of the cytoplasm was obtained (background).

FRET analysis

FRET sensor data analysis was done with a customized Image J FRET macro. Background emissions were measured by selecting a Region of Interest (ROI) adjacent to the cell cortex outside the cell. The background emissions were subtracted from both mTFP and YPet emissions and the YPet/mTFP ratio was calculated. Area selection was performed using thresholding and manual selection of the equatorial cell cortex.

C. elegans experiments

C. elegans strains were maintained on nematode growth medium (NGM) plates using standard procedures. RNAi was administered by feeding nematodes with E. coli expressing the appropriate double-stranded RNA (dsRNA) (Timmons and Fire, 1998). *Spd-1* (RNAi) clone (wormbase ID:sjj_Y34D9A_151.d) and *air-2* (RNAi) clone (wormbase ID:sjj2_B0207.4) were obtained from a RNAi feeding library (Kamath et al., 2003). HT115 bacterial cultures were grown in Luria broth with 100 µg/ml ampicillin overnight at 37°C. Cultures (250 µl) were seeded on NGM plates containing 100 µg/ml ampicillin and 1 mM isopropyl β-d-1-thiogalactopyranoside and incubated at room temperature (±23°C) for 8 hours. RNAi plasmids were obtained from a library produced by (Kamath et al., 2003). L4 hermaphrodites were picked onto feeding plates at 25°C at least 24 hours prior to dissection. To prepare one-cell embryos for imaging, gravid hermaphrodites were dissected into egg salt buffer on coverslips, mounted onto 2.5% agar pads and sealed with vaseline. For confocal imaging, embryos were imaged with a 63X/1.4 numerical aperture oil-immersion lens on a Zeiss Axioimager M1 equipped with a Yokogawa CSU-X1 spinning-disk unit (Solamere, Salt Lake City, UT) and illuminated with 50-mW, 488-nm and 50-mW, 561-nm lasers (Coherent, Santa Clara, CA). Images were captured on a Cascade 1K EM-CCD camera controlled by MetaMorph (Molecular Devices, Sunnyvale, CA). Image processing was performed with ImageJ. Time-lapse acquisitions were assembled into movies using Metamorph and ImageJ. MG731 (*nop-1(it142) III; xsSi43[cyk-4::gfp rRNAi, cb-unc-119(+)] II; mCherry::H2b; mCherry::PH)* and MG656 (*unc-119(ed3) III; ltIs44pAA173; [pie-1p-mCherry::PH(PLC1delta1) + unc-119(+)];xsIs7[Myo2::GFP;CYK-4::GFP-Pie-1 3'UTR;UNC-119(wt)]*) embryos were filmed by time-lapse confocal and DIC microscopy. In the mCherry::PH or the DIC images, the tip of the furrow was defined by an ROI in ImageJ at different stages of ingression. The maximum intensity of CYK-4::GFP in the ROI was determined in the corresponding frames. Using the same ROI, a maximum intensity in a random region of the cytoplasm was obtained. The extent of recruitment to the furrow tip was calculated as (max. furrow intensity/max. cytosolic intensity -1). These values were averaged across embryos of a given genotype.

Statistical analysis

Where indicated, the mean and standard deviation (SD) are shown. Statistical significance was calculated with a Chi-squared test or a Student's t-test using Prism 7 software.

Acknowledgements

We thank Dr. D. Gerlich (Institute of Molecular Biotechnlogy, Vienna, Austria) for the plasmid containing the Aurora B FRET sensor. This work is financially supported by the Netherlands Organization for Scientific Research (NWO-Vici 91812610 to S.M.A.L), by NIH R01GM085087 (to M.G.), and is part of the Oncode Institute which is partly financed by the Dutch Cancer Society.

The authors declare no competing financial interests.

Author contributions: I.E. Adriaans and S.M.A. Lens conceived the project. I.E. Adriaans, S.M.A. Lens, A. Basant, and M. Glotzer designed the experiments, and wrote the manuscript. I.E. Adriaans, B. Ponsioen, A. Basant, and M. Glotzer performed and analyzed the experiments.

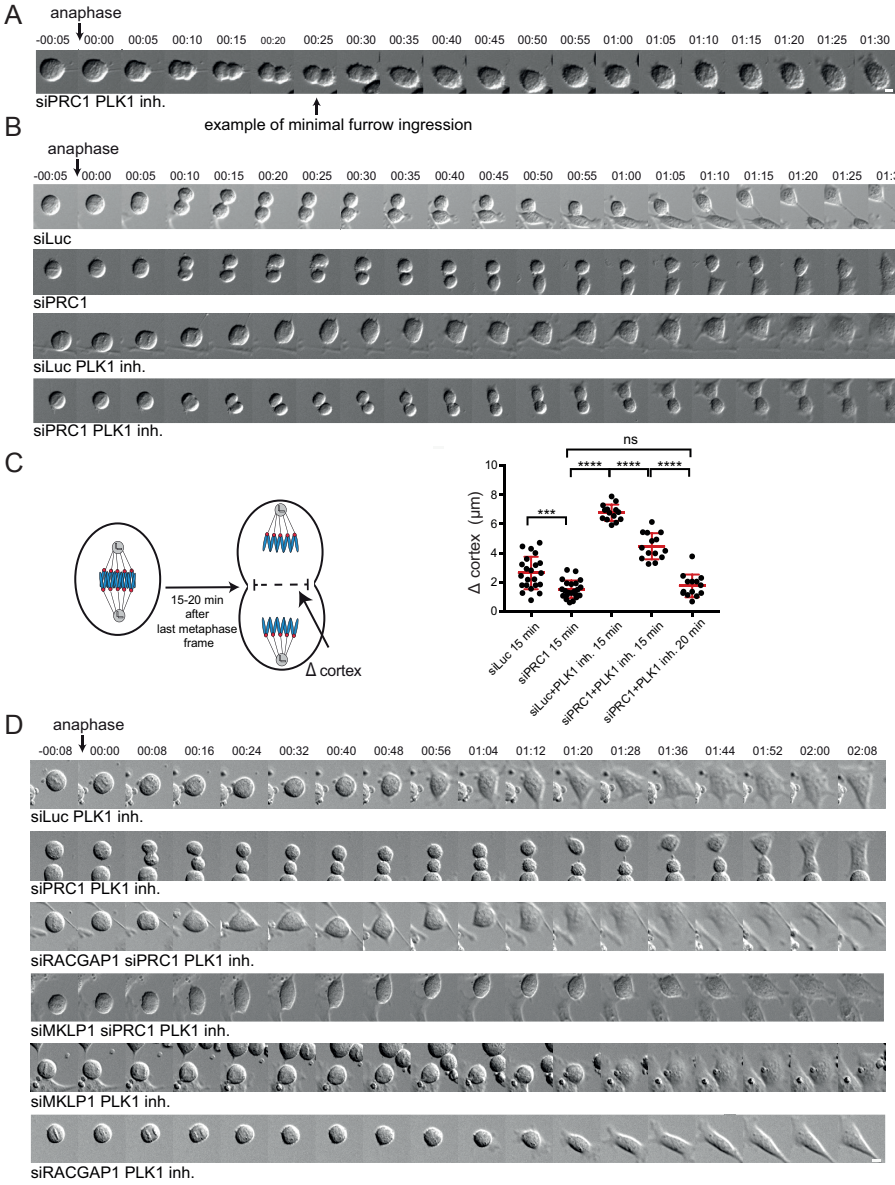

Supplemental Figure 1: PLK1 independent and centralspindlin dependent furrow ingression.
(A) Representative Differential Interference Contrast (DIC) stills of a cell showing minimal furrow ingression. (B) More DIC stills of the live cell imaging experiment shown in Fig. 1C of HeLa cells transfected with either siLuc or siPRC1 with (PLK1 inh.) or without addition of BI2536 (100 nM) prior to anaphase onset. Scale bar indicates 10 μm. Timepoint 00:00 (hours:minutes) refers to the first frame where we observed separating sisters. (C) Left: Scheme explaining how furrow ingression was measured 15-20 min. after the last frame in metaphase. Right: measurements of furrow ingression 15 min. after the last frame in metaphase. For the siPRC1 + PLK1 inh. condition also a 20 min. timepoint was measured. Each dot represents an individual cell. Error bars depict standard deviations of the mean. **** $p < 0.0001$, *** $p < 0.001$; Student's t-test for comparison of the indicated conditions, ns = not significant. (D) DIC stills of a live cell imaging experiment of HeLa cells treated with indicated siRNAs plus or minus addition of BI2536 (100 nM) prior to anaphase onset. Scale bar = 10 μm. Note that the top 4 rows are more DIC stills of the live imaging experiment shown in Fig. 2E.

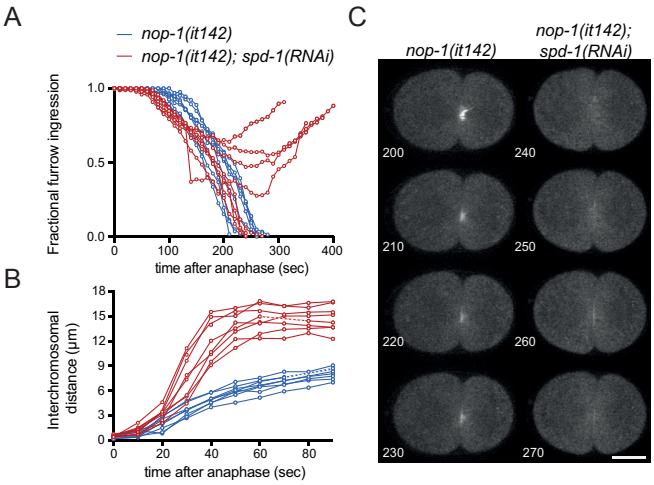

Supplemental Figure 2: Centralspindlin independent furrow ingression in C. elegans embryos.
(A,B) Quantification of the rate of furrow ingression (A) and chromosome separation (B) in *nop-1(it142)* embryos treated with *spd-1* (n=8 embryos) or *vector (RNAi)* (n=8 embryos). Dotted lines reflect missing timepoints on account of a filter wheel that was out of adjustment and failed to reposition itself for some timepoints. Embryos expressed mCherry::Histone and mCherry::PH as well as CYK-4::GFP. (C) Stills of embryos imaged 200, 210, 220 and 230 seconds for *vector (RNAi)*, or 240, 250, 260 and 270 seconds for *spd-1 (RNAi)* after anaphase onset. CYK-4::GFP is shown. Scale bar = 10 μm.

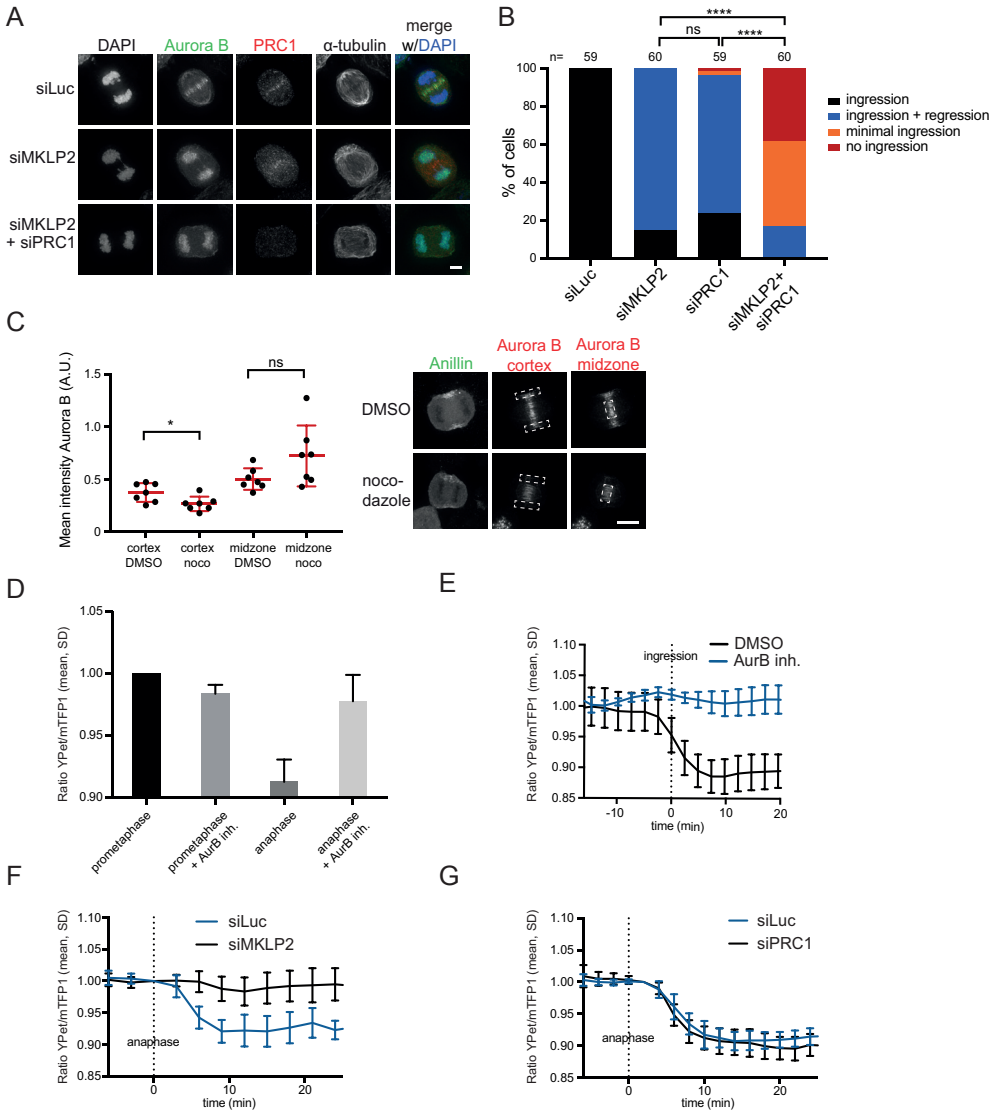

Supplemental Figure 3: Aurora B localization and activity at the equatorial cortex.
(A) IF for Aurora B, PRC1 and α-tubulin of HeLa cells in anaphase transfected with the indicated siRNAs. Scale bar = 5 μm. (B) HeLa cell lines were transfected with the indicated siRNAs and imaged live. The number of cells showing complete furrow regression, full furrow regression followed by regression, visible but minimal furrow ingression or no furrow ingression was scored. The number of cells analyzed is indicated (n). One representative experiment out of 2 is shown. **** = $p < 0.0001$; Chi-squared test for comparison of the indicated conditions, ns = not significant. (C) Left: Quantification of Aurora B fluorescent intensity at the equatorial cortex or the midzone with or without a low dose of nocodazole (83 nM). Each dot represents an individual cell. Error bars depict standard deviations of the mean. * = $p < 0.05$, ns = not significant (Student's t-test). Right: Example of ROIs to measure Aurora B fluorescence intensity at the equatorial cortex and in the midzone. Scale bar = 5 μm. Note that images are the same as shown in Fig. 3B. (D,E) HeLa cells stably expressing the Tubby-Aurora B FRET sensor and H2B-mCherry were synchronized in G2 using RO3306 and imaged live after release from the Cdk1 inhibitor. Thirty-five minutes after RO3306 release, DMSO or the Aurora B inhibitor ZM447439 was added. (D) The emission ratio at the equatorial cortex was calculated in prometaphase (~17 min before furrow ingression) and in anaphase (~3 min after furrow ingression). Data were derived from experiment presented in E. (E) The emission ratio at the equatorial cortex was calculated for each time point (interval = 3 min).

Mean ± SD of 11 (DMSO), or 10 (ZM447439) cells is shown. (F) HeLa cells stably expressing the Tubby-Aurora B FRET sensor and H2B-mCherry were treated with control (siLuc) or a MKLP2 siRNA and were synchronized in G2 using RO3306 and imaged live after release from the Cdk1 inhibitor. The emission ratio at the equatorial cortex was calculated for each time point (interval = 3 min). Mean ± SD of 15 (siLuc) and 14 (siMKLP2) cells is shown. (G) HeLa cells stably expressing the Tubby-Aurora B FRET sensor and H2B-mCherry were transfected with siLuc or siPRC1, synchronized in G2 using RO3306, and imaged live after release from the CDK1 inhibitor. The emission ratio at the equatorial cortex was calculated for each time point (interval = 3 min). Mean ± SD of 6 (siLuc) and 9 (siPRC1) cells is shown.

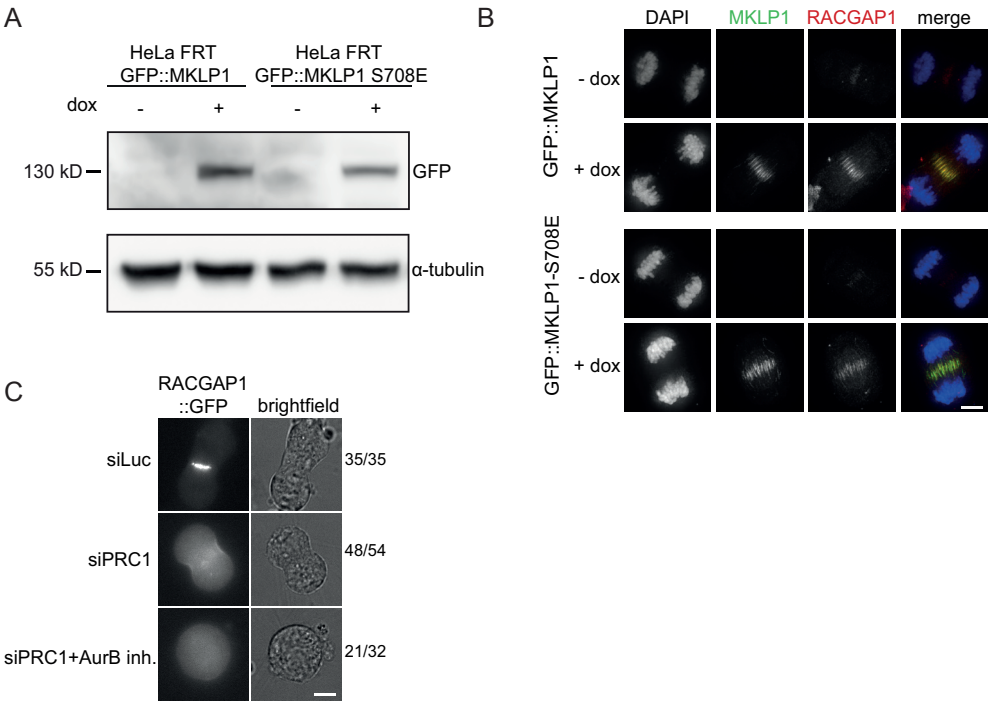

Supplemental Figure 4: Expression and localization of GFP-tagged MKLP1 and RACGAP1.
(A) Western blot of HeLa cells with doxycyclin (dox)-inducible expression of GFP::MKLP1 or GFP::MKLP1-S708E and treated with or without doxycyclin. The Western blot was probed with an anti-GFP antibody, and α-tubulin is shown as loading control. (B) HeLa cell lines with stable doxycycline (dox)-inducible expression of the indicated GFP-tagged (siRNA-insensitive) MKLP1 proteins were transfected with an siRNA for MKLP1 and processed for IF to visualize GFP-tagged MKLP1 and endogenous RACGAP1. For GFP::MKLP1 expressing cells, 49/50 cells, and for the GFP::MKLP1-S708E expressing cells 47/51 cells showed GFP midzone localization. DNA was visualized using DAPI. Scale bar = 5 μm. (C) Representative stills of HeLa cells with doxycycline (dox)-inducible expression of RACGAP1::GFP in anaphase and transfected with the indicated siRNAs and treated with (AurB inh.) or without ZM447439 (2 μM). Scale bar = 10 μm. Numbers indicate the number of times the depicted localization was observed / total number of cells that was imaged live.

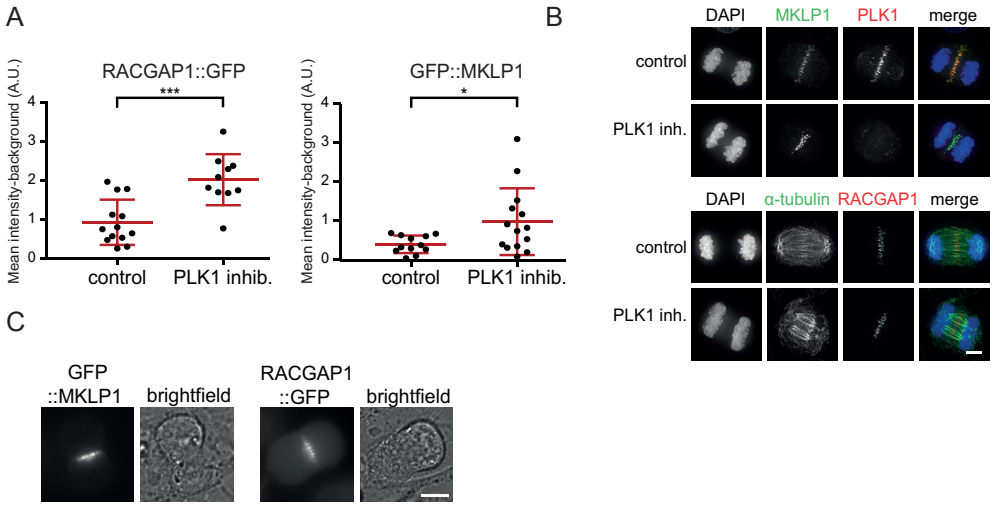

Supplemental Figure 5: Spindle midzone levels of MKLP1 and RACGAP1.
(A) Quantification of RACGAP1::GFP and GFP::MKLP1 levels on the spindle midzone in anaphases of living cells. Cells were treated with or without BI2536 (100 nM) prior to anaphase onset. One image per cell was captured and each dot represents an individual cell. For the control cells, fluorescence quantifications were performed on anaphases with visible, but not fully ingressed furrows. In case of PLK1 inhibition no furrow ingression was observed (see also Fig. 6C). (B) IF for MKLP1, PLK1, RACGAP1 and α-tubulin in cells with or without BI2536. DNA was visualized using DAPI. Scale bar = 5 μm. (C) Representative stills of live HeLa cells infected with lentiviruses expressing GFP::MKLP1 or RACGAP1::GFP. Scale bar = 10 μm.

Video material available online: http://jcb.rupress.org/content/218/4/1250

Video 1: HeLa cells transfected with siLuc were filmed (brightfield) starting at metaphase. Relevant stills are shown in Fig. 4A, row 1. Note that for the stills in Fig. 4A the best focus Z-plane is shown for each timepoint. For the video the best focus Z-plane was selected for furrow ingression. Frame interval time = 5 min.

Video 2: HeLa cells transfected with siLuc and treated with the Aurora B inhibitor ZM447439 (2 μM) were filmed (brightfield). Relevant stills are shown in Fig. 4A, row 2. Note that for the stills in Fig. 4A the best focus Z-plane is shown for each timepoint. For the video the best focus Z-plane was selected for furrow ingression. Frame interval time = 5 min.

Video 3: HeLa cells transfected with siPRC1 were filmed (brightfield) starting at prometaphase. Relevant stills are shown in Fig. 4A, row 3. Note that for the stills in Fig. 4A the best focus Z-plane is shown for each timepoint. For the video the best focus Z-plane was selected for furrow ingression. Frame interval time = 5 min.

Video 4: HeLa cells transfected with siPRC1 and treated with the Aurora B inhibitor ZM447439 (2 μM) were filmed starting at metaphase (brightfield). Relevant stills are shown in Fig. 4A, row 4. Note that for the stills in Fig. 4A the best focus Z-plane is shown for each timepoint. For the video the best focus Z-plane was selected for furrow ingression. Frame interval time = 5 min.

Video 5: *C. elegans* embryos expressing mCherry::PH membrane marker and CYK4::GFP were filmed starting at metaphase in the first division cycle. Only CYK4::GFP is shown in the movie. Montages with mCherry::PH are shown in Fig. 5E.

Video 6: *C. elegans* embryos expressing mCherry::PH membrane marker and CYK4::GFP were depleted of endogenous Aurora B (AIR-2) by RNAi and filmed starting at metaphase in the first division cycle. Only CYK4::GFP is shown in the movie. Montages with mCherry::PH are shown in Fig. 5E.

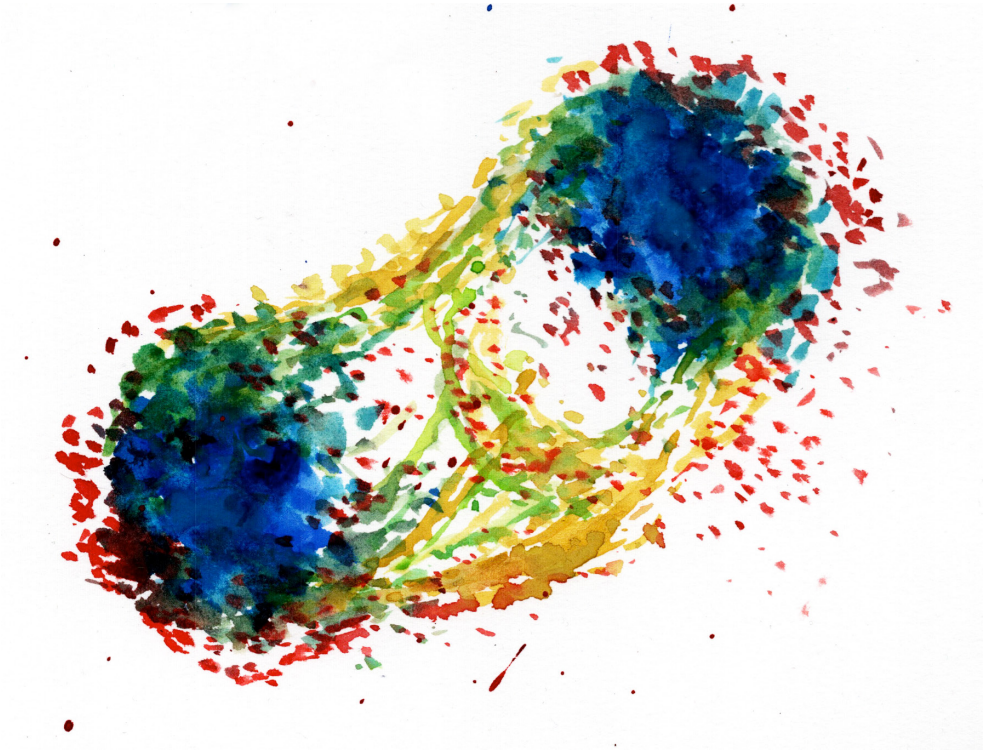

Chapter 3

MKLP2 is a motile kinesin that transports the Chromosomal Passenger Complex during anaphase

Ingrid E. Adriaans[1,2†], Peter Jan Hooikaas[3†], Amol Aher[3], Martijn J. M. Vromans[1,2], Robert M. van Es[1,2], Ilya Grigoriev[3], Anna Akhmanova[3‡*], Susanne M. A. Lens[1,2‡*]

[1]Oncode Institute and [2]Center for Molecular Medicine, University Medical Center Utrecht, Utrecht University, Utrecht, The Netherlands. [3]Cell Biology, Department of Biology, Faculty of Science, Utrecht University, Utrecht, The Netherlands.

[†]These authors contributed equally to this work. [‡]Shared senior authorship.

Submitted on 16th of September 2019

Summary

During cytokinesis, signals from the anaphase spindle direct the formation and position of a contractile ring at the cell cortex (Green et al., 2012). A pool of the chromosomal passenger complex (CPC) specifically enriched at the equatorial cortex participates in cytokinesis initiation in human cells (Adriaans et al., 2019). The mechanism underlying this anaphase-specific cortical localization of the CPC is currently unresolved. Accumulation of the CPC at the equatorial cortex requires the presence of microtubules and the mitotic kinesin-like protein 2 (MKLP2, KIF20A), a member of the kinesin-6 family (Murata-Hori and Wang, 2002; Kitagawa et al., 2013; Adriaans et al., 2019; Gruneberg et al., 2004; Cesario et al., 2006; Hümmer and Mayer, 2009), and this has led to the hypothesis that the CPC is transported along microtubules by MKLP2 (Murata-Hori and Wang, 2002; Gruneberg et al., 2004; Hümmer and Mayer, 2009; Kitagawa et al., 2013). However, the structure of the MKLP2 motor domain with its extended neck-linker region suggests that this kinesin might not be able to drive processive transport (Landino et al., 2017; Atherton et al., 2017). Furthermore, experiments in *Xenopus* egg extracts indicated that the CPC might be transported by kinesin-4, KIF4A (Nguyen et al., 2014; Wolfe et al., 2009). Finally, CPC-MKLP2 complexes might be directly recruited to the equatorial cortex via association with actin and myosin II in manner independent of kinesin activity (Kitagawa et al., 2013; Landino et al., 2017). Here, by using microscopy-based assays with purified proteins, we demonstrate that MKLP2 is a processive plus-end directed motor that can transport the CPC along microtubules *in vitro*. Live cell imaging of early anaphase revealed that a fraction of both MKLP2 and INCENP displays directional movement towards the equatorial cortex, and inhibition of the MKLP2 ATPase activity in anaphase perturbed CPC localization. Our data indicate that control of cytokinesis initiation by the CPC requires its directional MKLP2-dependent transport towards the equatorial cortex.

Results and discussion

The extended neck and coiled coil domain of MKLP2 binds to the CPC via the N-termini of INCENP and Borealin

To test the hypothesis that MKLP2 is a transporting motor for the CPC, we first performed a detailed mapping of the interaction between MKLP2 and the CPC. The CPC is a complex of four proteins; INCENP, Survivin, Borealin and Aurora B kinase, and previous work suggested that the C-terminal half of MKLP2 binds to the very N-terminus of INCENP (Hümmer and Mayer, 2009; Kitagawa et al., 2014). We generated several GFP-tagged fragments of MKLP2 and INCENP, expressed these in HEK293T cells and assessed their ability to immunoprecipitate (IP) endogenous CPC proteins or MKLP2, respectively (Figure 1A-D). Since endogenous CPC proteins and MKLP2 are poorly expressed in interphase (Hill et al., 2000; Kimura et al., 2004; Chang et al., 2006; Li et al., 1998), we enriched for mitotic cells by the addition of S-trityl-L-cysteine (STLC), an inhibitor of the mitotic kinesin-5 Eg5 (DeBonis et al., 2004). Although Cyclin B-Cdk1 dependent phosphorylation of either INCENP or MKLP2 has been described to interfere with CPC-MKLP2 binding (Hümmer and Mayer, 2009; Kitagawa et al., 2014), we consistently co-immunoprecipitated from these extracts endogenous CPC with MKLP2::GFP, as well as endogenous MKLP2 with INCENP::GFP (Figure 1B,D, S1A,B). It is possible that in mitotic cells a fraction of INCENP and MKLP2 is not phosphorylated, and this could be the fraction we pulled down.

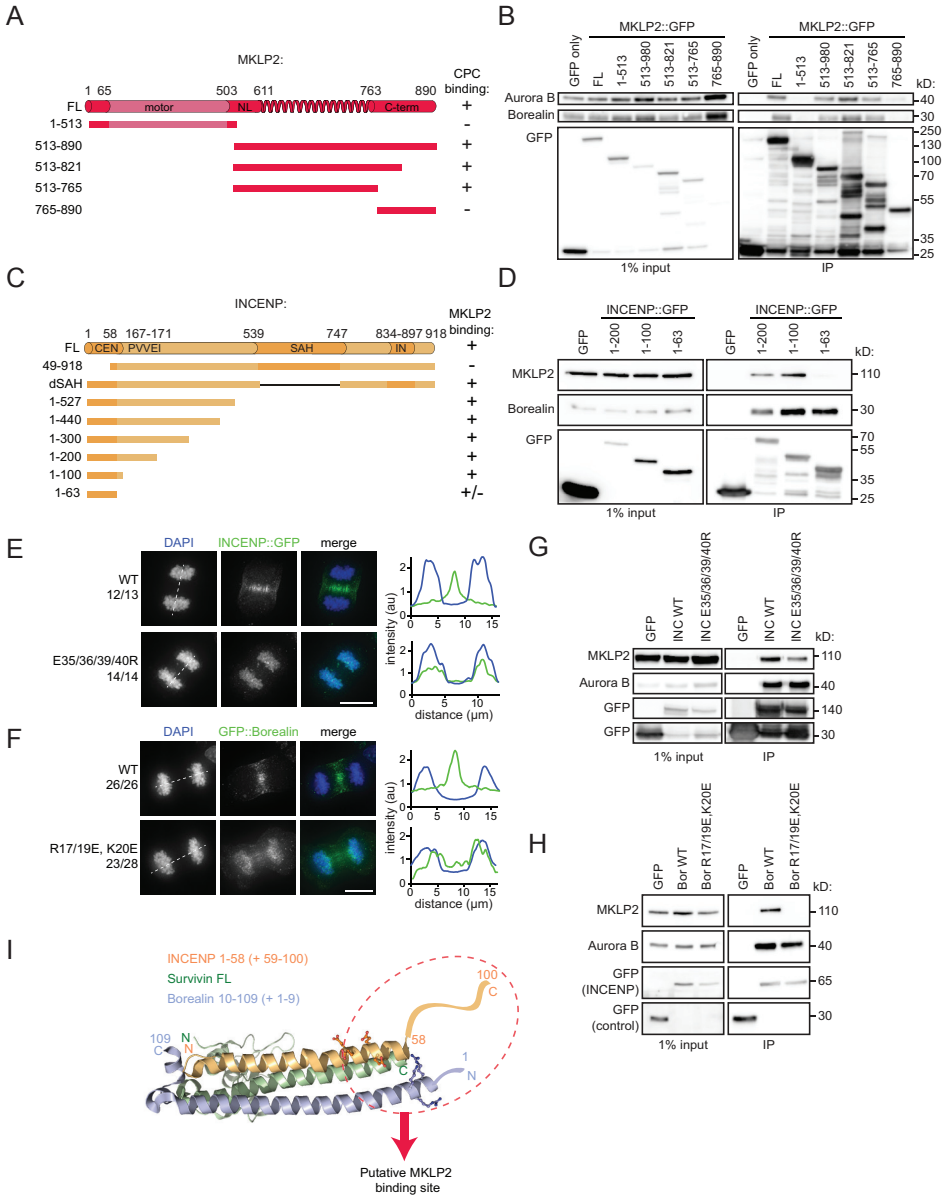

Figure 1: The extended neck and coiled coil domain of MKLP2 bind to the CPC via the N-termini of INCENP and Borealin

A) Schematic representation of full length (FL) human MKLP2 protein and MKLP2 fragments used in this study. NL = neck linker region, C-term = C-terminal domain. The ability of MKLP2 fragments to pull down detectable amounts of endogenous CPC (determined by Western blotting for Aurora B and Borealin) is indicated on the right. B) HEK293T cells were transfected with the indicated MKLP2 plasmids. Immunoprecipitations were performed with GFP-Trap beads, and samples were analyzed by Western blotting using antibodies specific for the indicated proteins. C) Schematic representation of FL human INCENP and the deletion mutations of INCENP used in this study. CEN = centromere targeting domain that interacts with Borealin and Survivin, PVVEI = HP1 binding motif, SAH = single alpha helix, IN =

IN box that interacts with Aurora B. The ability of INCENP fragments to pull down detectable amounts of endogenous MKLP2 (determined by Western blotting) is indicated on the right. D) HEK293T cells were transfected with the indicated INCENP plasmids. Immunoprecipitations were performed with GFP-Trap beads, and samples were analyzed by Western blotting using antibodies specific for the indicated proteins. E-F) IF for GFP of HeLa cells in anaphase expressing INCENP::GFP or INCENP E35/36/39/40R::GFP (E), or expressing GFP::Borealin or GFP::Borealin R17/19E, K20E (F). DNA was visualized using DAPI. Dotted line indicates the position of the line scan for GFP and DAPI shown on the right. Scale bar = 10 μm. Numbers on the left indicate the number of times the depicted localization was observed/total number of cells that were imaged. G-H) HEK293T cells were transfected with the indicated plasmids. Immunoprecipitations were performed with GFP-Trap beads, and samples were analyzed by Western blotting using antibodies specific for the indicated proteins. I) Ribbon representation of the 3-helix bundle structure of the CPC core complex, consisting of INCENP (light orange; aa 1-58), Borealin (light blue; aa 10-109) and Survivin (light green; aa 1-140) (Jeyaprakash et al., 2007) with amino acids side chains E35/36/39/40 in INCENP (dark orange) and R17/19, and K20 in Borealin (dark purple) indicated (PDB = 2QFA). The hypothetical location of the C-terminal aa 59-100 of INCENP and N-terminal aa 1-9 of Borealin is added to the crystal structure.

We found that the interaction with the CPC depends on a small MKLP2 region (aa 513-765), which is composed of the extended neck and the coiled coil domain of the kinesin (Fig 1A, B). A recombinant N-terminal fragment of INCENP (aa 1-58, referred to as CEN-box), essential for the centromere targeting of the CPC and known to bind Borealin and Survivin (Jeyaprakash et al., 2007; Klein et al., 2006; Mackay et al., 1993; Ainsztein et al., 1998) has been shown to interact with recombinant MKLP2 (Kitagawa et al., 2014). However, we found that INCENP 1-63 did not bind endogenous MKLP2 efficiently (Figure 1D). In contrast, a somewhat longer N-terminal fragment of INCENP (aa 1-100) precipitated endogenous MKLP2 equally well as full length INCENP (Figure 1C,D, S1B). Importantly, both INCENP fragments efficiently co-precipitated Borealin (Figure 1D), indicating that both INCENP fragments were properly folded. We therefore conclude that there are additional interactions between MKLP2 and INCENP outside the CEN-box. An N-terminal deletion mutant of INCENP (49-918) failed to pull down endogenous MKLP2, whilst it efficiently precipitated Aurora B (Figure S1A). The latter rules out Aurora B as an important direct interaction partner of MKLP2, in contrast to what has been suggested previously (Gruneberg et al., 2004), and it implies that aa 49-100 in INCENP are necessary but not sufficient for MKLP2 binding. To further define CPC-MKLP2 interaction sites, we mutated a conserved set of exposed glutamic acids in the N-terminus of INCENP to positively charged residues (E35/36/39/40R), or mutated several positively charged residues in the N-terminus of Borealin to negatively charged residues (R17/19/K20E). These mutations do not interfere with the interactions between the CPC members (Jeyaprakash et al., 2007), but do perturb the translocation of the CPC from centromeres in (pro)metaphase to the spindle midzone in anaphase, very similar to what is seen after knock-down of MKLP2 (Jeyaprakash et al., 2007; Gruneberg et al., 2004; Hümmer and Mayer, 2009; Kitagawa et al., 2013) (Figure 1E,F, S1C). We found that both the INCENP E35/36/39/40R and Borealin R17/19/K20E mutant were less efficient in precipitating MKLP2 than their wild-type counterparts (Figure 1G,H).

INCENP 1-58, Borealin 10-109 and Survivin form a three-helix bundle structure *in vitro* (Jeyaprakash et al., 2007). We used this structural information to map the location and orientation of the residues in INCENP and Borealin involved in MKLP2 binding, and found they are positioned towards one side of the three-helix bundle. Moreover, aa 63-100 of INCENP would be oriented towards the N-terminus of Borealin (Figure 1I). We propose that the N-terminus of Borealin together with an extended N-terminal

part of INCENP forms the binding interface for MKLP2. Whether Survivin also makes direct contacts with MKLP2 is currently unclear. Given the orientation of the residues in INCENP and Borealin, it seems more likely that Survivin contributes to MKLP2 binding mostly by participating in the formation of the three-helix bundle with INCENP and Borealin.

MKLP2 is a motile kinesin that becomes more processive in the presence of the CPC

We next set out to investigate whether MKLP2 can transport the CPC complex *in vitro* by using *in vitro* reconstitution assays in combination with Total Internal Reflection Fluorescence (TIRF) microscopy. In these assays, dynamic microtubules were grown from GMPCPP-stabilized microtubule seeds that are attached to the surface of a glass coverslip (Bieling et al., 2007). Imaging was performed using fluorescently labeled proteins and (un)labeled tubulin and the data are analyzed using kymographs, as described previously (Hooikaas et al., 2019). As a first step, we assessed whether MKLP2 alone shows processive motility along microtubules. Full length GFP-tagged human MKLP2 (MKLP2::GFP) was purified from HEK293T cells using StrepII-tag affinity purification (Figure S2A). Analysis of fluorescence intensity of single MKLP2::GFP molecules showed that they were homodimers (Figure S2B). Mass spectrometry analysis revealed MKLP2 as the main protein present in the elution, although some contaminants were present. In particular, a few KIF4A peptides were detected, but intensity-based quantification estimated the KIF4A protein abundance to be at least 9000 times less than that of the MKLP2 protein (Figure S2C). We used a similar approach to purify GFP::StrepII- or mCherry::StrepII-tagged human CPC, but the complex containing full length INCENP was highly unstable. We therefore generated a recombinant "coreCPC" consisting of full length Survivin and Borealin with INCENP(1-100)::GFP/mCherry (Figure 2A, S2D). In addition, we also generated a complex which contained full length Survivin, Borealin and INCENP(1-100)-linker-INCENP(834-918)::GFP/mCherry. Since the C-terminal part of INCENP interacts with Aurora B (Sessa et al., 2005; Honda et al., 2003), it could be loaded with either wild type (WT) or a kinase-dead (KD) variant of Aurora B (Figure 2A, S2E,F). We refer to this complex as "miniCPC". Aurora B kinase activity in miniCPC containing WT Aurora B but not the KD mutant was confirmed by an *in vitro* kinase assay (Figure S2G).

In our assays, single MKLP2::GFP molecules exhibited plus-end directed movement on dynamic microtubules with an average run length of 1.1 ± 1.2 µm and a velocity of 0.15 ± 0.05 µm/s (Figure 2B-D, S2H-I). Importantly, this velocity differs from the single molecule properties described for the mouse KIF4A motor fragment (0.92 ± 0.15 µm/s) and for the full length *X. laevis* KIF4A homolog Xklp1 (0.8 µm/s) (Yue et al., 2018; Bieling et al., 2010), making it highly unlikely that the observed motility was caused by co-purified KIF4A. In fact, MKLP2 is relatively slow compared to other processive kinesin motors like KIF5B, KIF1A, KIF21A and B, which all move at speeds higher than 0.5 µm/s (Monroy et al., 2018; Hooikaas et al., 2019; van Riel et al., 2017; van der Vaart et al., 2013). We performed the same motor assay in the presence of mCherry-tagged coreCPC and observed that MKLP2::GFP became more processive with an increased run length of 1.5 ± 1.6 µm (Figure 2B,C, S2H). Note that this value might be an underestimation because it is based on the analysis of "complete" motor tracks, where both the landing and dissociation of the motor were observed, and does not include tracks exceeding the duration

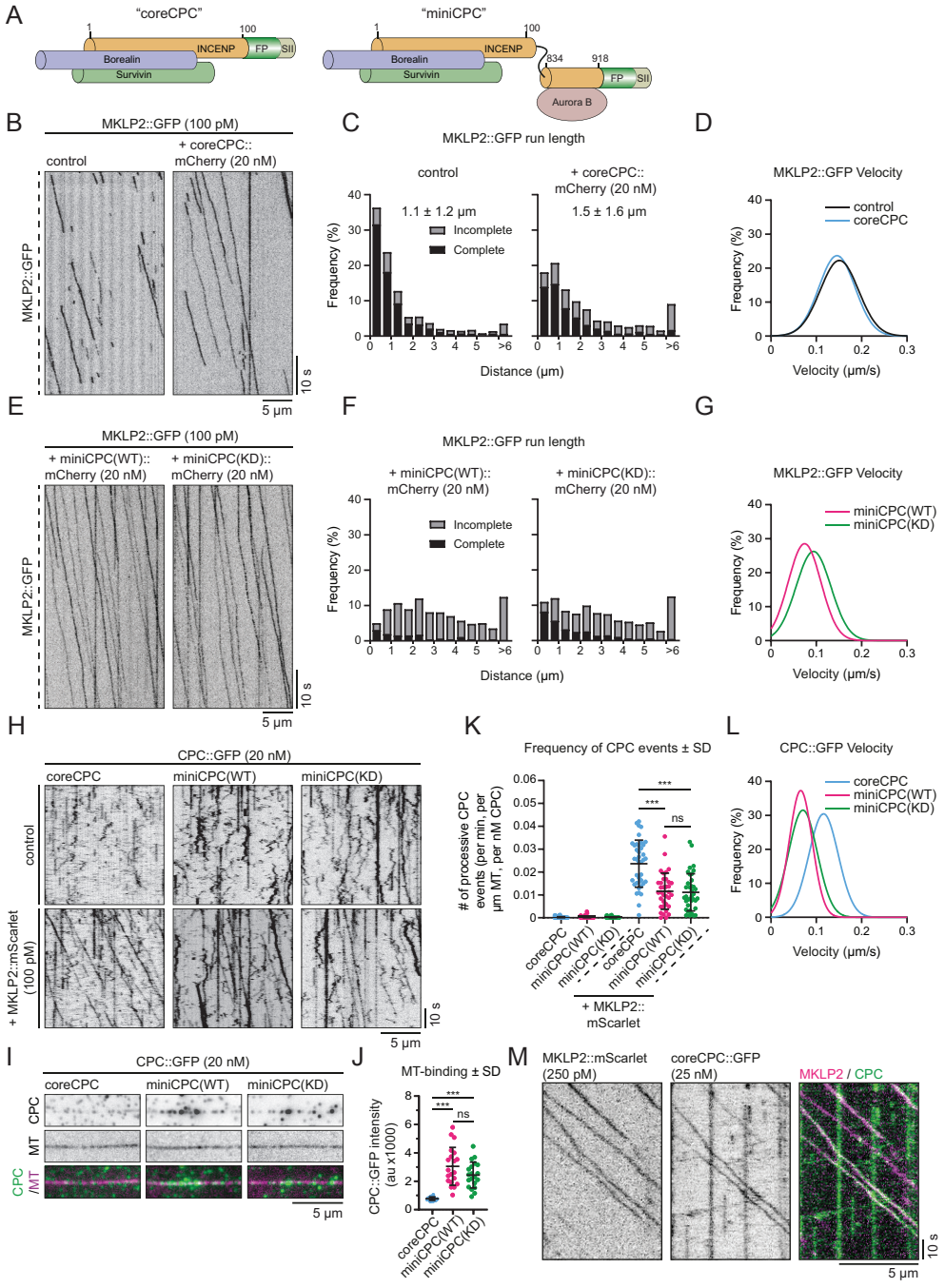

Figure 2: MKLP2 is a motile motor that transports CPC complexes in vitro

A) Schematic representation of the purified coreCPC and miniCPC complexes. FP = fluorescent protein (either GFP or mCherry), SII = StrepII-tag. B) Representative kymographs of MKLP2::GFP on dynamic microtubules (MTs) in control conditions or in the presence of coreCPC::mCherry. Image acquisition was performed at 10 frames per second (fps). C)

Histograms of MKLP2::GFP run length. Observed motor tracks were subdivided in complete tracks, where both landing and dissociation of the motor was observed, or incomplete tracks, which were tracks that exceeded the 90 s acquisition time or partially took place outside the acquisition area. Average run length of complete tracks is indicated for each condition, and the corresponding plot is shown in Figure S2H. n = 1145 and 1137 kinesin runs from three independent experiments. D) Gaussian fits of MKLP2::GFP velocities. Histograms are shown in Figure S2I. E) Representative kymographs of MKLP2::GFP on dynamic MTs in the presence of miniCPC::mCherry loaded with active Aurora B kinase (WT) or inactive Aurora B (kinase-dead, KD). Image acquisition was performed at 10 fps. (F) Histograms of MKLP2::GFP run length in the presence of miniCPC::mCherry. Observed motor tracks were subdivided in complete and incomplete tracks as in Figure 2C. n = 459 and 657 kinesin runs from two independent experiments. G) Gaussian fits of MKLP2::GFP velocities. Histograms are shown in Figure S2K. H) Kymographs of core- and miniCPC::GFP on dynamic MTs in control conditions or in the presence of MKLP2::mScarlet. Image acquisition was performed at 4 fps. I) Representative images showing core- or miniCPC on dynamic rhodamine-labeled MTs in vitro. J) Quantification of core- and CPC::GFP intensities on dynamic MTs using images acquired under identical conditions on a TIRF microscope. n = 20 MTs for all conditions. K) Quantification of processive CPC events per MT and corrected for MT length, time of acquisition and CPC concentration. n = 44, 48, 47, 40, 35 and 37 MTs from three independent experiments. L) Gaussian fits of core- and miniCPC::GFP velocities. Histograms are shown in Figure S2M. M) Kymographs of dual-color *in vitro* reconstitution experiments with MKLP2::mScarlet and coreCPC::GFP. Image acquisition was performed at 2 fps.

of 90 s or that partially took place outside the camera's field of view ("incomplete" tracks). In addition to increasing processivity of MKLP2, coreCPC negatively affected the landing frequency of MKLP2::GFP while the velocity of the motor remained unchanged (Figure 2B,D, S2I,J).

Next, we assayed the influence of Aurora B kinase on MKLP2::GFP motility using mCherry-tagged miniCPC complexes, with either WT or KD Aurora B. Whilst coreCPC caused a modest increase of MKLP2::GFP processivity by 48.3%, the presence of miniCPC made MKLP2::GFP motors hyperprocessive. For most tracks, no start and/or end point could be detected in our experimental setup, and run length could thus not be determined accurately (Figure 2E,F). Furthermore, MKLP2::GFP velocity was decreased to 0.08 ± 0.03 μm/s by miniCPC (WT) and to 0.10 ± 0.04 μm/s by miniCPC (KD), respectively (Figure 2E,G, S2K). Interestingly, the kinase activity of Aurora B had no clear effect on any of the measured motility parameters, as miniCPC (KD) showed similar effects as miniCPC (WT) (Figure 2E-G, S2K,L). Thus, MKLP2 is a motile kinesin that displays increased processivity in the presence of CPC.

MKLP2 transports the CPC along microtubules in vitro

We then investigated whether the CPC could be transported by MKLP2 along microtubules *in vitro*. In the absence of MKLP2, both core- and miniCPC showed some binding and diffusive behavior on microtubules. Since, the microtubule binding SAH (single alpha-helix) domain of INCENP is not present in our recombinant complexes (Mackay et al., 1993; Tseng et al., 2010; van der Horst et al., 2015; Ainsztein et al., 1998; Samejima et al., 2015), their ability to interact with microtubules most likely involves Borealin and the extended N-terminus of INCENP, in line with the fact that both co-pellet with microtubules *in vitro* (Wheatley et al., 2001; Trivedi et al., 2019b). Interestingly, the miniCPC bound to microtubules significantly better than coreCPC (Figure 2H-J), suggesting that the INCENP C-terminus together with Aurora B increases microtubule binding affinity of the complex. Addition of MKLP2::mScarlet to both core- and miniCPC induced processive plus-end directed movement of CPC on microtubules (Figure 2H,K). CoreCPC movement was seen more frequently than that of miniCPC, whilst Aurora B activity

again did not seem to affect motility (Figure 2H,K). In agreement with the observation that miniCPC, but not coreCPC slowed down MKLP2::GFP (Fig. 2D,G), miniCPC::GFP moved at a lower velocity (WT: 0.07 ± 0.03 µm/s, KD: 0.08 ± 0.03 µm/s) compared to coreCPC::GFP (0.11 ± 0.03 µm/s) in the presence of MKLP2::mScarlet (Figure 2L, S2M). These data suggest that the interaction of miniCPC with microtubules promotes processivity of an MKLP2-CPC complex at the expense of velocity, likely because miniCPC exerts some drag on the motor. Finally, using dual-color TIRF imaging, we confirmed that MKLP2 tracks correspond to those of moving coreCPC on a single microtubule (Figure 2M). In summary, we show that MKLP2 is a motile kinesin capable of transporting a CPC complex along microtubules *in vitro*.

MKLP2 and INCENP display directional motility towards the midzone and equatorial cortex in anaphase cells

To investigate if MKLP2 and CPC also show directional motility in cells, we generated HeLa cell lines with stable, doxycycline inducible expression of MKLP2::GFP and INCENP::GFP (Figure S3A,B). Live cell imaging of MKLP2::GFP and INCENP::GFP during anaphase revealed the presence of discrete particles

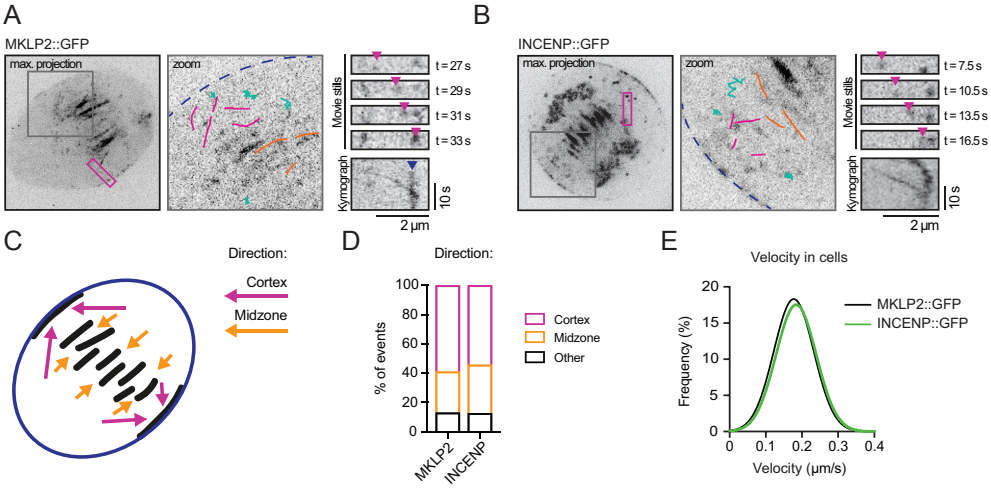

Figure 3: MKLP2 and INCENP display directional motility in cells

A-B) Representative still images (left panel) and corresponding zooms (grey, middle panel) of HeLa cells in anaphase with stable inducible expression of MKLP2::GFP (A) and INCENP::GFP (B). A number of representative particles were traced per movie and categorized as non-directional events (turquoise), which could be diffusive or static, and directional events going towards the equatorial cortex (magenta) or the spindle midzone (orange). The cell cortex is indicated with a blue dotted line in the zoom. Still images of different timepoints and a corresponding kymograph show an example of a directional event going towards the equatorial cortex (right panels). The position of the moving GFP-tagged molecule and corresponding area where the event took place are indicated with the magenta arrows in the stills or the magenta box in the left panels, respectively. Blue arrow in the kymograph (panel A) indicates the cell cortex. Note that we frequently detected ectopically expressed INCENP::GFP on chromatin in anaphases of otherwise untreated cells. This has been described before by others (Landino et al., 2017). C) Cartoon showing an anaphase cell with the midzone and equatorial cortex (black) and arrowheads displaying the two main orientations of directional MKLP2::GFP and INCENP::GFP motility events: towards the equatorial cortex (magenta) and midzone (orange). D) Quantification of MKLP2::GFP and INCENP::GFP particle directionality in HeLa cells. n = 107 events from 32 cells (MKLP2) and n = 94 events from 19 cells (INCENP). E) Gaussian fits of MKLP2::GFP (black) and INCENP::GFP (green) velocities. Histograms are shown in Figure S3C and D. n numbers correspond to those of panel D.

for both MKLP2::GFP and INCENP::GFP (Figure 3A,B). In line with previous work (Landino et al., 2017), we found that the majority of particles showed diffusive behavior or remained static (turquoise tracks in Figure 3A,B). However, motile events displaying clear directionality were also observed. Quantification of unidirectional events with a duration > 2.5 s and a velocity > 0.05 µm/s revealed that both in MKLP2::GFP and INCENP::GFP expressing cells, the majority (59% and 54%, respectively) of these directional events were oriented towards the equatorial cortex (magenta tracks). Tracks directed towards the midzone (orange tracks) constituted 28% (MKLP2) and 33% (INCENP) of all directional tracks, while the remaining tracks showed no preferred direction (Figure 3A-D). Strikingly, the directional MKLP2 and INCENP events had similar velocities of 0.19 ± 0.05 µm/s and 0.19 ± 0.06 µm/s, respectively (Figure 3A,B,E, S3C,D). The MKLP2 and INCENP velocities in cells were slightly higher compared to those measured *in vitro* (Figure 2D,G,L, S2I,K,M). This could be explained by the fact that our *in vitro* assays were performed at 30°C, whereas cell culture experiments were carried out at 37°C. Furthermore, the influence of additional cellular factors on velocity cannot be ruled out. In short, we show that MKLP2 and INCENP show not only diffusive, but also directional motility in cells during anaphase.

MKLP2 motor activity specifies CPC localization in anaphase

Our findings imply that MKLP2 is a processive motor that can transport CPC complexes *in vitro* and in cells. To test if MKLP2-mediated transport of the CPC is involved in the typical localization of the CPC in anaphase, we made use of the MKLP2 inhibitor, paprotrain (Tcherniuk et al., 2010). This compound was shown to be a specific inhibitor of MKLP2 ATPase activity that is uncompetitive with ATP. Other mitotic kinesins, such as the two MKLP2-related kinesin-6 motors MKLP1 (KIF23) and MPP1 (KIF20B) and KIF4A are not affected by paprotrain (Tcherniuk et al., 2010). In the *in vitro* assays, paprotrain severely perturbed MKLP2 movement. At 50 µM, the average run length of MKLP2::GFP was reduced from 1.1 ± 1.2 µm (DMSO) to 0.2 ± 0.3 µm (Figure 4B), the landing frequencies were diminished (Figure 4C) and motor velocity was strongly decreased, with 47% of events being static (Figure 4D,E, S4A).

We next added 50 µM paprotrain to cells, 50 min after the release from a Cdk1 inhibitor block for the duration of 10 min. Inhibition of MKLP2 ATPase activity at this time point did not prevent the translocation of either MKLP2 and CPC (here detected by immunofluorescent staining for Aurora B) from the chromosomes to the spindle midzone (Figure 4F, upper panel). However, inhibition of MKLP2 motor activity resulted in a loss of MKLP2 and CPC from the equatorial cortex, the latter visualized by IF for Anillin (Figure 4F, middle panel, G) and in a reduced and more dispersed localization of MKLP2 and CPC on the spindle midzone (Figure 4F,G). Importantly, localization of the microtubule crosslinker PRC1, which concentrates on the antiparallel microtubule overlaps in the anaphase spindle midzone and bundles midzone microtubules (Mollinari et al., 2002; Zhu et al., 2006; Pamula et al., 2019; Bieling et al., 2010), was not affected (Figure 4F, lower panel). The unperturbed PRC1 localization suggests that the size of the antiparallel microtubule overlaps was not affected by the 10 min treatment with paprotrain, making it more likely that the observed change in CPC and MKLP2 localization was caused by impaired motor-based transport.

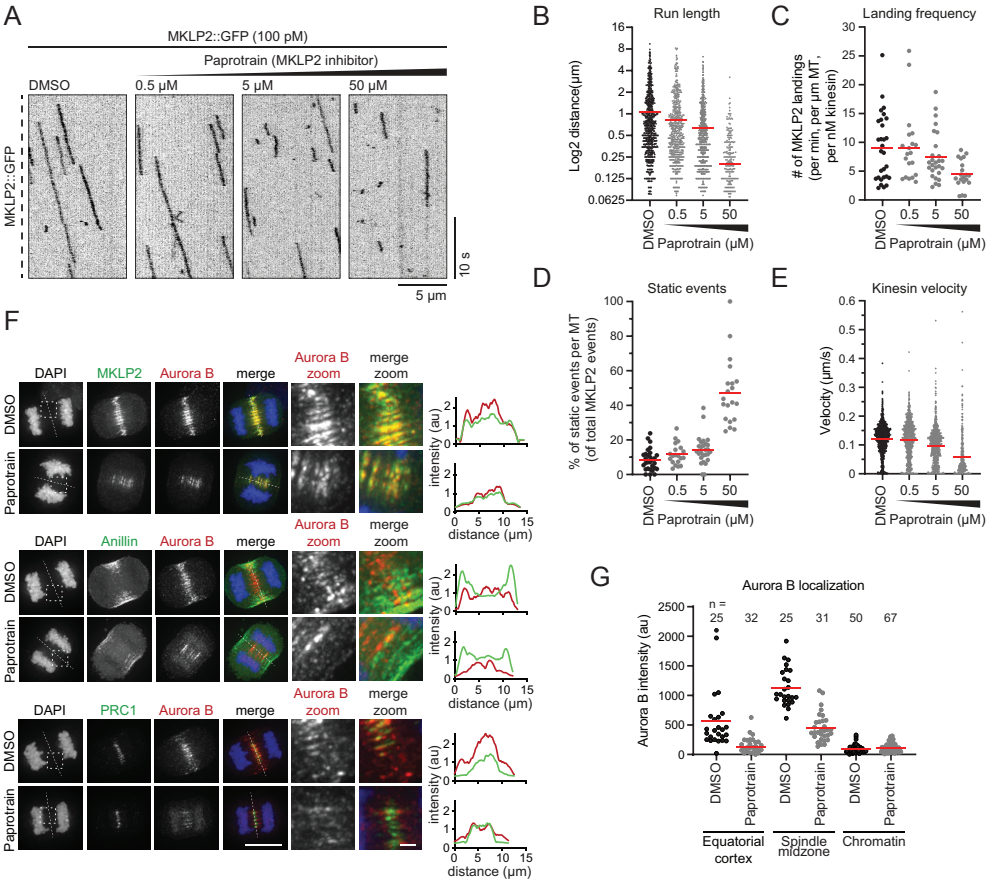

Figure 4: Inhibition of MKLP2 activity perturbs CPC localization in anaphase

A) Representative kymographs of MKLP2::GFP on dynamic MTs in DMSO (control) conditions or in the presence of increasing concentrations MKLP2 inhibitor paprotrain. Image acquisition was performed at 10 fps. B) Quantification of MKLP2::GFP run length. n = 847, 626, 778 and 337 kinesins from two or three independent experiments. Mean values are indicated with red bars. C) Quantification of MKLP2::GFP landing frequencies per MT corrected for MT length, time of acquisition and kinesin concentration. n = 29, 20, 27, 20 MTs from two or three independent experiments. Mean values are indicated with red bars. D) Quantification of static MKLP2::GFP events per MT as a percentage of the total number of MKLP2::GFP events observed per MT. Events were categorized as static when the velocity was < 0.025 µm/s. n = 29, 20, 27, 20 MTs from two or three independent experiments. Mean values are indicated with red bars. E) Quantification of MKLP2::GFP velocities. n = 1262, 899, 1014 and 423 kinesins from two or three independent experiments. Mean values are indicated with red bars. F) IF images of HeLa cells in anaphase stained for Aurora B, MKLP2, Anillin and PRC1 with or without the addition of 50 µM paprotrain (10 min treatment, fixation 60 min after Cdk1 inhibitor release). DNA was visualized using DAPI. Scale bar = 10 µm. Dotted box in DAPI indicates zoom area, scale bar in zoom = 1 µm. Dotted line indicates the position of the line scans for respectively MKLP2, Anillin, and PRC1 (green) with Aurora B (red) shown on the right. G) Quantification of Aurora B intensity levels on the equatorial cortex (marked by Anillin), the spindle midzone (marked by PRC1), and on chromatin (DAPI) in anaphase cells treated with either DMSO or 50 µM paprotrain. The number of cells analyzed per condition is indicated at the top of the graph. Mean values are indicated with red bars.

Conclusions

Our combined *in vitro* and *in cellulo* experiments indicate that MKLP2 functions as a processive motor that focuses the CPC at the antiparallel microtubule overlaps of the anaphase spindle midzone and transports the CPC along microtubules towards the equatorial cortex. We propose that upon arrival at the cortex, both MKLP2 and CPC might dock there through interactions with actin and myosin II (Landino et al., 2017; Kitagawa et al., 2013). In spite of the fact that the motor domain of MKLP2 has an atypical structure and mechanochemistry (Atherton et al., 2017), full length MKLP2 can move processively along microtubules, albeit with a velocity that is lower than that characteristic of many other transporting kinesins. Furthermore, our *in vitro* reconstitution experiments suggest that the interaction with the CPC promotes processivity of MKLP2 at the expense of its velocity. This property is likely caused by direct interactions of different CPC components with microtubules (Mackay et al., 1993; Tseng et al., 2010; van der Horst et al., 2015; Trivedi et al., 2019b; Wheatley et al., 2001; Ainsztein et al., 1998), although some effects on the conformation of the MKLP2 molecule may also be involved. Since miniCPC, used in our experiments, lacks the microtubule binding SAH domain of INCENP, we cannot exclude that in the presence of full length INCENP motor velocity is further reduced. However, we deem it unlikely that MKLP2 is stalled by binding to full length CPC, as both MKLP2 and INCENP exhibit directional motility with similar velocities in cells. Why only a subset of MKLP2-CPC complexes moves directionally in cells is currently unclear. Post-translational modification of MKLP2, the CPC or microtubules, or the presence of specific microtubule associated proteins may control the motility of MKLP2-CPC complexes or their preference for specific microtubule tracks. Overall, our data provide a mechanism for anaphase-specific CPC accumulation at the equatorial cortex that regulates initiation of cytokinesis.

Acknowledgments

We thank Drs M. Glotzer and S. Wheatley for their generous gift of reagents, Dr. M. Hadders for his help with Figure 1I, and Dr. H.R. Vos for proteomics support. This work is financially supported by The Netherlands Organization for Scientific Research (NWO-Vici 91812610 to S.M.A.L and NWO ALW Open Program grant 824.15.017 to A.A.). Proteomics was supported by the Proteins at Work Initiative (NWO 184.032.201). The group of S.M.A.L is part of Oncode Institute which is partly financed by the Dutch Cancer Society.

Author contributions

I.E. Adriaans and S.M.A. Lens conceived the project.. I.E.A, P.J.H, A.A. and S.M.A.L, designed the experiments. I.E.A., P.J.H., A. Aher, M.J.M.V, R.M. van E, and I.G. performed the experiments. I.E.A and P.J.H analyzed the experiments. I.E.A, P.J.H, A.A. and S.M.A.L wrote, reviewed and edited the manuscript. S.M.A.L. and A.A. supervised the project.

Material and methods

Cell lines and cell culture

HeLa Flp-In T-Rex and human embryonic kidney 239T (HEK293T) cells were cultured in Dulbecco's modified Eagle's Medium (DMEM, Sigma-Aldrich) supplemented with 6% Fetal Calf Serum (FCS, Sigma-

Aldrich), 2 mM UltraGlutamine (Lonza), 100 units/ml penicillin and 100 μg/ml Streptomycin (Sigma). HeLa Flp-In T-Rex cells were additionally supplemented with 4 μg/ml Blasticidin (PAA Laboratories). Cell lines were cultured at 37°C with 5% CO_2. Polyclonal Hela Flp-In T-Rex cells with stable integration of GFP-tagged INCENP, GFP-tagged Borealin and GFP-tagged MKLP2 were cultured in the presence of 800 μg/ml Hygromycin B (Sigma-Aldrich) and 6% Tet-approved HyClone Fetal Bovine Serum (GE Healthcare). Protein expression was induced with 1 μg/ml of doxycycline (Sigma-Aldrich) for minimal 12 hours.

Plasmids

Full length MKLP2 (aa 1-890) was obtained by PCR from a human thymus cDNA library and was subsequently cloned into a pEGFP-N1 vector to generate MKLP2::GFP. This plasmid was used to generate the deletion mutants aa 1-513, aa 513-890, aa 513-821, aa 513-765 and aa 765-890 by PCR and restriction cloning into pEGFP-N1. Full length MKLP2::GFP was cloned into a pcDNA5/FRT/TO-hygromycin B vector (Invitrogen) for stable cell line production. Full length MKLP2 cDNA was also cloned into a pTT5 vector (Novopro labs) containing a C-terminal GFP::StrepII- or mScarlet::StrepII-tag used for protein purification.

Full length VSV-tagged INCENP, INCENP 49-918 (delta CEN-box) and INCENP d539-747 (deletion of single alpha helix, SAH) constructs were made as previously described (van der Horst et al., 2015; Vader et al., 2007, 2006). Full length INCENP cDNA was used to generate the following INCENP fragments: aa 1-63, 1-100, 1-200, 1-300, 1-440 and 1-527, by PCR and restriction enzyme-based cloning into pEGFP-N1. Site directed mutagenesis was used to generate the INCENP mutant R35/36/39/40E. INCENP WT and INCENP R35/36/39/40E were subsequently cloned into a pcDNA5/FRT/TO-hygromycin B vector (Invitrogen) for stable cell line generation. INCENP (aa 1-100) and INCENP (aa 1-100) linker (GGGGS) INCENP (aa 834-918) were also cloned into a pTT5 vector (Novoprolabs) with a C-terminal GFP::StrepII- or mCherry::StrepII-tag for protein purification. A plasmid encoding full length Borealin (pCR3; Invitrogen), and previously described (Vader et al., 2006), was used as a template for site directed mutagenesis to generate the GFP::Borealin mutant R17/19E, K20E. The N-terminally GFP-tagged Borealin WT and Borealin R17/19E, K20E were subsequently cloned into a pcDNA5/FRT/TO-hygromycin B vector (Invitrogen) for stable cell line production. Full length Borealin, Survivin and Aurora B were amplified by PCR from previously described plasmids (Vader et al., 2007; Hengeveld et al., 2012; Vader et al., 2006) and cloned into a pTT5 vector lacking GFP and StrepII coding DNA (Novoprolabs) and these were used for protein purification together with INCENP. The Aurora B (K106R), kinase dead, mutant was generated by site directed mutagenesis of pTT5-Aurora B. All newly generated plasmids were checked by DNA sequencing. Due to a point mutation in the stop codon of Aurora B K106R the protein has a short extension of 15 amino acids which is visible by Western blot in Figure S2F.

siRNA and plasmid transfection

HeLa Flp-In T-Rex cells were transfected with siRNAs for either INCENP (Dharmacon/3'UTR; GGCUUGGCCAGGUGUAUAUdTdT) or Borealin (Dharmacon/3'-UTR; AGGUAGAGCUGUCUUCAdTdT) using HiPerfect Transfection Reagent (#301705; Qiagen) and a standard HiPerfect transfection protocol with a 3:1 ratio for siRNA:HiPerfect (37ºC for 20 min) in Opti-MEM culture medium. The final concentration

of siRNAs was 20 nM. Cells were analyzed 48 hrs after siRNA transfection. Transient transfection of plasmids was performed with X-tremeGENE™ 9 DNA Transfection Reagent (Roche) according the manufacturer's protocol. To generate stable cell lines with doxycyclin-inducible expression of wild type (WT) or E35/36/39/40R INCENP::GFP; WT or R17/19E,K20E GFP::Borealin; or MKLP2::GFP, HeLa Flp-In T-Rex cells were co-transfected with pOG44 (Invitrogen) and pcDNA5/FRT/TO-hygromycin B plasmids encoding the indicated proteins. After transfection, cells were selected in medium supplemented with 800 µg/ml hygromycin B and 4 µg/ml blasticidin (Invitrogen). Polyclonal cell lines expressing the indicated GFP-tagged proteins were used for analysis. HEK293T cells were transfected with pTT5 plasmids using Polyethylenimine (PEI, Polysciences) with a 3:1 ratio for plasmid:PEI. Alternatively, HEK293T were transfected with pEGFP-N1 plasmids using a standard Calcium Phosphate transfection protocol.

Immunoprecipitation (IP)

HeLa Flp-In T-Rex cells were plated in 2.5 mM thymidine (Sigma-Aldrich) for 24 hrs and released into 20 µM of the Eg5 inhibitor S-Trityl-L-Cysteine (STLC, Tocris Bioscience) for 16 hrs, to enrich for mitotic cells. Where indicated, doxycycline (1 µg/ml, Sigma-Aldrich) was added together with STLC to induce protein expression. HeLa Flp-In T-Rex cells or HEK293T cells transfected with plasmids encoding GFP-tagged MKLP2, INCENP and Borealin constructs were collected and washed twice in ice-cold PBS. Cell pellets were lysed in lysis buffer (50 mM Tris-HCl, 150 mM NaCl, 0.5% NP-40, 0.1% sodium deoxycholate, 40 mM glycerol phosphate, 10mM NaF, 0.3 mM $NaVO_3$, 100 µM ATP, 100 µM $MgCl_2$, 100 nM okaidic acid and supplemented with protease inhibitors (Roche)) with 4 U/ml MNase (New England Biolabs) and 30 µg/ml RNase (Sigma). After clearing debris by centrifugation, a standard Bradford assay was performed to measure protein concentration, and cell lysates were incubated with 15 µl of GFP-Trap beads (Chromotek) for 2 hrs at 4°C while rotating. Beads were washed 3 times with washing buffer (50 mM Tris-HCl, 400 mM NaCl, 0.5% NP-40, 0.1% sodium deoxycholate, 40 mM glycerol phosphate, 10 mM NaF, 0.3 mM $NaVO_3$, 100 µM ATP, 100 µM $MgCl_2$, 100 nM okaidic acid and supplemented with protease inhibitors (Roche)). Proteins were eluted by adding 20 µl of standard SDS sample buffer and by boiling the samples for 5 min. Samples were stored at -20°C until SDS-PAGE and Western blotting.

Protein purification and Aurora B kinase assay

HEK293T cells transfected with single (MKLP2::GFP::StrepII or MKLP2::mScarlett::StrepII) or multiple (coreCPC or miniCPC::GFP::StrepII or mCherry::StrepII, see Figure 2A) pTT5 plasmids were collected and washed twice in ice-cold PBS. Cells were lysed in ice-cold lysis buffer (50 mM HEPES, 300 mM NaCl, 0.5% Triton X-100, pH 7.4) supplemented with protease inhibitors (Roche). After clearing debris by centrifugation at 4°C, cell lysates were incubated with StrepTactin beads (StrepTactin Sepharose High Performance, GE Healthcare) for one hour at 4°C. Beads were washed 3 times with ice cold washing buffer (50 mM HEPES, 150 mM NaCl, 0.01% Triton X-100). For MKLP2 proteins, beads were washed an additional time with a high salt wash buffer (1M NaCl). The proteins were subsequently eluted in elution buffer (50 mM HEPES, 150 mM NaCl, 0.01% Triton X-100 and 2.5 mM desthiobiotin) for 10 min. Protein concentration was determined by SDS-PAGE and Coomassie Blue staining using InstantBlue (Expedeon), using purified BSA titration as a reference. Purified proteins were snap-frozen and stored

at −80°C. A kinase assay was performed by adding 5 µg of purified miniCPC with either Aurora B WT or KD, into a reaction mixture containing kinase buffer (10 mM $MgCl_2$, 25 mM HEPES pH 7.5, 25 mM β-glycerophosphate, 0.5 mM DTT, 0.5 mM vanadate, 100 µM ATP), and 0.2 mg/ml Histone H3 as substrate (Roche Diagnostics). Either DMSO or 2 µM Aurora B inhibitor (ZM447439, Tocris) was added to the reaction as well. After 30 min incubation at 30°C, the reaction was stopped by the addition of sample buffer. Samples were analyzed by Western blot using a primary antibody specific for phosphorylated Serine 10 in Histone H3 (H3S10ph).

Western blotting

Mitotic HeLa or transfected HEK293T cells were collected and lysed in standard Laemmli buffer. Protein concentration was determined using a Lowry assay. Protein samples of either whole cell extracts or IP's were separated by SDS-PAGE and transferred to nitrocellulose membranes. Membranes were blocked in 4% milk in Tris-buffered saline containing 0.5% Tween-20 (TBST) and subsequently incubated with a primary antibody for 2 hrs. Primary antibodies used were rabbit anti-MKLP2 (Bethyl (ITK) A300-879A), rabbit anti-Aurora B (Abcam 2254-100), rabbit anti-Borealin (gift from Dr. S. Wheatley), rabbit anti-Survivin (R&D Systems AF886), mouse anti-INCENP (Invitrogen 39-2800), rabbit anti-H3S10ph (Upstate 06-570) and mouse anti-GFP (Roche 11814460001). Membranes were washed 3x with TBST, and subsequently incubated with goat anti-mouse or anti-rabbit horseradish peroxidase (HRP)-conjugated secondary antibodies (Bio-Rad). An ECL chemiluminescence detection kit (GE Healthcare) was used to visualize the protein-antibody complex.

Sample preparation for and analysis by mass spectrometry

Eluted MKLP2::GFP::StrepII or GFP::StrepII samples (three technical replicates of each) were first denatured and alkylated by adding alkylation buffer (10 mM tris(2-carboxyethyl)phosphine (TCEP), 40 mM 2-chloroacetamide (CAA), 8 M urea, 1 M ammonium bicarbonate. After 30 min of incubation the samples were diluted fourfold with 1 M ammonium bicarbonate and 250 ng Trypsin/Lys-C protease (Promega) was added and followed by overnight digestion at 37°C on a shaker. The samples were then cleaned up using homemade C18 stagetips (Rappsilber et al., 2007), and a quarter was used for the analysis with LC-MS (Thermo Easy-nLC 1000, Thermo Orbitrap Fusion Tribrid) running a 140 min gradient (300 nl/min, 30 cm 1.9 µm C18 column) with 240k (at 200 m/z) full MS resolution and a 1 s MS2 duty cycle (top speed, highest to low intensity, HCD fragmentation). Raw files were analyzed with Maxquant software, version 1.6.3.4. For identification, the Human Uniprot database was searched with oxidation of and carbamidomethylation of cysteine set as fixed modification, while peptide and protein false discovery rates were set to 1%. The median intensity of the iBAQ values was then plotted as Log2 transformed values with a red line (x=0) and a green line (x+5) added as visual aid.

Immunofluorescence microscopy

For immunofluorescence (IF) of anaphase cells, HeLa Flp-In T-Rex cells were plated in 2.5 mM thymidine (Sigma-Aldrich) for 24 hrs in 24 well plates containing 12 mm High Precision coverslips (Superior-Marienfeld GmbH & Co) and subsequently released into medium containing 5 µM Cdk1 inhibitor RO3306 (Calbiochem) for another 16 hrs to synchronize cells in G2. Where indicated, doxycycline (1 µg/ml, Sigma-Aldrich) was added together with RO3306 to induce protein expression. Cells were released from the

RO3306-induced G2 block by washing three times with warm medium. Where indicated, 50 μM paprotrain (Millipore) was added 50 min. after the release. Sixty minutes after release from the Cdk1 inhibitor, cells were processed for IF. Cells were fixed with 4% PFA in PBS for 7 min. and permeabilized in 0.25% Triton X-100 in PBS for 5 min. Cells were blocked in PBS containing 3% BSA and 0.1% Tween-20. Primary antibodies used were: rabbit anti-MKLP2 (Bethyl (ITK) A300-878A), rabbit anti-PRC1 (Santa Cruz sc-8356), mouse anti-Aurora B (BD Transduction labs 611083), rabbit anti-Anillin (a kind gift from Michael Glotzer) and mouse anti-GFP (Roche 11-814-460-001). Secondary antibodies used were: goat anti-mouse or goat anti-rabbit IgG-Alexa 488, goat anti-mouse or goat anti-rabbit IgG-Alexa 568 (Invitrogen). 4',6-Diamidino-2-Phenylindole (DAPI, Sigma) was used for DNA staining and coverslips were mounted in ProLong Antifade (Molecular Probes). Images were taken with a Personal DeltaVision system (Applied Precision) equipped with a 100x / NA 1.40 UPLS Apo-UIS2 objective (Olympus) and a CoolSNAP HQ CCD camera (Photometrics). Images were deconvolved in Softworx. For each experiment, all images were acquired with identical illumination settings. Images are projections of deconvolved Z-stacks, unless stated otherwise.

In vitro microtubule (MT) dynamics assays

Doubly cycled GMPCPP MT seeds were prepared as described before (Mohan et al., 2013), by incubating a tubulin mix containing 70% unlabeled porcine brain tubulin (Cytoskeleton), 18% biotin-tubulin (Cytoskeleton) and 12% rhodamine-tubulin (Cytoskeleton) at a total final tubulin concentration of 20 μM with 1 mM GMPCPP (Jena Biosciences) at 37°C for 30 min. MTs were pelleted by centrifugation in an Airfuge for 5 min at 119,000 × g and then depolymerized on ice for 20 min. This was followed by a second round of polymerization at 37°C with 1 mM GMPCPP. MT seeds were then pelleted as above and diluted in MRB80 buffer containing 10% glycerol, snap frozen in liquid nitrogen and stored at −80°C.

Reconstitution of MT growth dynamics *in vitro* was performed as described previously (Montenegro Gouveia et al., 2010). Flow chambers, assembled from sticking plasma-cleaned glass coverslips onto microscopic slides with a double sided tape were functionalized by sequential incubation with 0.2 mg/ml PLL-PEG-biotin (Susos AG, Switzerland) and 1 mg/ml NeutrAvidin (Invitrogen) in MRB80 buffer (80 mM piperazine-N,N[prime]-bis(2-ethanesulfonic acid), pH 6.8, supplemented with 4 mM $MgCl_2$, and 1 mM EGTA. MT seeds were attached to the coverslip through biotin-NeutrAvidin interactions. Flow chambers were further blocked with 1 mg/ml κ-casein (Sigma). The *in vitro* reaction mixture consisted of 18 μM tubulin, 50 mM KCl, 0.1% methylcellulose, 0.5 mg/ml κ-casein, 1 mM GTP, an oxygen scavenging system (20 mM glucose, 200 μg/ml catalase, 400 μg/ml glucose-oxidase, and 4 mM DTT), 2 mM ATP, MKLP2 motors at indicated concentrations (concentrations were calculated for monomeric proteins), and CPC protein complexes at indicated concentrations. After centrifugation in an Airfuge for 5 min at 119,000 g, the reaction mixture was added to the flow chamber containing the MT seeds and sealed with vacuum grease. The experiments were conducted at 30°C, and data were collected using total internal reflection fluorescence (TIRF) microscopy. For most experiments, the reaction mixture was composed of 17.5 μM tubulin supplemented with 0.5 μM rhodamine-labeled tubulin to properly visualize MTs in the assay. All tubulin products were purchased from Cytoskeleton Inc.

TIRF Microscopy

In vitro reconstitution assays were imaged on a TIRF microscope setup as described previously (Mohan et al., 2013) or on an ILAS-2 TIRF setup. The former system consisted of an inverted research microscope Nikon Eclipse Ti-E (Nikon) with the perfect focus system (Nikon), equipped with Nikon CFI Apo TIRF 100x 1.49 N.A. oil objective (Nikon) and controlled with MetaMorph 7.7.5 software (Molecular Devices). The microscope was equipped with TIRF-E motorized TIRF illuminator modified by Roper Scientific France/PICT-IBiSA, Institut Curie. To keep the *in vitro* samples at 30°C, a stage top incubator model INUBG2E-ZILCS (Tokai Hit) was used. For excitation, 491 nm 100 mW Calypso (Cobolt) and 561 nm 100 mW Jive (Cobolt) lasers were used. We used ET-GFP 49002 filter set (Chroma) for imaging of proteins tagged with GFP or ET-mCherry 49008 filter set (Chroma) for imaging of rhodamine-labeled tubulin or proteins tagged with mScarlet or mCherry. For simultaneous imaging of green and red fluorescence, we used an Evolve512 EMCCD camera (Photometrics) and ET-GFP/mCherry filter cube (59022; Chroma) together with an Optosplit III beamsplitter (Cairn Research Ltd) equipped with double-emission filter cube configured with ET525/50m, ET9630/75m and T585lprx (Chroma). Fluorescence was detected using an EMCCD Evolve 512 camera (Roper Scientific) with the intermediate lens 2.5X (Nikon C mount adapter 2.5X). The final magnification using EMCCD camera was 0.063 µm/pixel.

ILAS-2 system (Roper Scientific, Evry, France) is a dual laser illuminator for azimuthal spinning TIRF (or Hilo) illumination and with a custom modification for targeted photomanipulation. This system was installed on Nikon Ti microscope (with the perfect focus system, Nikon), equipped with 150 mW 488 nm laser and 100 mW 561 nm laser, 49002 and 49008 Chroma filter sets. For simultaneous imaging of green and red fluorescence, we used an Evolve512 EMCCD camera (Photometrics) and ET-GFP/mCherry filter cube (59022; Chroma) together with an Optosplit III beamsplitter (Cairn Research Ltd) equipped with double-emission filter cube configured with ET525/50m, ET9630/75m and T585lprx (Chroma). Fluorescence was detected using an EMCCD Evolve mono FW DELTA 512x512 camera (Roper Scientific) with the intermediate lens 2.5X (Nikon C mount adapter 2.5X). The setup was controlled with MetaMorph 7.8.8 software (Molecular Device). To keep the *in vitro* samples at 30°C, a stage top incubator model INUBG2E-ZILCS (Tokai Hit) was used. The final resolution using EMCCD camera was 0.065 µm/pixel.

Single-molecule intensity analysis

Sample preparation for the fluorescence intensity analysis was performed by immobilizing diluted GFP or MKLP2::GFP full length proteins non-specifically to the plasma cleaned glass coverslips in flow chambers. After protein addition, the flow chambers were washed with MRB80 buffer, sealed with vacuum grease and immediately imaged with a TIRF microscope. Approximately 10 images of previously unexposed coverslip areas were acquired. GFP and MKLP2::GFP full length proteins were located in different chambers of the same coverslip, so identical imaging conditions could be preserved. All acquisitions were obtained under identical laser power, exposure time and TIRF angle.

Live cell microscopy

Imaging of MKLP2::GFP and INCENP::GFP in HeLa Flp-In T-Rex cells was done in Lab-tek (8 well, Chambered Coverglass W/Cover #1.5 Borosilicate Sterile, Thermo Fisher Scientific). Cells were blocked

in late G2 by overnight Cdk1 inhibition (RO-3306) and released prior to imaging by 3x washing with Leibovitz's medium (Sigma). Medium was changed to Leibovitz's medium (Sigma) supplemented with 10% FCS (FBS, Sigma-Aldrich), 2 mM UltraGlutamine (Lonza) and 100 units/ml penicillin and 100 µg/ml streptomycin (Sigma). Spinning disk microscopy was performed on an inverted research microscope Eclipse Ti-E with the Perfect Focus System (Nikon), equipped with Plan Apo VC 100x N.A. 1.40 oil objective, a Yokogawa CSU-X1-A1 confocal head with 405-491-561 triple-band mirror and GFP, mCherry, and GFP/mCherry emission filters (Chroma), ASI motorized stage MS-2000-XYZ with Piezo Top Plate (ASI), a Photometrics Evolve 512 electron-multiplying charge-coupled device (CCD) camera (Photometrics), and controlled by MetaMorph 7.7 software (Molecular Devices). The microscope was equipped with a custom-ordered illuminator (MEY10021; Nikon) modified by Roper Scientific France/PICT-IBiSA, Institut Curie. Cobolt Calypso 491 nm (100 mW) and Vortran Stradus 642 nm (110 mW) lasers (Cobolt) were used as light sources. To keep cells at 37°C, we used a stage top incubator (model INUBG2E-ZILCS; Tokai Hit).

Single molecule GFP counting assays

ImageJ plugin Comdet v.0.3.61 and DoM_Utrecht v1.1.1.5 (https://github.com/ekatrukha/DoM_Utrecht) were used for detection and fitting of single molecule fluorescent spots as described previously (Yau et al., 2014). With this method, individual spots were fitted with 2D Gaussian, and the amplitude of the fitted Gaussian function was used as a measure of the fluorescence intensity value of an individual spot. These fitted peak intensity values were used to build fluorescence intensity histograms which could be fitted to a Gaussian curve using GraphPad Prism 7.

Analysis of in vitro reconstitution data

Images and videos were processed and analyzed with Fiji image processing software (ImageJ). Maximum intensity projections were made using z projection. Kinesin velocities, run lengths and landing frequencies were obtained from kymograph analysis using ImageJ plugin KymoReslideWide v.0.4 (https://github.com/ekatrukha/KymoResliceWide). Kinesin parameters were quantified for processive events that last > 1 s. Static events were not included in velocity and run length quantifications. Quantification of landing frequencies was corrected for MT length, time of acquisition and kinesin concentration. Processive events were quantified and subdivided into "complete" and "incomplete" tracks. Tracks where both kinesin landing and detachment were observed were defined as complete, whereas incomplete tracks were tracks that exceeded the 90 s acquisition time or partially took place outside of the acquisition area. In cases of hyperprocessive events (imaging of miniCPC::GFP, or MLKP2::GFP in the presence of miniCPC) with many incomplete tracks, the observed event frequency per MT was quantified instead of landing frequency. Again, these data were corrected for MT length, time of acquisition and kinesin or CPC concentration. To distinguish directional and processive CPC events from diffusively behaving particles, only unidirectional events with a duration > 2.5 s were quantified. CPC::GFP labelling intensities on *in vitro* polymerized dynamic MTs were measured from 2 pixel wide line scans along MTs. An adjacent line scan 10 pixels away from the same MT was used as a background intensity measurement. MT labelling intensity was corrected by subtraction of this background intensity measurement. Imaging conditions

were kept identical for all samples in the same experiment.
For *in vitro* experiments with paprotrain, kinesin motility parameters were quantified for events that last > 1 s. Kinesin runs with a velocity < 0.025 µm/s were classified as static events. The percentage of static events per MT was quantified as a percentage of all kinesin events per MT. In the experiments with paprotrain, non-motile (static) events were included in velocity and run length quantifications. Kinesins running on GMPCPP MT seeds were excluded from the analysis.

Analysis of live cell imaging data
Image analysis was performed with Fiji image processing software (ImageJ). MKLP2 and INCENP velocities were obtained from kymograph analysis using ImageJ plugin KymoReslideWide v.0.4 (https://github.com/ekatrukha/KymoResliceWide). To distinguish directional MKLP2::GFP and INCENP::GFP events in cells from diffusive or statically behaving particles, only unidirectional events with a relatively constant velocity > 0.05 µm/s and a duration > 2.5 s were quantified. In addition, only events that could be measured using a kymograph were quantified in these experiments.

Analysis of immunofluororescence intensities in fixed cells
Images were deconvolved in Softworx (Applied Precision). For each experiment, all images were acquired with identical illumination settings. Images are projections of deconvolved z stacks. Image analysis was performed with Fiji image processing software (ImageJ). To quantify and compare the mean fluorescence intensities (MFIs) of Aurora B on the equatorial cortex (marked by Anillin), the spindle midzone (marked by PRC1), and on chromatin (DAPI), a regions of interest (ROIs) were made on the basis of Anillin, PRC1 or DAPI localization. A random region of the cytoplasm was used as background measurement, and background intensity per cell was subtracted from the fluorescence intensity measured in the indicated ROIs. Line plots were performed with Fiji image processing software (ImageJ) and visualized in Graphpad Prism 7 software.

Statistical analysis
Statistical significance was analyzed either using the Mann-Whitney *U* test or *t* test, as indicated in the figure legends. For the *t* tests, data distribution was checked for normal distribution of the data. Kinesin and CPC velocities are represented using frequency distributions and Gaussian curve fits. For this fitting, data distributions were assumed to be normal, but this was not formally tested. Statistical analysis was performed with Graphpad Prism 7 or Prism 8 software.

DATA AND CODE AVAILABILITY
The mass spectrometry proteomics data have been deposited to the ProteomeXchange Consortium via the PRIDE (Perez-Riverol et al., 2019) partner repository with the dataset identifier PXD014665.
Username: reviewer91799@ebi.ac.uk
Password: nclY8CjQ

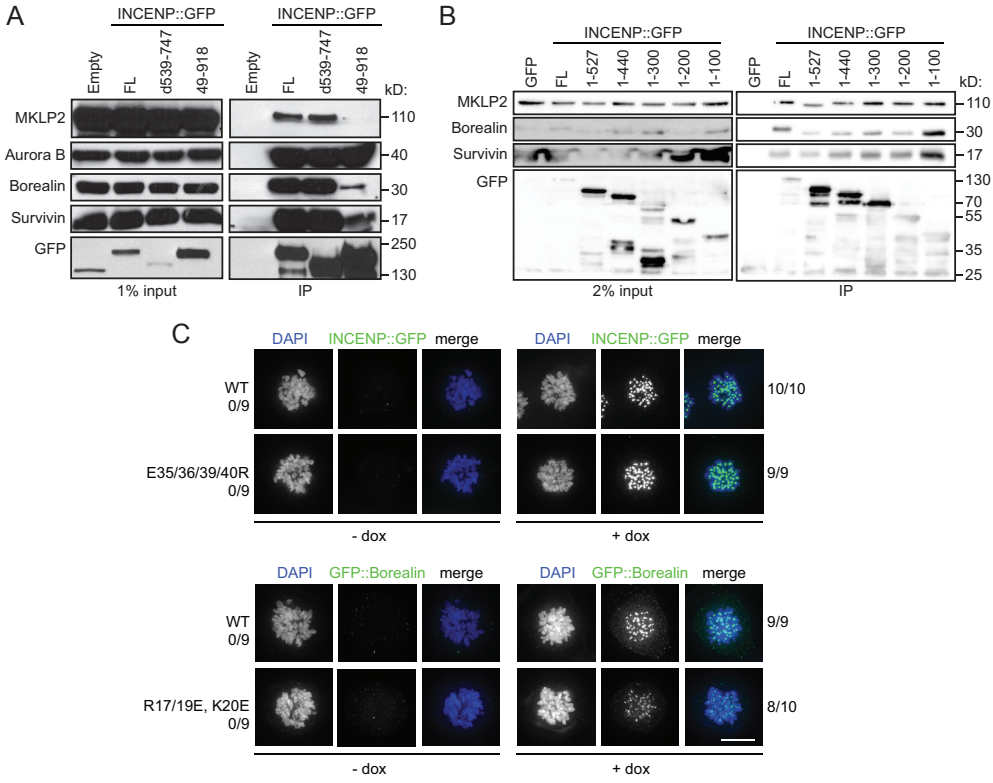

Figure S1, related to Figure 1: Mapping of the MKLP2-CPC interaction

A) IPs of GFP-tagged INCENP full length (FL), INCENP-dSAH (d539-747) and INCENP 49-918 from mitotic HeLa cells stably expressing the dox-inducible indicated protein. Blots were stained for MKLP2, Aurora B, Borealin, Survivin and GFP. The anti-GFP antibody gave a background band in the "empty' HeLa cell line, which did not show up in the IP. B) HEK293T cells were transfected with the indicated INCENP plasmids. Immunoprecipitations were performed with GFP-Trap beads, and samples were analyzed by Western blotting using antibodies specific for the indicated proteins. C) IF for GFP of HeLa cells expressing INCENP::GFP or INCENP E35/36/39/40R::GFP, and expressing GFP::Borealin or GFP::Borealin R17/19E,K20E from a dox-inducible promotor. Cells were synchronized in mitosis by addition of STLC. DNA was visualized using DAPI. Scale bar = 10 mm. Numbers on the left indicate the number of times the depicted localization was observed/total number of cells that were imaged. Scale bar = 10 mm

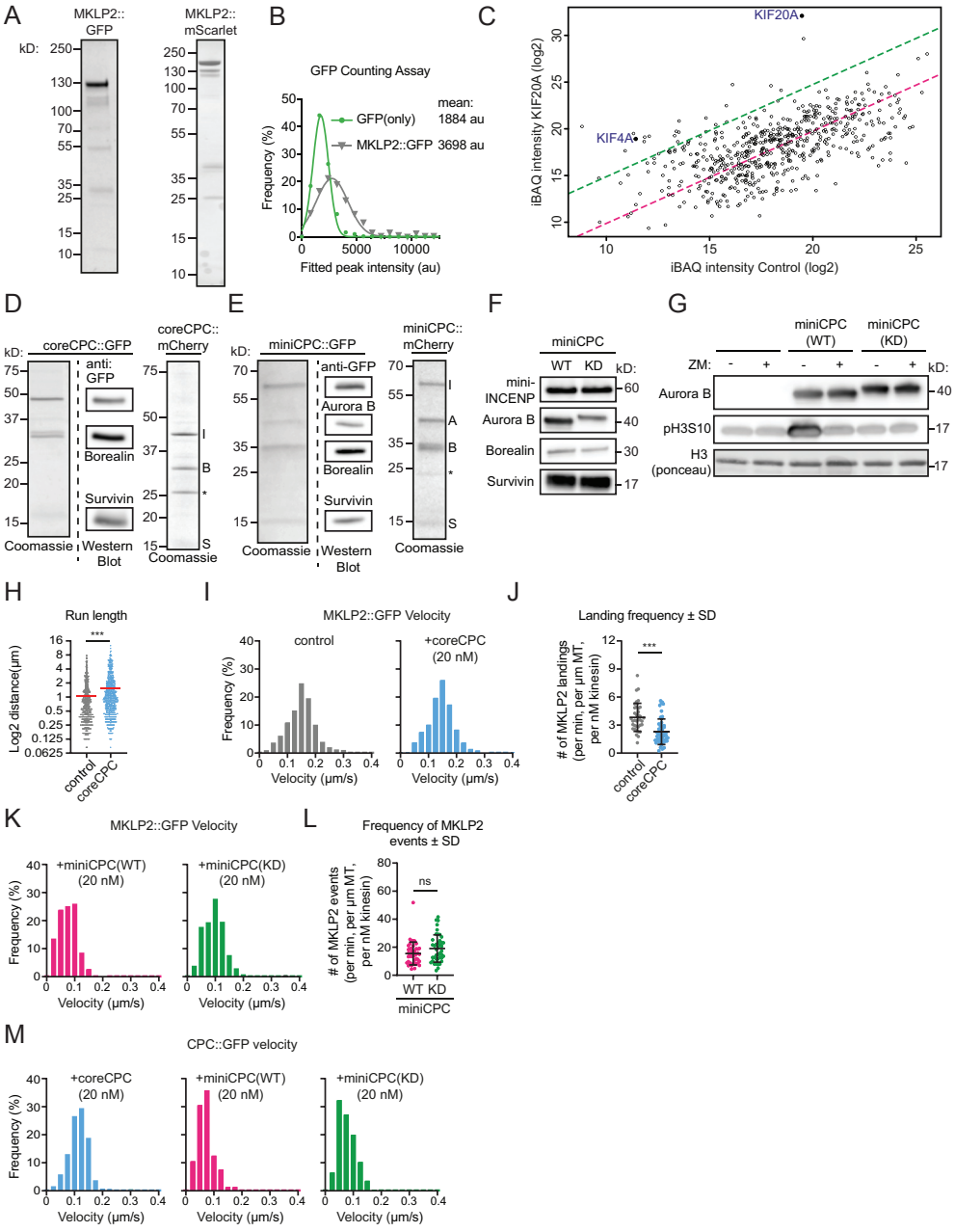

Figure S2, related to Figure 2: Analysis of purified MKLP2 and CPC

A) SDS-PAGE of full length MKLP2::GFP and MKLP2::mScarlet purified from HEK293T cells. Gels were stained with Coomassie Brilliant Blue. B) Histograms of fluorescence intensities of single GFP (green dots) and MKLP2::GFP molecules (grey triangles) immobilized on coverslips in two separate chambers on the same coverslip and the corresponding Gaussian fits (green and grey lines). Imaging conditions were identical for both conditions. n = 1909 (GFP) and n = 324 (MKLP2::GFP) molecules. Fluorophore density was approximately 0.04-0.10 µm^{-2}. Mean values for each condition are indicated in the plot. C) Scatter plot of protein abundance comparison between MKLP2::GFP and

GFP purified from HEK293T cells using LC MS/MS. Enrichment of proteins is estimated using a linear model through all median iBAQ intensities of identified proteins (N=3) (Red line). Green line indicates 32 (2^5) times enrichment based on the linear model. KIF20A and KIF4A are indicated. Raw data/spectra can be found on ProteomeXchange Consortium via the PRIDE partner repository with the dataset identifier PXD014665. D) SDS-PAGE of purified coreCPC::GFP (left panel) and coreCPC::mCherry (right panel). Gels were stained with Coomassie Brilliant Blue. In the middle panel, individual proteins of coreCPC::GFP were visualized by Western blot probed with the indicated antibodies. INCENP 1-100 is visualized with anti-GFP. *An additional band around 25 kD appeared in the coreCPC::mCherry preparation, which corresponds to mCherry. E) SDS-PAGE of purified miniCPC::GFP (left panel) and miniCPC::mCherry (right panel) loaded with Aurora B WT. Gels were stained with Coomassie Brilliant Blue. In the middle, individual proteins of miniCPC::GFP were visualized by Western blot probed with the indicated antibodies. INCENP (1-100)-linker-INCENP (834-918) is visualized with anti-GFP. *An additional band around 25 kD appeared in the coreCPC::mCherry preparation, which corresponded to mCherry. F) Western blot of purified miniCPC loaded with either wild type Aurora B (WT) or kinase dead Aurora B (KD). Blots were probed with antibodies specific for GFP, Aurora B, Borealin and Survivin. G) *In vitro* kinase assay for purified miniCPC loaded with either WT or KD Aurora B. The kinase reaction was separated by SDS-PAGE and Western blots were probed with antibodies specific for Aurora B and phosphorylated serine 10 in Histone H3. Bottom panel is a Ponceau staining of Histone H3. H) Quantification of MKLP2::GFP run length in control condition or in the presence coreCPC::m herry. *** $p < 0.001$, Mann-Whitney U test. n = 832 (control), n = 618 kinesins (coreCPC) from three independent experiments. Mean values are indicated with red bars. I) Histograms of MKLP2::GFP velocities. n = 1145 and 1137 kinesin runs from three independent experiments. Histograms correspond to the velocity fits shown in Figure 2D. J) Quantification of MKLP2::GFP landing frequency in control condition or in the presence coreCPC::mCherry normalized for MT length, time of acquisition and kinesin concentration. *** $p < 0.001$, Mann-Whitney U test. n = 37 MTs (control), n = 49 MTs (coreCPC) from three independent experiments. K) Histograms of MKLP2::GFP velocities. n = 459 and 657 kinesin runs from two independent experiments. Histograms correspond to the velocity fits shown in Figure 2G. L) Quantification of MKLP2 event frequency corrected for MT length, time of acquisition and kinesin concentration. n = 43 (WT) and n = 42 (KD) MTs from three independent experiments. M) Histograms of CPC::GFP velocities. n = 708, 305 and 372 kinesin runs from three independent experiments. Histograms correspond to the velocity fits shown in Figure 2L.

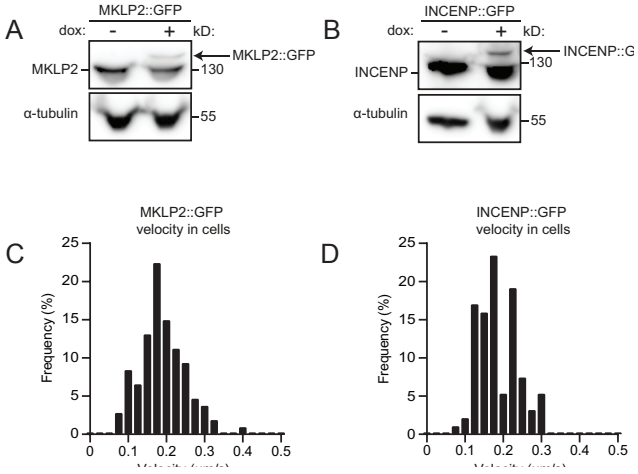

Figure S3, related to Figure 3: Characterization of the dynamics of MKLP2 and INCENP in HeLa cells in anaphase
A, B) Western blot of the MKLP2::GFP (A) and INCENP::GFP (B) expressing cell lines probed with antibodies specific for MKLP2 (A) or INCENP (B) and α-tubulin (A,B). Expression of the exogenous GFP-tagged proteins was induced by addition of doxycycline (dox). C-D) Histograms showing the velocities of directional motility events of MKLP2::GFP (C) and INCENP::GFP (D) measured in HeLa cells. n = 107 (C) and 94 kinesin (D) runs from two or three independent experiments. Histograms correspond to the velocity fits shown in Figure 3E.

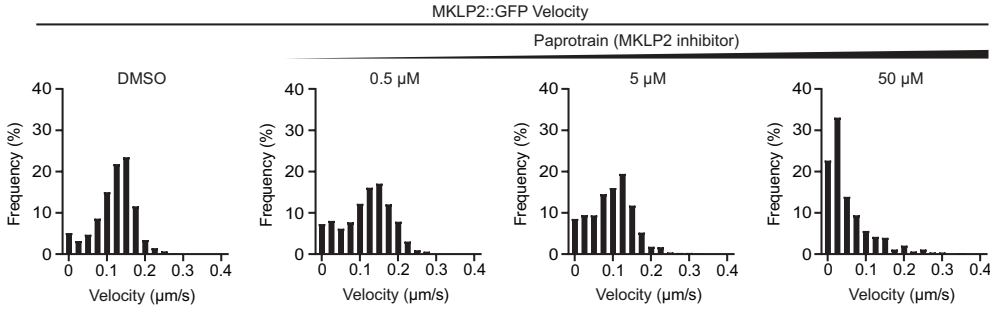

Figure S4, related to Figure 4: Analysis of MKLP2 motor parameters in the presence of paprotrain
Histograms of MKLP2::GFP velocities in DMSO (control) conditions or in the presence of increasing paprotrain concentrations, n = 1262, 899, 1014 and 423 kinesins from two or three independent experiments. Histograms correspond to the quantification shown in Figure 4E.

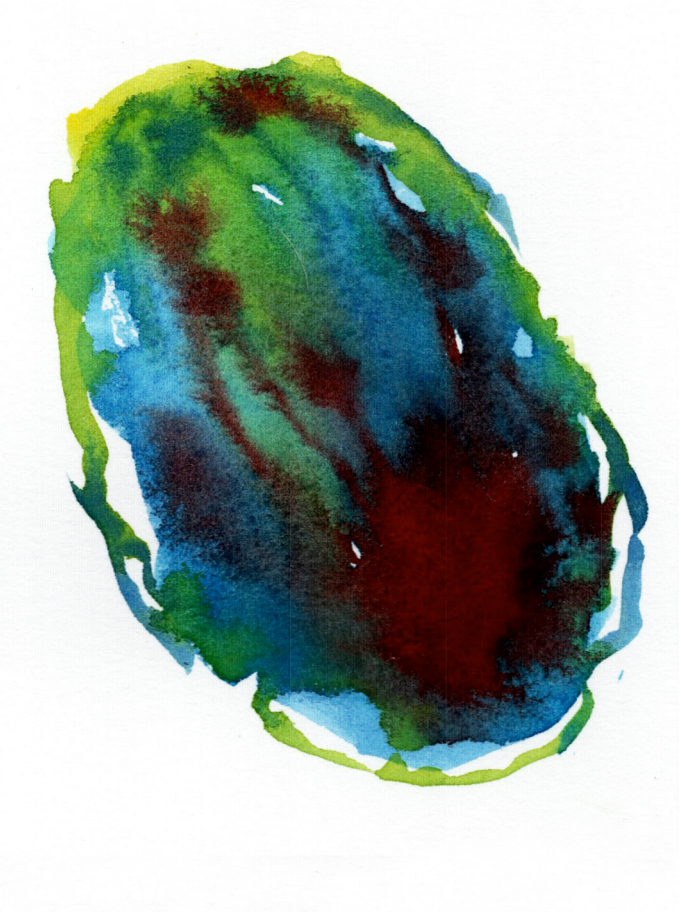

Chapter 4

MAP7 proteins specify the localization of MKLP2 and the CPC during anaphase

Ingrid E. Adriaans[1,2], Peter Jan Hooikaas[3], Robert M. van Es[1,2], Anna Akhmanova[3], Susanne M. A. Lens[1,2]

[1]Oncode Institute and [2]Center for Molecular Medicine, University Medical Center Utrecht, Utrecht University, Utrecht, The Netherlands. [3]Cell Biology, Department of Biology, Faculty of Science, Utrecht University, Utrecht, The Netherlands.

Manuscript in preparation

Abstract

At anaphase onset, the Chromosomal Passenger Complex (CPC), consisting of Aurora B, INCENP, Survivin and Borealin, translocates from the chromosomes to the antiparallel microtubule overlaps of the spindle midzone and to the equatorial cortex. We recently demonstrated that this typical anaphase localization of the CPC is in part dependent on microtubule-based transport by the kinesin-6 motor protein, MKLP2 (KIF20A). However, how directed motility of MKLP2 is regulated in cells remains unclear. Here we identify the MAP7 proteins (MAP7, MAP7D1, MAP7D2 and MAP7D3) as interactors of MKLP2 and demonstrate that the MAP7 proteins are required for the proper localization of MKLP2 and the CPC in anaphase. *In vitro*, MAP7 has a minimal effect on the motor function of MKLP2. In cells lacking MAP7 proteins, MKLP2 and the CPC appear as foci between the segregating chromosomes and are no longer confined to the antiparallel microtubule overlaps of the spindle midzone. The origin of these foci is unknown, but they require the presence of microtubules and resemble liquid-liquid phase-separated droplets. We propose that the MAP7 proteins anchor MKLP2/CPC complexes to the antiparallel-microtubule overlaps of the spindle midzone, and that in the absence of MAP7 proteins, MKLP2 and the CPC form liquid condensates induced by microtubules.

Introduction

The Mitotic Kinase-Like Protein 2 (MKLP2, also known as KIF20A or Rab-6 kinesin) is a member of the kinesin-6 family together with MKLP1 (KIF23) and MPP1 (KIF20B) (Echard et al., 1998; Neef et al., 2003; Lawrence et al., 2004), and is required for successful cytokinesis (Neef et al., 2005; Kitagawa et al., 2013; Hill et al., 2000). In anaphase, MKLP2 colocalizes with the Chromosomal Passenger Complex (CPC) on the antiparallel microtubule overlaps of the anaphase spindle midzone and at the equatorial cortex (Kitagawa et al., 2013, 2014; Gruneberg et al., 2004; Hümmer and Mayer, 2009). In fact, MKLP2 and the CPC form a complex in anaphase and they mutually depend on each other for spindle midzone and cortical localization (Gruneberg et al., 2004; Adriaans et al., 2019; Hümmer and Mayer, 2009). We recently demonstrated that MKLP2 is a motile plus-end directed motor protein that can transport the CPC along microtubules *in vitro* (chapter 3). However, in anaphase cells, MKLP2 and the CPC subunit, INCENP, display both non-directed, diffusive motility, as well as directed motility towards the spindle midzone and the equatorial cortex (chapter 3) (Landino et al., 2017). The molecular mechanisms that determine directional movement of MKLP2 in cells are currently unknown. The spatiotemporal control of kinesin localization and activity depends on multiple factors such as post-translational modifications, the presence of cargo adaptors, and the interaction with other proteins such as microtubule (MT) associated proteins (MAPs) (Verhey and Hammond, 2009; Akhmanova and Hammer, 2010; Fu and Holzbaur, 2014; Barlan and Gelfand, 2017). Indeed, in (pro)metaphase, MKLP2 is phosphorylated by Cdk1-cyclin B and bound to the mitotic checkpoint protein Mad2. This post-translational modification and protein-protein interaction prevents MKLP2 to bind microtubules and to interact with the CPC before anaphase onset (Lee et al., 2010; Hümmer and Mayer, 2009; Kitagawa et al., 2014). However, whether MKLP2 associates with other proteins, such as MAPs, that could explain its differential activity in anaphase remains to be tested. In this study, we performed Mass Spectrometry (MS) analysis of overexpressed MKLP2 protein purified from HEK293T cells and revealed an interaction between MKLP2 and Microtubule Associated

Protein 7 (MAP7) and MAP7 Domain-containing protein 2 (MAP7D2).

MAP7 proteins are represented by four isoforms encoded by different genes in mammals: MAP7 (Ensconsin), MAP7D1, MAP7D2 and MAP7D3. With the exception of MAP7D2, which is expressed in brain tissue, MAP7 proteins are widely expressed (Koizumi et al., 2017; Tymanskyj et al., 2018; Niida and Yachie, 2011). The four MAP7 proteins are structured in a similar manner, with two conserved helical domains separated by an unstructured linker domain. The N-terminal helical domain interacts with microtubules and the C-terminal helical domain, known as the MAP7 domain, interacts with kinesin-1 (Bulinski and Bossler, 1994; Metzger et al., 2012; Yadav et al., 2014; Monroy et al., 2018; Sun et al., 2011). All four MAP7 proteins act as positive regulators of kinesin-1, increasing the recruitment of kinesin-1 to MTs and its processivity (Sung et al., 2008; Metzger et al., 2012; Barlan et al., 2013; Métivier et al., 2018; Monroy et al., 2018; Hooikaas et al., 2019; Pan et al., 2019). In contrast, MAP7 acts as a negative regulator of kinesin-3, (Monroy et al., 2018) and MAP7D3 counteracts DDA3-mediated recruitment of the kinesin-13 protein KIF2A to the mitotic spindle, thereby limiting minus-end MT dynamics (Kwon et al., 2016). This indicates that MAP7 proteins regulate the spatiotemporal activity of different motor proteins in various ways.

To understand if and how MAP7 proteins affect the function of MKLP2, we here investigated the interaction between MAP7 proteins and MKLP2 in detail and studied its contribution to MKLP2 function. We show that MKLP2 binds the N-terminal domain of MAP7, and that MT binding and processivity of MKLP2 are not enhanced by MAP7. However, we find that the localization of MKLP2 and the CPC during anaphase is markedly changed when the MAP7 proteins are absent. MKLP2 and CPC are no longer confined to the antiparallel MT overlaps of the spindle midzone, but instead localize in the area between the separating sister chromatids as foci. These MKLP2-CPC foci are reduced when microtubules are depolymerized by nocodazole suggesting that they associate with or form on microtubules. Immunofluorescence for EB1 indicated that MKLP2 and CPC do not specifically localize to the (+)-ends of dynamic microtubules in the absence of MAP7 proteins. Interestingly, the catalytic subunit of the CPC, Aurora B, was activated in these foci and cells proceeded through cytokinesis seemingly normal. In conclusion, the MAP7 proteins specify MKLP2 and CPC localization to the antiparallel-microtubule overlaps in anaphase. Whether this involves a direct association between MAP7 proteins and spindle midzone proteins such as PRC1, or whether MAP7 proteins inhibit the binding of MKLP2-CPC to parts of the spindle that do not form anti-parallel overlaps remains to be determined.

Results

Identification of MKLP2 interacting proteins

To identify proteins interacting with MKLP2, we overexpressed MKLP2::GFP::StrepII or GFP::StrepII in HEK239T cells and immunoprecipitated MKLP2::GFP::StrepII or GFP::StrepII with StrepTactin beads. LC/MS analysis revealed an enrichment of peptides for Histones (HIST1H2BL, HIST2H3PS2, HIST1H4A), MAD2L1 (Mitotic Arrest Deficient 2-like 1), INCENP (INner CENtromere Protein), LMAN1 (Lectin, Mannose binding 1), FBXW11 (F-box and WD repeat domain containing protein 11), MAP7

and MAP7D2 in the MKLP2::GFP::StrepII pulldown compared to the GFP::StrepII pulldown (Figure 1A). Whilst INCENP and MAD2L1 are known interactors of MKLP2 (Lee et al., 2010; Gruneberg et al., 2004; Kitagawa et al., 2013, 2014; Hümmer and Mayer, 2009 and chapter 3), to our knowledge, the other proteins have not been reported as potential MKLP2 binding proteins. Given the described role of MAP7 proteins in the regulation of kinesin activity (Sung et al., 2008; Metzger et al., 2012; Barlan et al., 2013; Métivier et al., 2018; Monroy et al., 2018; Hooikaas et al., 2019; Pan et al., 2019; Kwon et al., 2016) and our recent finding that MKLP2 is a motile kinesin (chapter 3), we choose to follow-up the potential interaction between MKLP2 and the MAP7 proteins.

MKLP2 preferentially interacts with MAP7D2 and MAP7 via its coiled coil domain

To confirm the interaction between MKLP2 and MAP7 proteins, we immunoprecipitated overexpressed pBio-mCherry-tagged MAP7 proteins from HEK293T cells and tested if they could co-IP endogenous MKLP2. We included all four mammalian MAP7 isoforms (MAP7, MAP7D1, MAP7D2, MAP7D3) because of their reported functional redundancy and similarity (Figure 1B)(Hooikaas et al., 2019; Pan et al., 2019). Each MAP7 protein co-precipitated endogenous MKLP2, although MAP7D3 appeared to be less efficient, and MAP7D2 most efficient in precipitating MKLP2 (Figure 1C). In the reverse experiment, different fragments of MKLP2 were overexpressed in HEK293T cells and tested for their ability to co-IP endogenous MAP7, MAP7D1, MAP7D2 and MAP7D3 (figure 1D-F). In contrast to the other MAP7 proteins, MAP7D2 is poorly expressed in HEK293T cells (undetectable in whole cell extracts by western blot, figure 1E). Yet, the latter protein was clearly detected in the MKLP2::GFP IP, suggesting a high affinity of MAP7D2 for MKLP2. We did not detect MAP7D1 and relatively low levels of MAP7 and MAP7D3 in the MKLP2::GFP IP. The MKLP2 fragment representing the neck linker region and coiled coil domain of MKLP2 (aa 489-765) immunoprecipitated MAP7 and MAP7D2. This part of MKLP2 also interacts with the CPC, here represented by the non-enzymatic subunits Borealin and Survivin (Figure 1E,F and chapter 3). Remarkably, the binding of MAP7D2 to MKLP2 was strongly decreased in the presence of the C-terminal (aa 765-890) part of MKLP2, suggesting regulation of this interaction by an intramolecular mechanism. This regulation appeared to be specific for MAP7D2 binding, as MAP7 or MAP7D3 binding was not enhanced by deletion of the MKLP2 C-terminus. Based on these combined experiments we propose the following preference of MKLP2 for MAP7 proteins: MAP7D2 > MAP7 > MAP7D1/MAP7D3. Because of the weak association with MAP7D1 and D3, and the fact that MAP7D2 is only expressed in neuronal tissue (Niida and Yachie, 2011) we next focussed mainly on MAP7.

In contrast to kinesin-1, which interacts with the C-terminal part of the MAP7 proteins, we find that the kinesin-6 protein MKLP2 preferentially binds the N-terminal half of MAP7 (Figure 1G). Whether this interaction involves the MT binding domain of MAP7, in either a direct or indirect, MT dependent, manner is currently unclear. In summary, we have identified the MAP7 proteins as genuine interactors of MKLP2, and show this interaction involves the neck linker and coiled-coil region of MKLP2 and the N-terminus of MAP7. Whether this interaction is direct or indirect is not yet clear. Moreover, why MAP7D2 displays a much higher affinity for MKLP2 than the other MAP7 isoforms also remains to be resolved.

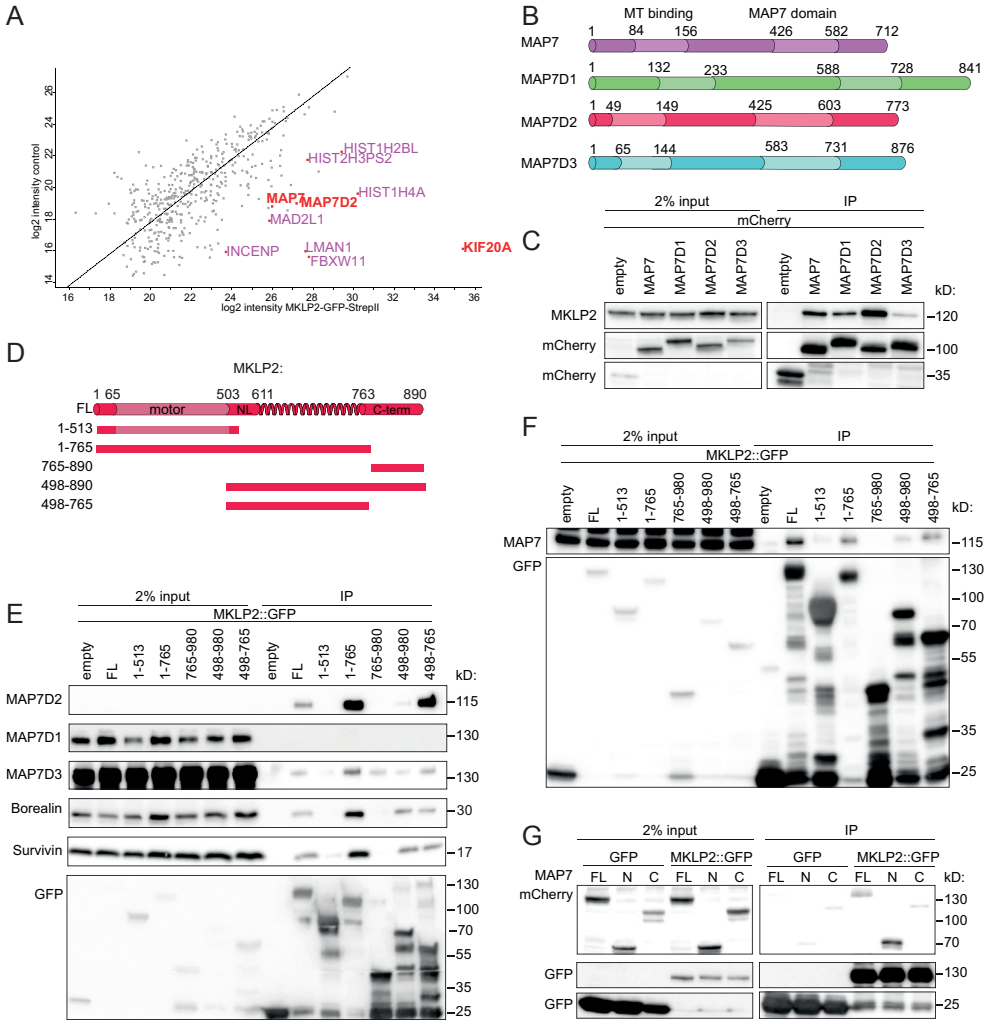

Figure 1: MAP7 proteins interact with the extended neck and coiled coil domain of MKLP2

A) Scatter plot of protein abundance of comparison between MKLP2::GFP::StrepII and GFP::StrepII purified from HEK293T cells using LC MS/MS. Proteins of significance are indicated in purple and red. Only the proteins indicated in red are followed-up in this study. B) Schematic representation of the domain structures of MAP7, MAP7D1, MAP7D2 and MAP7D3. Numbers indicate amino acids. C) HEK293T cells were transfected with the indicated mCherry tagged MAP7 plasmids. Immunoprecipitations were performed with RFP-Trap beads, and samples were analysed by Western blotting using antibodies specific for the indicated proteins. D) Schematic representation of full length (FL) MKLP2 protein and the deletion mutants of MKLP2 used to pull down endogenous MAP7 proteins. E) HEK293T cells were transfected with the indicated MKLP2 plasmids. Immunoprecipitations were performed with GFP-Trap beads, and samples were analysed by Western blotting using antibodies specific for the indicated proteins. F) HEK293T cells were transfected with the indicated MKLP2 plasmids. Immunoprecipitations were performed with GFP-Trap beads, and samples were analysed by Western blotting using antibodies specific for the indicated proteins. G) HEK293T cells were transfected with the indicated MKLP2 and MAP7 plasmids. FL = mCherry::MAP7 full length. N = mCherry::MAP7 N-term (aa1-301,d176-212) and C = pBio-mCherry::MAP7 C-term (aa301-749). Immunoprecipitations were performed with GFP-Trap beads, and samples were analysed by Western blotting using antibodies for the indicated proteins.

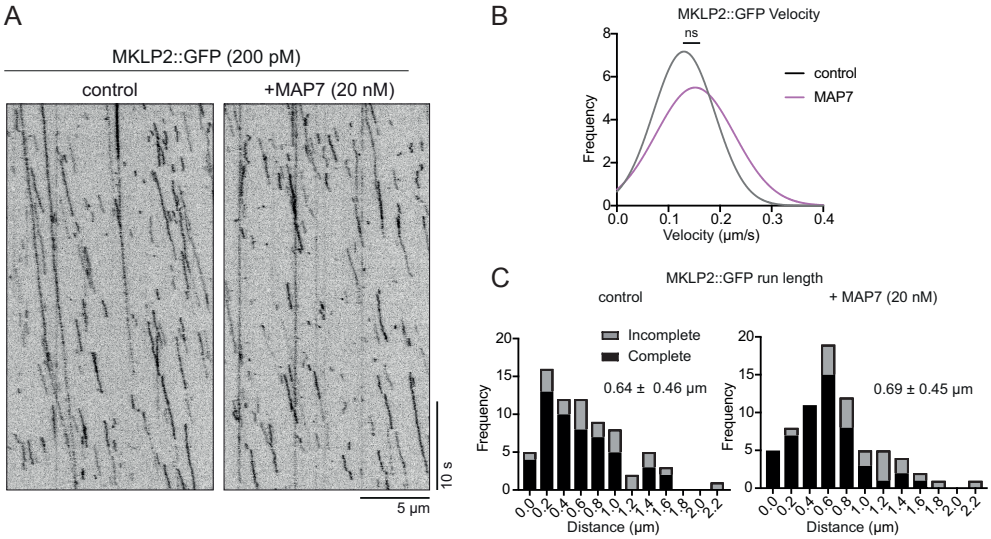

Figure 2: MAP7 proteins do not influence MKLP2 motor function in vitro

A) Representative kymographs of MKLP2::GFP on dynamic MTs in control conditions or in the presence of 20 nM MAP7. Image acquisition was performed at 10 frames per second (fps). B) Gaussian fits of MKLP2::GFP velocities plus or minus 20 nM MAP7. Histograms are shown in Supplemental figure S1. Quantification the velocity of MKLP2 with or without 20 nM MAP7. C) Histograms of MKLP2::GFP run length in the presence or absence of 20 nM MAP7. Observed motor tracks were subdivided in complete and incomplete tracks. n = 73 for both control and MAP7 kinesin runs from one experiment.

4

MKLP2 motor function in the presence of MAP7

Since binding of MAP7 proteins to kinesins can either positively (kinesin-1) or negatively (kinesin-3) regulate their activity, we next assessed the impact of MAP7 binding on MKLP2 activity *in vitro*, by using *in vitro* reconstitution assays in combination with Total Internal Reflection Fluorescence (TIRF) microscopy. Dynamic microtubules were grown from GMPCPP-stabilized microtubule seeds that are attached to the surface of a glass coverslip (Bieling et al., 2007). Imaging was performed using GFP-tagged MKLP2 and (un)labeled tubulin and the data are analyzed using kymographs, as described previously (Hooikaas et al., 2019). First, the presence of MAP7, which strongly binds to microtubules (Hooikaas et al., 2019), did not interfere with, nor promoted MT binding of MKLP2 *in vitro* (Figure 2A). We analysed the movement and MKLP2::GFP in the absence or presence of purified MAP7 protein and observed that addition of MAP7 slightly enhanced the mean velocity (0.13 ± 0.06 µm/s without, versus 0.15 ± 0.07 µm/s with MAP7), and run length (0.64 ± 0.69 µm to 0.46 ± 0.45 µm) of MKLP2 (Figure 2A-C, S1). Of note, the calculated run lengths of MKLP2::GFP are shorter than reported in chapter 3, which could be due to the lack of Potassium Chloride (KCl) in this reaction. Thus, similar to kinesin-1, MAP7 might increase MKLP2 velocity and run length (Sung et al., 2008; Metzger et al., 2012; Barlan et al., 2013; Métivier et al., 2018; Monroy et al., 2018; Hooikaas et al., 2019). However, these increases are minimal and statistically not significant.

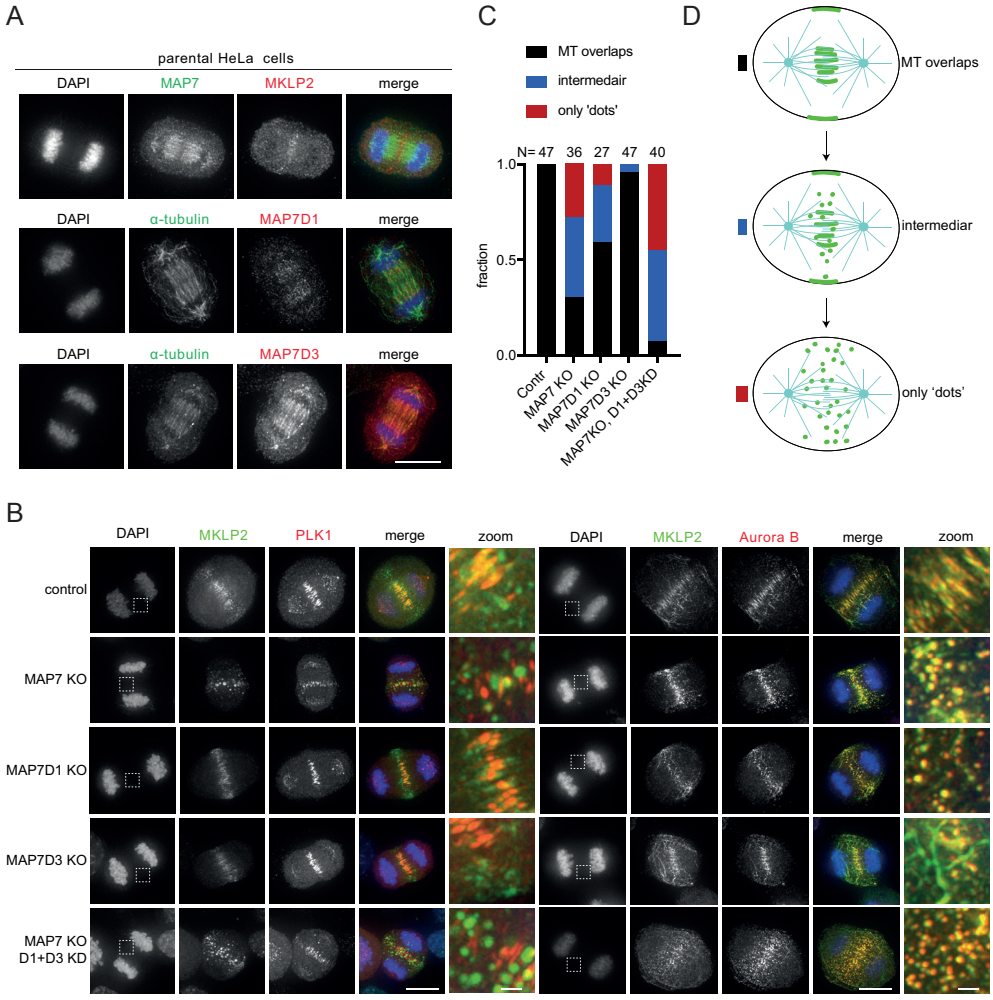

Figure 3: MAP7 specifies MKLP2 and CPC localization to the microtubule overlaps of the spindle midzone
A) IF for MAP7, MAP7D1, MAP7D3 and α-tubulin in anaphase HeLa cells. DNA was visualized using DAPI. Scale bar = 10 µm. B) IF for MKLP2 and PLK1 and MKLP2 and Aurora B in control cells, MAP7, MAP7D1 or MAP7D3 KO cells or MAP7 KO cells with MAP7D1 and MAP7D3 knock-down using siRNA (KD). DNA was visualized using DAPI. Scale bar = 10 µm and 1 µm in zoom. Squares in DAPI image indicates the position of the enlarged area. C) Quantification of localization phenotype observed in B). N= the number of cells analysed per condition. D) Schematic representation of the phenotype that was scored in C).

MAP7 proteins decorate the anaphase spindle

Since MKLP2 exerts its function in dividing cells after metaphase (Gruneberg et al., 2004; Hümmer and Mayer, 2009; Kitagawa et al., 2014, 2013), we next wanted to know if and where the MAP7 proteins localize during anaphase. We performed immunostainings for endogenous MAP7, MAP7D1 and MAP7D3 in HeLa cells (Figure 3A). As motioned earlier, MAP7D2 is not expressed in most cell types including HeLa cells (Niida and Yachie, 2011), and it was therefore not included in the analysis. MAP7, MAP7D1 and

MAP7D3 decorated the microtubules of the anaphase spindle. In fact, the immunostaining pattern of the MAP7 proteins was very similar to that of α-tubulin (Figure 3A). Of note, the IF intensity of MAP7D1 was reduced compared to the intensity of MAP7 and MAP7D3, however signal intensity increased in MAP7 KO cells (Figure S2A,B). Similarly, the signal intensity of MAP7D3 on the anaphase spindle increased when MAP7D1 was absent, suggesting competition and redundancy between the MAP7 proteins in MT binding in anaphase (Figure S2B). The MAP7 proteins did not detectably colocalize with MKLP2 in the spindle midzone (Figure 3A). However, due to the very compact microtubule bundling in the spindle midzone, α-tubulin antibodies are known to be excluded, resulting in an α-tubulin 'dark zone' in the middle of the anaphase spindle (Saxton and McIntosh, 1987; Hu et al., 2012a). We deem it likely, that also antibodies for the MAP7 proteins are excluded from the spindle midzone, giving rise to a similar 'dark zone'. This could mean that the MAP7 proteins are in fact colocalizing with MKLP2 in the spindle midzone.

MAP7 proteins specify MKLP2 and CPC localization in anaphase

An important cellular function of MKLP2 is to translocate the CPC from the chromosomes to the spindle midzone and the equatorial cortex at anaphase onset (Hümmer and Mayer, 2009; Gruneberg et al., 2004; Kitagawa et al., 2013). We next investigated if this function of MKLP2 requires the presence of MAP7 proteins, using HeLa cell lines in which the MAP7, MAP7D1 and MAP7D3 encoding genes were mutated by CRISPR-Cas9 (Hooikaas et al., 2019). Because of the previously reported redundancy in kinesin-1 regulation, we also analysed cells in which MAP7D1 and MAP7D3 were knocked-down (KD) by siRNA in the MAP7 knockout (KO) background (Hooikaas et al., 2019). Knockout of MAP7 was confirmed by western blot and the knockout or knock-down of MAP7D1 and MAP7D3 was confirmed by IF (Figure S2A,B). Successful MAP7 KO with MAP7D1 + MAP7D3 KD was further confirmed by observing the clustering of mitochondria, caused by inactivation of kinesin-1, prior to cell seeding for IF (data not shown) (Hooikaas et al., 2019).

The localization of MKLP2 was altered in the absence of MAP7, and more dramatically in the triple KO/KD condition. MKLP2 localization was no longer confined to the spindle midzone, but instead appeared as foci or condensates spread out in the area between the separating chromosomes (Figure 3B-D). In marked contrast, the localization of Polo-like kinase 1 (PLK1) and protein regulator of cytokinesis 1 (PRC1) was not affected (Figure 3B-D and S2C). Both proteins localize to the anti-parallel MT overlaps in the spindle (Mollinari et al., 2002, 2005; Burkard et al., 2009) and their unaltered localization thus suggests that these overlaps were still present and that spindle midzone formation was not impaired by the absence of MAP7 proteins (Figure 3B and S2C). Strikingly, Aurora B, the enzymatic subunit of the CPC, behaved exactly the same as MKLP2 in the absence of MAP7 proteins: it colocalized with MKLP2 in the foci (Figure 3B-D). Although anaphase localization of Aurora B was clearly altered, it localized in the midzone area and was not retained on chromosomes. The phenotype of MAP7-less cells is thereby very different from cells lacking MKLP2 or with inhibited MKLP2, since in these cells the CPC is retained on the chromosomes in anaphase (van der Horst et al., 2015; Gruneberg et al., 2004; Ahonen et al., 2009; Hümmer and Mayer, 2009; Kitagawa et al., 2014, 2013; Tcherniuk et al., 2010). This indicates that in the absence of MAP7 proteins, the CPC is successfully removed from the chromosomes by MKLP2 at

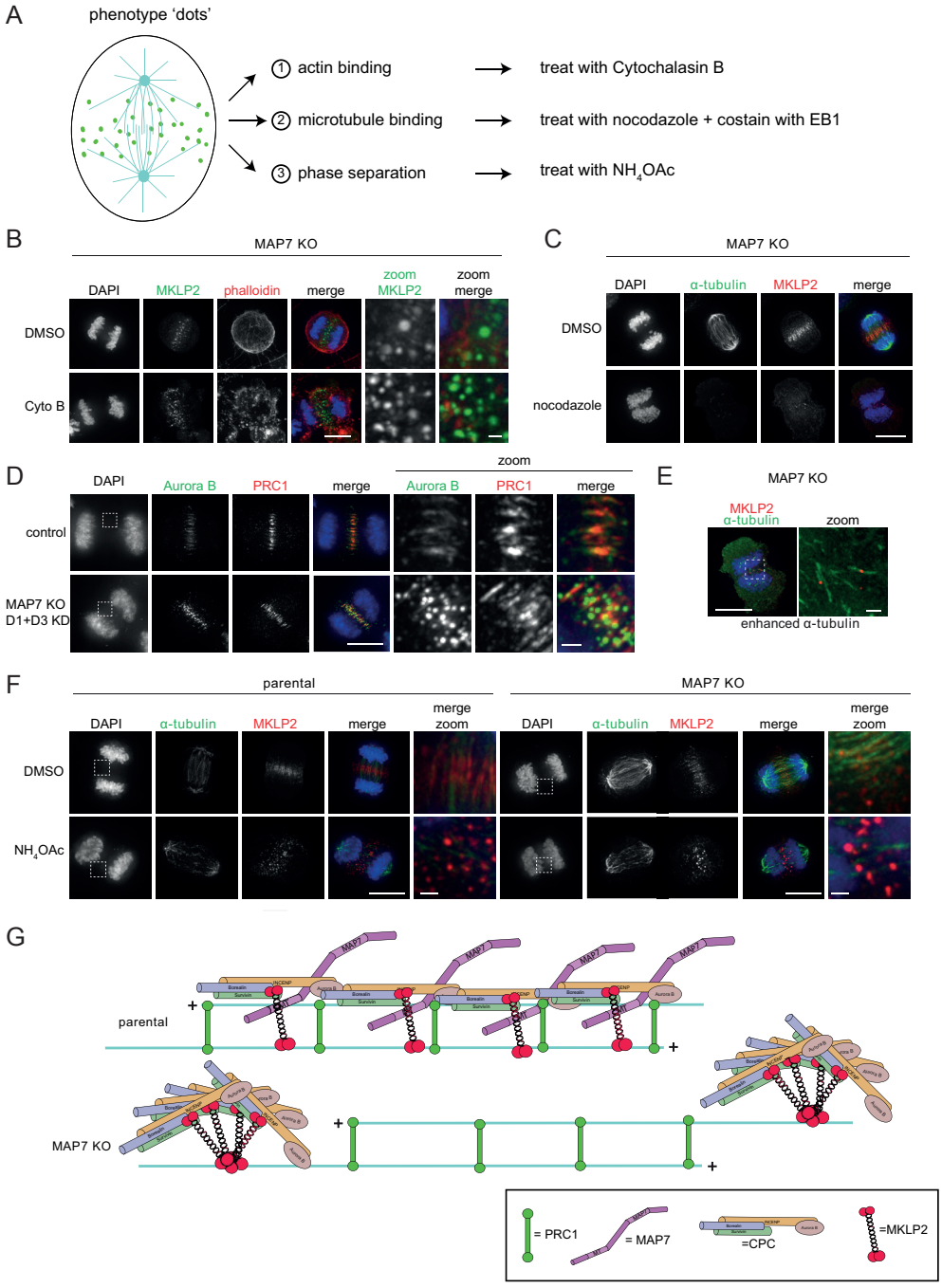

Figure 4: The alternative MKLP2 and CPC localization in cells lacking MAP7 proteins is microtubule dependent
A) Schematic representation of the distribution of MKLP2/CPC in cells lacking MAP7 proteins and the three proposed explanation for this dot-like distribution, including the method to test these hypotheses. B) IF of MKLP2 and actin (detected with phalloidin) in MAP7 KO cells in anaphase treated with or without Cytochalasin B (5 µg/m for 30 minutes).

Scale bar = 10 μm and 1 μm in zoom. C) IF of α-tubulin and MKLP2 in MAP7 KO cells in anaphase treated with or without nocodazole (5 μM for 10 minutes). Scale bar = 10 μm. D) IF of Aurora B and PRC1 in the parental HeLa cell line and in MAP7 KO, MAP7D1+D3 KD cells. Scale bar = 10 μm and 1 μm in zoom. Squares in DAPI images indicates enlarged area in zoom. E) Enhancement of α-tubulin and MKLP2 fluorescent signal of nocodazole-treated cell from (D) Scale bar = 10 μm and 1 μm in zoom. Square in DAPI image indicates enlarged area in zoom, shown on the right. F) IF of α-tubulin and MKLP2 in the parental HeLa cell line and in MAP7 KO, MAP7D1+D3 KD cells treated with or without NH_4OAc (90 mM for 2 minutes). Scale bar = 10 μm and 1 μm in zoom. Squares in DAPI images indicates enlarged area in zoom.E) G) Schematic representation of MKLP2 and CPC localization on the antiparallel microtubule overlaps of the spindle midzone in the parental HeLa cell line and of the dot-like localization of in cells lacking MAP7 proteins.

anaphase onset, but that the MKLP2/CPC complex is somehow unable to properly localize or dock on the antiparallel MT overlaps of the spindle midzone.

Do MAP7 proteins counteract liquid-liquid phase separation of MKLP2/CPC complexes in anaphase?

We next aimed to apprehend how the MAP7 proteins promote localization of MKLP2 and the CPC to the antiparallel microtubule overlaps of the spindle midzone, by understanding the alternative localization of the MKLP2/CPC complexes in the absence of MAP7 proteins (Figure 4A). We considered and tested three possibilities. 1) MAP7 proteins counteract MKLP2/CPC binding to actin, thus in their absence MKLP2/CPC prefers to bind actin filaments. This idea was fuelled by the proposed actin-based localization of MKLP2 and CPC in monopolar anaphases which resembled MKLP2 and CPC localization in the MAP7 proteins KO/KD background (Hu et al., 2008; Landino et al., 2017). To test this, we depolymerized actin filaments in anaphase MAP7 KO cells by addition of Cytochalasin B (Landino et al., 2017). Phalloidin staining and the observed membrane blebbing confirmed that the Cytochalasin B treatment was successful (Figure 4B and data not shown). However, it did not change the dot-like appearance of MKLP2 in the MAP7 KO cells, suggesting that the alternative behaviour of MKLP2 in these cells is not explained by localization to actin filaments (Figure 4B and S3B).

2) MAP7 proteins somehow promote the binding of MKLP2/CPC to stable antiparallel microtubule overlaps and, in their absence, MKLP2/CPC localizes to more dynamic microtubules. To test this hypothesis, we treated anaphase cells briefly with a high dose of nocodazole (5 μM) to depolymerize all microtubules. MKLP2 foci largely disappeared in the MAP7 KO cells when microtubules were absent (Figure 4C). However, MKLP2 foci did not colocalize with the microtubule (+)tip tracking protein EB1 (Figure S3A), excluding the possibility that MKLP2 would prefer binding to the plus ends of dynamic MTs in the absence of MAP7. Moreover, close examination of Aurora B localization in MAP7 KO cells showed that many Aurora B foci localized in the vicinity of microtubules (Figure 4D). Furthermore, the few MKLP2 foci that were still visible after the nocodazole treatment colocalized with the remaining microtubules (Figure 4E and S3D). Collectively, these findings suggest a role for microtubules in either formation or localization of the MKLP2/CPC foci when MAP7 is absent.

3) The MKLP2/CPC foci in the MAP7 KO cells represent liquid-liquid phase-separated droplets (Hyman et al., 2014), and MAP7 proteins prevent phase separation of MKLP2/CPC by promoting their binding to the antiparallel-microtubule overlaps of the spindle midzone. It was recently demonstrated that the non-enzymatic CPC subunits undergo phase separation in *vitro* and evidence was provided that the CPC may exist in a phase-separated state at the inner centromere during mitosis (Trivedi et al., 2019a).

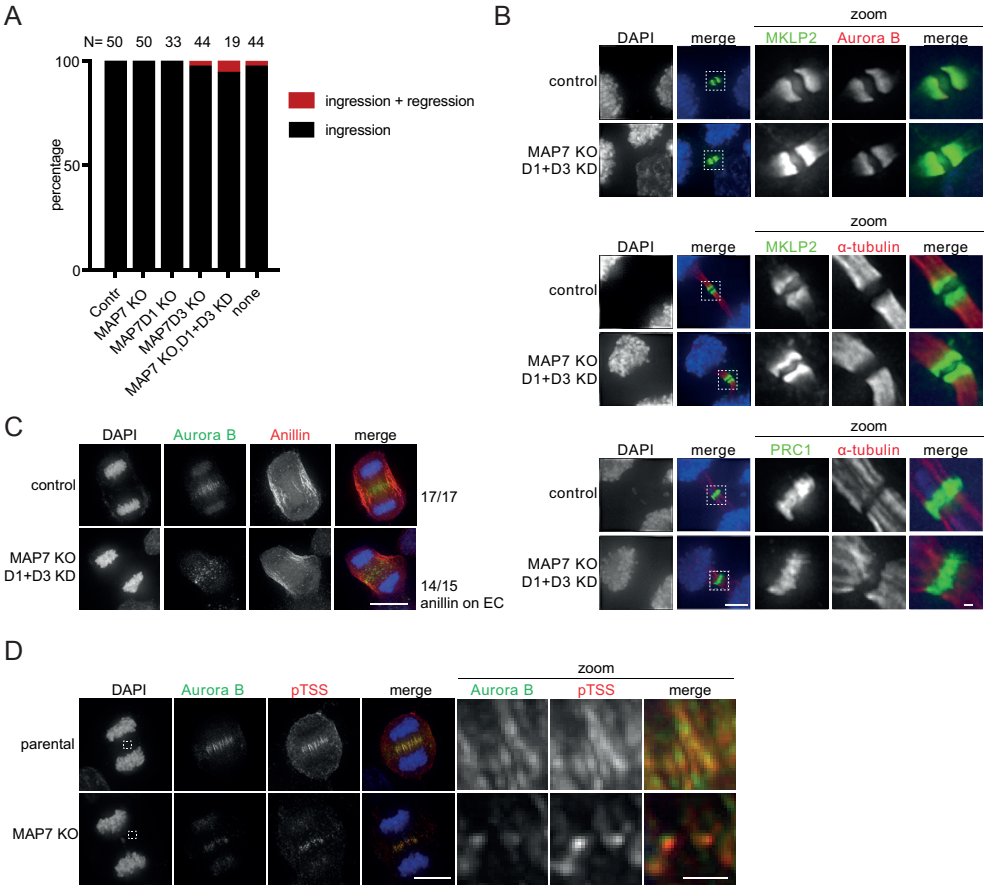

Figure 5: MAP7 proteins are not required for successful cytokinesis
A) Quantification of live cell imaging experiment. Cells were scored for furrow ingression and for furrow ingression followed by regression of the furrow. Failure to form a cleavage furrow was not observed. N = the number of cells analysed per condition. Contr. indicates transfection with siLuc, none indicates none transfected cells. B) IF of MKLP2 and Aurora B, MKLP2 and α-tubulin and PRC1 and α-tubulin in the parental HeLa cell line and in MAP7 KO, MAP7D1+D3 KD cells. Scale bar = 10 µm and 1 µm in zoom. Squares in DAPI images indicates enlarged area in zoom. C) IF of Aurora B and Anillin in the parental HeLa cell line and in MAP7 KO, MAP7D1+D3 KD cells. Scale bar = 10 µm. The presence of Anillin was scored (17/17 for control cells and 14/15 for MAP7 KO, MAP7D1+D3 KD cells). D) IF of Aurora B and INCENP phospho (p) TSS in the parental HeLa cell line and in MAP7 KO cells. Scale bar = 10 µm and 1 µm in zoom. Squares in DAPI images indicates enlarged area in zoom.

To obtain an initial indication if the MKLP2/CPC foci represent liquid-liquid phase separated droplets, we briefly treated anaphase cells with ammonium acetate (NH_4OAc), previously described to disturb phase separation (Jain and Vale, 2017; Trivedi et al., 2019a). Interestingly, treatment with NH_4OAc did not abolish the dot-like localization of MKLP2 in the MAP7 KO cells. Instead, NH_4OAc exposure seemed to increase the amount of MKLP2 foci in the MAP7 KO cells, and to induce a dot-like appearance of MKLP2 in the parental cell line (Figure 4F). Although we used a low concentration of NH_4OAc (90mM), we cannot exclude that in cells this concentration causes certain proteins to precipitate that may be visible as

aggregates. Alternatively, it may break certain protein-protein interactions that could cause MKLP2/CPC complexes to phase separate. Hence, the observation that NH_4OAc did not dissolve the MKLP2 foci in MAP7 KO does not exclude phase separation and more study is needed.

In summary, the alternative anaphase localization of MKLP2 and the CPC in MAP7 KO cells, requires the presence of microtubules but does not represent microtubule tip tracking. We propose that the MAP7 proteins direct and fixate MKLP2/CPC complexes to the antiparallel-microtubule overlaps of the spindle midzone, and that in the absence of MAP7 proteins, MKLP2 and the CPC form liquid condensates induced by microtubules (Figure 4G).

MAP7 proteins are not required for successful cytokinesis

Given the dramatic change in localization of MKLP2 and the CPC we next asked if this would affect the function of these proteins in promoting successful cytokinesis (Neef et al., 2005; Gruneberg et al., 2004; Kitagawa et al., 2013). MAP7 KO and MAP7 KO, MAP7D1 + MAP7D3 KD cells were followed from anaphase onset to the end of cytokinesis by live cell imaging. Surprisingly, cytokinesis initiation (furrow ingression) and completion (no furrow regression) appeared unaffected (Figure 5A). In line with this, anillin (an indicator of RhoA activation (Hickson and O'Farrell, 2008)) accumulated in the equatorial cortex in MAP7 KO, MAP7D1 + MAP7D3 KD cells (Figure 5C). Moreover, midbody formation was not impaired by the loss of MAP7 proteins as MKLP2, Aurora B and PRC1 localized normally to this structure in telophase (Figure 5B). Since Aurora B kinase within the CPC/MKLP2 complex is the important driver of cytokinesis (Adriaans et al., 2019), this suggested that the alternative localization of MKLP2/CPC in anaphase does not impair Aurora B kinase activity. In support of this, Aurora B localized in the foci in MAP7 KO cells was active, based on the presence of phosphorylated INCENP (TSS site), a bona fide substrate of Aurora B (Honda et al., 2003; Sessa et al., 2005) (Figure 5D). Thus, despite the dramatic change in MKLP2/CPC localization in anaphase, cytokinesis is not impaired.

Discussion

We here asked the question if an interaction between MKLP2 and MAPs could explain the differences in MKLP2 motions observed in cells (chapter 3). MAP binding to MKLP2 could inhibit its directed motility, and explain why events are either stationary or diffusive (chapter 3). Alternatively, MAP binding could enhance kinesin speed and processivity and the directed movements of MKLP2 in cells could reflect MAP-bound populations of MKLP2. We here identified the MAP7 proteins as either direct or indirect interactors of MKLP2. Although all four MAP7 isoforms could interact with MKLP2, MAP7D2 appeared to have the highest affinity for the kinesin-6 protein, followed by MAP7. Our preliminary in vitro experiments with recombinant MKLP2 and MAP7 suggest that MAP7 neither promotes nor inhibits velocity or processivity of MKLP2, and does not promote or block the binding of MKLP2 to MTs. This suggests that at least MAP7 binding may not explain MKLP2's motile behaviour in cells. Although, we did not track MKLP2::GFP in MAP7 KO cells to determine if and how MKLP2 was altered. Moreover, it would be important to test how the other MAP7 proteins affect MT binding and motor function of MKLP2 *in vitro*, in particular MAP7D2. Given that MAP7D2 is only expressed in brain tissue (and apparently HEK293T cells), it would be

interesting to figure out if MKLP2 is involved in the transport of organelles in neurons. Of note, Aurora B was recently identified as negative regulator of retrograde mitochondrial transport in hippocampal axons (Shlevkov et al., 2019). Whether MKLP2 is responsible for this transport and regulated by MAP7D2 and Aurora B in these cells, remains to be determined.

Although we have not yet answered the question what determines the mobile behaviour of MKLP2 during anaphase, we did uncover a role for the MAP7 proteins in localizing MKLP2 and the CPC to the antiparallel MT overlaps of the spindle midzone. In the absence of MAP7 proteins, MKLP2 and the CPC appeared as foci or condensates between the segregating chromosomes in HeLa cells, and this alternative localization required the presence of microtubules. Interestingly, we regularly observe small dots of MKLP2 and CPC near the equatorial cortex in cells expressing the MAP7 proteins, which could mean that the microtubules involved in depositing MKLP2 and the CPC to the equatorial cortex do not bind MAP7 proteins. How MAP7 proteins direct or anchor MKLP2 and the CPC to the antiparallel microtubule overlaps of the spindle midzone remains unclear. It could be that some of the MAP7 proteins inhibit the MT association of MKLP2 to parts of spindle that do not form antiparallel overlaps, or that they actively promote the association of MKLP2/CPC complexes to these antiparallel MT overlaps, perhaps via binding to other proteins localizing to these overlaps.

Finally, the appearance of MKLP2 and CPC in cells lacking the MAP7 proteins resembles liquid-liquid phase separated droplets. Treatment with ammonium acetate seemed to enhance the distribution of MKLP2 and CPC in foci in the parental cell line as well as in the MAP7 KO cell line. Although counterintuitive, the result suggests that the state of these MKLP2/CPC foci is influenced by increases in ionic strength (Trivedi et al., 2019a). Further study is needed to confirm or exclude that MKLP2 and the CPC phase separate in anaphase when MAP7 proteins are absent. For future experiments, we propose live cell imaging of triple KO/KD cells expressing GFP tagged MKLP2 to visualize if the dots display fusion and fission. Moreover, by Fluorescence Recovery After Photobleaching (FRAP) of MKLP2::GFP we can determine if the molecular dynamics of MKLP2 changes when it appears in a dot then when bound to the antiparallel MT overlaps of the spindle midzone (Alberti et al., 2019). Finally, it would be interesting to follow the localization of MKLP2 and the CPC in the absence of MAP7 proteins over time be live cell imaging. From the moment that the CPC leaves the chromatin in early anaphase to midbody formation in telophase. Do the foci form immediately after removal of the CPC from the chromosomes? And do they gradually coalesce when the furrow ingresses and do they ultimately accumulate in the midbody?

In conclusion, we have uncovered a role for MAP7 proteins in specifying the localization of MKLP2 and the CPC to the spindle midzone anaphase. This specific localization does not seem to be critical for successful cytokinesis. However, given the redundancy in the signalling pathways that regulate cytokinesis, the MAP7 protein-controlled localization of MKLP2/CPC may only become apparent when the robustness of cytokinesis is weakened in mammalian cells. In addition, we did not analyse anaphase timing, anaphase spindle formation or stability. Therefore, further study is needed to assess the function of the MAP7 proteins during anaphase.

Acknowledgments

We thank Drs M. Glotzer for his generous gift of reagents and Dr. H.R. Vos for proteomics support. This work is financially supported by The Netherlands Organization for Scientific Research (NWO-Vici 91812610 to S.M.A.L and NWO ALW Open Program grant 824.15.017 to A.A.). Proteomics was supported by the Proteins at Work Initiative (NWO 184.032.201). The group of S.M.A.L is part of Oncode Institute which is partly financed by the Dutch Cancer Society.

The authors declare no competing financial interests.

Material and methods

Cell lines and tissue culture

HeLa cell lines were cultured in DMEM (Sigma-Aldrich) supplemented with 6% Fetal Calf Serum (FCS, Sigma-Aldrich), 2mM UltraGlutamine and 100 units/ml penicillin and 100 μg/ml Streptomycin (Lonza). Human embryonic kidney 239T (HEK293T) cells were cultured in DMEM (Sigma-Aldrich) supplemented with 10% Fetal Calf Serum (FCS, Sigma-Aldrich), 2mM UltraGlutamine and 100 units/ml penicillin and 100 μg/ml Streptomycin (Lonza). Cell lines were grown at 37°C with 5% CO2. HeLa MAP7, MAP7D1 and MAP7D3 knockout cell lines were previously made using CRISPR-Cas9 (Hooikaas et al., 2019; Ran et al., 2013).

siRNA and plasmid transfection

MAP7D1 and MAP7D3 were knocked-down by transfection of 100 nM siRNA for each target using HiPerfect (Qiagen). The siRNAs used were siMAP7D1 (5′-TCATGAAGAGGACTCGGAA-3′), siMAP7D3 (5′-AACCTACATTCGTCTACTGAT-3′), and siLuciferase as a control (5′-TCGAAGTATTCCGCGTAC G-3′). A standard HiPerfect transfection protocol was used with a 3:1 ratio for siRNA:HiPerfect in Opti-MEM. Incubation of siRNA/HiPerfect mixture was done at 37°C for 20 minutes. HEK293T cells were transfected with eGFP-N1 empty, full length MKLP2::GFP, MKLP2 1-513::GFP, MKLP2 765-890::GFP, MKLP2 498-980::GFP and MKLP2 498-765::GFP, pBio-mCherry empty, pBio-mCherry::MAP7, pBio-mCherry::MAP7 N-term (aa1-301,d176-212), pBio-mCherry::MAP7 C-term (aa301-749), pBio-mCherry::MAP7D1, pBio-mCherry::MAP7D2 and pBio-mCherry::MAP7D3 using Polyethylemimine (PEI) transfection with a 3:1 ratio for plasmid/PEI. For the production of purified MKLP2 a pTT5 MKLP2::GFP::StrepII plasmid was used.

Cell synchronization and treatment

For live cell imaging and IF of anaphase cells, HeLa cells were plated in 2.5 mM thymidine (Sigma-Aldrich) for 24 h and released into 5 μM RO3306 (Calbiochem) for 16 h. Cells were released from the RO3306 block by washing three times with medium. HeLa cells were either filmed immediately after release from RO3306 or fixed 60 min after RO3306 release. Where indicated, cells were treated with the following drugs prior to fixation: Cytochalasin B (5 μg/m for 30 minutes, Sigma), nocodazole (5 μM for 10 minutes, Sigma) and NH_4OAc (90 mM for 2 minutes, Sigma).

Immunoprecipitation

HEK293T cells transfected with MKLP2::GFP constructs or pBio-mCherry-MAP7 constructs were collected in ice cold PBS and washed. Cells were lysed in lysis buffer (50 mM Tris-HCl, 150mM NaCl, 0.5% NP-40, 0.1% sodium deoxycholate, 40mM Glycerol phosphate, 10mM NaF, 0.3mM NaVO3, 100 µM ATP, 100 µM MgCl2, 100 nM, mM Okaidic Acid and supplemented with protease inhibitors (Roche)) with 4U/ml MNase (New England Biolabs) and 30 µg/ml RNase (Sigma). After clearing debris by centrifugation, a standard Bradford assay was performed to measure protein concentration and cell lysates were incubated with GFP-Trap beads (Chromotek) for 2 hours at 4°C while rotating. GFP-Trap or RFP-Trap Beads (Chromotek) were washed 3 times with wash buffer (50 mM Tris-HCl, 400 mM NaCl, 0.5% NP-40, 0.1% sodium deoxycholate, 40mM glycerol phosphate, 10mM NaF, 0.3 mM NaVO3, 100 µM ATP, 100 µM MgCl2, 100 nM, mM okaidic acid and supplemented with protease inhibitors (Roche)). Proteins were eluded by adding standard SDS samples buffer and boiling the samples for 5 minutes and stored at -20°C until SDS-page and western blotting.

Western blotting

Mitotic HeLa parental or MAP7 KO cells were collected and lysed in standard Laemmli buffer. Protein concentration was determined using a Lowry assay. Protein samples of either whole cell extracts or IP's were separated by SDS-PAGE and transferred to nitrocellulose membranes. Membranes were blocked in 4% milk in Tris-buffered saline containing 0.5% Tween-20 (TBST) and subsequently incubated with a primary antibody for 2 hrs. Primary antibodies used were rabbit anti-MKLP2 (Bethyl (ITK) A300-879A), rabbit anti-Borealin (gift from Dr. S. Wheatley), rabbit anti-Survivin (R&D Systems AF886), rabbit anti-MAP7D1 (Sigma, A97171), rabbit anti-MAP7D2 (Sigma, R61350), rabbit anti-MAP7D3 (Sigma, A114972), rat anti-RFP (Chromotek, 5F8) and rabbit anti-MAP7 (Abnova, H00009053-B01P). After washing the membranes with TBST, they were incubated with horseradish peroxidase (HRP)-conjugated secondary antibodies (Bio-Rad). An ECL chemiluminescence detection kit (GE Healthcare) was used to visualize the protein/antibody complex.

Protein purification for microtubule tracking experiment and Mass Spectrometry

HEK293T cells transfected with pTT5 MKLP2::GFP::StrepII or GFP::StrepII were collected and washed twice in ice-cold PBS. Cells were lysed in ice-cold lysis buffer (50 mM HEPES, 300 mM NaCl, 0.5% Triton X-100, pH 7.4) supplemented with protease inhibitors (Roche). After clearing debris by centrifugation at 4°C, cell lysates were incubated with StrepTactin beads (StrepTactin Sepharose High Performance, GE Healthcare) for one hour at 4°C. Beads were washed 3 times with ice cold washing buffer (50 mM HEPES, 150 mM NaCl, 0.01% Triton X-100). Beads were washed an additional time with a high salt wash buffer (1M NaCl) except for the Mass Spectrometry samples. The proteins were subsequently eluted in elution buffer (50 mM HEPES, 150 mM NaCl, 0.01% Triton X-100 and 2.5 mM desthiobiotin) for 10 min. Protein concentration was determined by SDS-PAGE and Coomassie Blue staining using InstantBlue (Expedeon), using purified BSA titration as a reference. Purified proteins were snap-frozen and stored at −80°C. Purified MAP7 protein from E. coli was produced previously (Hooikaas et al., 2019).

Sample preparation for and mass spectrometry

Eluted MKLP2::GFP::StrepII or GFP::StrepII samples were first denatured and alkylated by adding alkylation buffer (10 mM tris(2-carboxyethyl)phosphine (TCEP), 40 mM 2-chloroacetamide (CAA), 8 M urea, 1 M ammonium bicarbonate. After 30 min of incubation, Trypsin/Lys-C protease (Promega) was added to the samples and left for overnight digestion at 37°C on a shaker. The samples were cleaned up using homemade C18 stagetips (Rappsilber et al., 2007), and used for the analysis with LC-MS (Thermo Easy-nLC 1000, Thermo Orbitrap Fusion Tribrid) running a 140 min gradient (300 nl/min, 30 cm 1.9 µm C18 column) with 240k (at 200 m/z) full MS resolution and a 1 s MS2 duty cycle (top speed, highest to low intensity, HCD fragmentation). Raw files were analysed with Maxquant software, version 1.6.3.4. For identification, the Human Uniprot database was searched with oxidation and carbamidomethylation of cysteine set as fixed modification, while peptide and protein false discovery rates were set to 1%. The intensity of the values was plotted as Log2 transformed values with a black line (x=0) added as visual aid.

Immunofluorescence

Cells were grown on 12 mm High Precision coverslips (Superior-Marienfeld GmbH & Co). Cells were fixed with 4% PFA in PBS for 7 minutes and permeabilized in in 0.25% Triton X-100 in PBS for 5 minutes. Cells were blocked with PBS containing 3% BSA and 0.1% Tween-20. Primary antibodies used were rabbit anti-KIF20A (Bethyl (ITK) A300-879A), rabbit anti-PRC1 (Santa Cruz sc-8356), mouse anti-Aurora B (BD Transduction labs 611083), mouse anti-α-tubulin (Sigma, T5168), rabbit anti-MAP7D1 (Sigma, A97171), rabbit anti-MAP7D3 (Sigma, A114972), rabbit anti-MAP7 (Abnova, H00009053-B01P), mouse anti-PLK1 (Santa Cruz, sc-17783), rabbit anti-anillin (kind gift of Dr. M. Glotzer), phalloidin-Alexa 633 (Invitrogen, A22284), mouse anti-EB1 (BD, 610534) and rabbit anti-phosphoINCENP S893/894 (kind gift of Dr. M. Lampson (Salimian et al., 2011)). Secondary antibodies used were goat anti-mouse or goat anti-rabbit IgG-Alexa 488, goat anti-mouse or goat anti-rabbit IgG-Alexa 568 (Invitrogen). 4',6-Diamidino-2-Phenylindole (DAPI) was used for DNA staining and coverslips were mounted using ProLong Antifade (Molecular Probes).

Imaging of fixed cells

Images of fixed cells were taken with a Personal DeltaVision system (Applied Precision) equipped with a 100x / NA 1.40 UPLS Apo-UIS2 objective (Olympus) and a CoolSNAP HQ CCD camera (Photometrics). Images were deconvolved in Softworx. For each experiment all images were acquired with identical illumination settings. Images are projections of deconvolved Z-stacks, unless stated otherwise.

Live cell microscopy

Cells were seeded in µ-Slides (ibiTreat; Ibidi). Medium was changed to Leibovitz's medium (Sigma-Aldrich) supplemented with 10% FCS (FBS; Sigma-Aldrich), 2 mM UltraGlutamine, and 100 U/ml penicillin and 100 µg/ml streptomycin (Lonza) before live cell imaging. Images were acquired using an Olympus IX-81 microscope with a 20× DIC UPLFLN NA 0.5 objective and a Hamamatsu ORCA-ER CCD camera and a 37°C heated chamber, controlled by Cell-M software. Movies were scored for the occurrence of ingression and regression for 12 hours.

Microtubule tracking experiment

In vitro reconstitution assays were imaged on a TIRF microscope setup as described previously (Mohan et al., 2013, and in Chapter 3).

Statistical analysis and computer software

Image analysis was performed with Fiji image processing software (ImageJ). Statistical analysis was performed with Prism 7 software

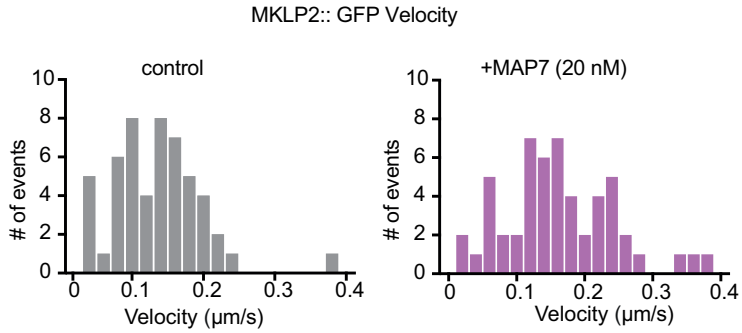

Supplemental figure 1: Histograms of MKLP2 velocities
Histograms of MKLP2::GFP velocities. n = 73 for both conditions from one experiment. Histograms correspond to the velocity fits shown in Figure 2B.

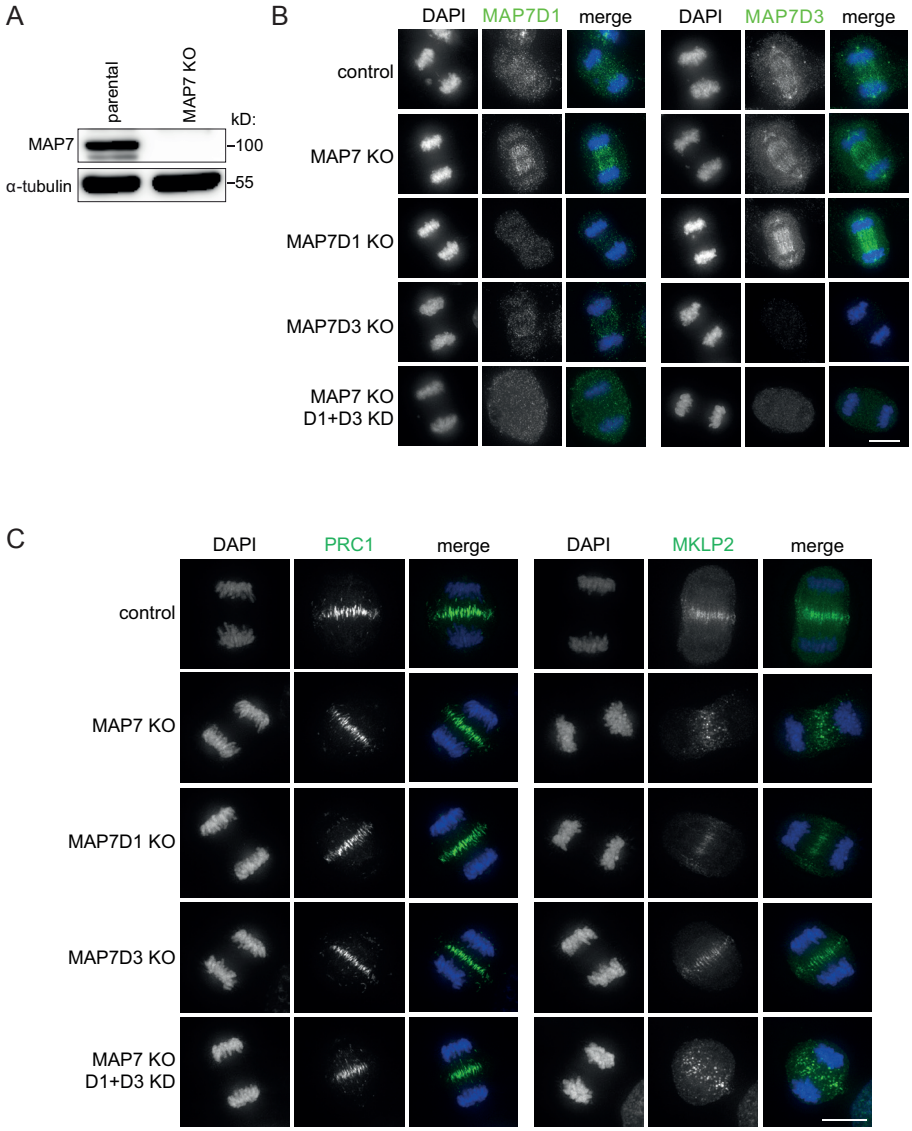

Supplemental figure 2: Analysis of parental HeLa cell line and the MAP7 KO, MAP7D1+D3 KD HeLa cells.
A) Western blot of parental or MAP7 KO HeLa cells probed with anti-MAP7 antibody. α-tubulin is shown as loading control. B) IF for MAP7D1 and MAP7D3 in control cells, MAP7, MAP7D1 or MAP7D3 KO cells or MAP7 KO cells with MAP7D1 and MAP7D3 knock-down by siRNA. DNA was visualized using DAPI. Scale bar = 10 µm. C) IF for PRC1 and MKLP2 in control cells, MAP7, MAP7D1 or MAP7D3 KO cells or MAP7 KO cells with MAP7D1 and MAP7D3 knock-down by siRNA. DNA was visualized using DAPI. Scale bar = 10 µm.

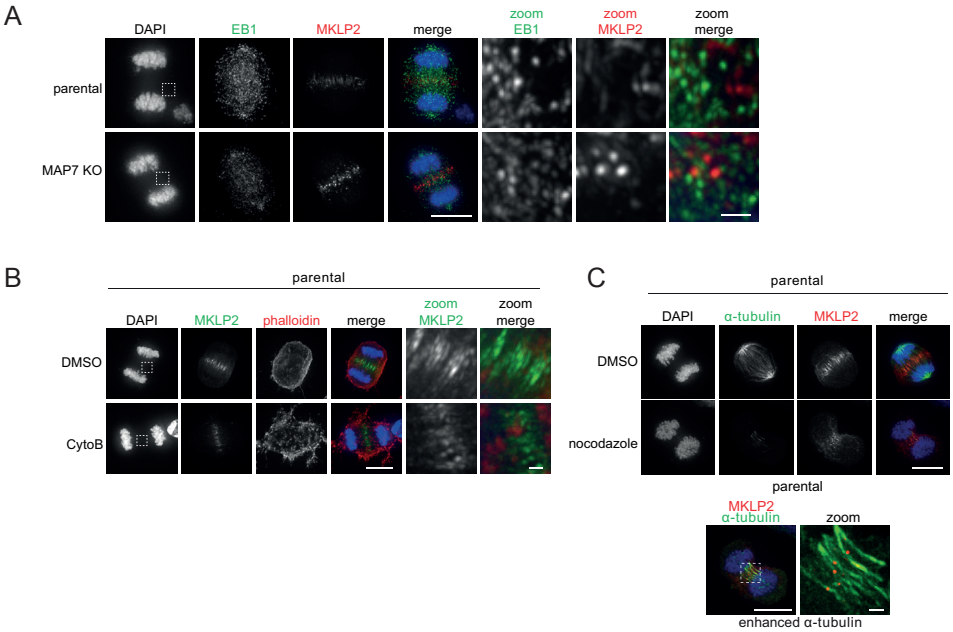

Supplemental figure 3: The alternative MKLP2 and CPC localization in cells lacking MAP7 proteins is microtubule dependent

A) IF of EB1 and MKLP2 in the parental HeLa cell line and in MAP7 KO cells. Scale bar = 10 μm and 1 μm in zoom. Squares in DAPI images indicate enlarged area in zoom. B) IF of MKLP2 and actin (detected with phalloidin) in the parental HeLa cell line, treated with or without Cytochalasin B (5 μg/m for 30 minutes). Scale bar = 10 μm and 1 μm in zoom. Squares in DAPI images indicate enlarged area in zoom. C) IF of α-tubulin and MKLP2 in the parental HeLa cell line, with or without nocodazole (5 μM for 10 minutes). Scale bar = 10 μm. D) Enhancement of α-tubulin and MKLP2 fluorescent signal of nocodazole-treated cell from (C) Scale bar = 10 μm and 1 μm in zoom. Square in DAPI image indicates enlarged area in zoom.

Chapter 5

Summarizing discussion

Ingrid E. Adriaans

Summarizing discussion

Cytokinesis drives the physical separation of daughter cells at the end of mitosis, and failure to either initiate or complete cytokinesis gives rise to cells with twice the number of chromosomes and centrosomes. Because these cells are at risk of becoming aneuploid, proper execution and completion of cytokinesis is essential for genomic stability.

A spindle midzone- and PLK1-independent route to cytokinesis initiation

In animal cells, cytokinesis starts in anaphase with the formation of an actomyosin-based contractile ring. The ring forms at the equatorial cortex and drives ingression of the cleavage furrow. Formation and contractility of the contractile ring requires activation of the small GTPase RhoA by the Guanine Nucleotide Exchange Factor (GEF), ECT2, at the equatorial cortex. The current models on how spatiotemporal activation of RhoA and subsequent cleavage furrow ingression is achieved in mammalian cells, emphasize an important role for the anaphase spindle midzone, for Polo-like kinase-1 (PLK1) (Burkard et al., 2009; Brennan et al., 2007; Wolfe et al., 2009; Petronczki et al., 2007), and for a tetrameric protein complex consisting of RACGAP1 and MKLP1, known as centralspindlin (Somers and Saint, 2003; Yüce et al., 2005; Nishimura, 2006). PLK1 is recruited to the spindle midzone by Protein Regulator of Cytokinesis 1 (PRC1), where it phosphorylates RACGAP1 of the centralspindlin complex. This phosphorylation event results in the activation of ECT2 (Petronczki et al., 2007; Burkard et al., 2009; Wolfe et al., 2009). In this prevailing model PRC1 *promotes* RhoA activity by recruiting PLK1 to the spindle midzone. In **chapter 2** we uncover an alternative route to cytokinesis initiation that is *inhibited* by PRC1, which changes the current view on how cleavage furrow ingression in mammalian cells is regulated (Figure 1).

The starting point of the study described in **chapter 2**, was the observation that knock-down of PRC1, which disrupts the organization of the spindle midzone, does not impair RhoA activation and cleavage furrow ingression in mammalian cells (Jiang et al., 1998; Mollinari et al., 2005; Zhu and Jiang, 2004; Zhu et al., 2006). This implied that spindle midzone-independent cues could specify and activate RhoA in mammalian cells. Indeed, we show in **chapter 2** that in the absence of PRC1, RhoA is activated at the equatorial cortex by cortical Aurora B activity and centralspindlin (Figure 1). Remarkably, we find that in PRC1-deficient cells, cytokinesis can be initiated in the absence of PLK1 activity, and we provide evidence that this alternative, PLK1-independent, route to RhoA activation has gone unnoticed because of an unrecognized inhibitory effect of PLK1 on PRC1 in anaphase. We demonstrate that PLK1 acts as a “brake” on PRC1 in anaphase which most likely serves two purposes: it limits PRC1’s microtubule bundling activity allowing elongation of the anaphase spindle (unpublished observations), and second, it promotes the release of a pool of centralspindlin from the spindle midzone, to activate ECT2 and RhoA at the equatorial cortex (Figure 1).

How PLK1 regulates PRC1 in anaphase is not yet fully understood. We deem it likely that it might be similar to the way it is inhibited before anaphase onset (Hu et al., 2012b). In (pro)metaphase and anaphase PRC1 is directly phosphorylated by PLK1 on multiple sites, including T602 (Hu et al., 2012b; Neef et al., 2007). Mutation of this site into alanine was shown to mimic the effect of PLK1 inhibition in metaphase, which

is the premature recruitment of PRC1 and centralspindlin (RACGAP1 and MKLP1) to the metaphase spindle (Hu et al., 2012b). Expressing the PRC1 T602A mutant in a PRC1 knock-down background could reveal if this mutant has a similar effect on centralspindlin sequestering on the anaphase spindle midzone as PLK1 inhibition. Moreover, it would be interesting to see if this mutant induces hyperbundling of the microtubules of the anaphase spindle, similar to PLK1 inhibition (chapter 2). If not, then it would indicate that the sequestration of centralspindlin is directly linked to (phosphorylated) PRC1 instead of an indirect consequence of MT hyperbundling by overactive PRC1. Although a seemingly simple experiment, it appears challenging to avoid artefacts caused even by only mild overexpression of PRC1 (Hu et al., 2012 and unpublished observations). An *in vitro* approach with recombinant fluorescently labeled PRC1, PLK1 and tubulin and TIRF microscopy might be a more suitable way to study how active PLK1 affects the microtubule bundling and spindle midzone organizing activity of PRC1 (Bieling et al., 2010; Hannabuss et al., 2019).

How does Aurora B activate ECT2 at the equatorial cortex?

Previous studies demonstrated that the phosphorylation of RACGAP1 by PLK1 is an important requirement for the activation of ECT2 (Petronczki et al., 2007; Burkard et al., 2009; Wolfe et al., 2009). However, in **chapter 2**, we show that cytokinesis can be initiated in the absence of PLK1 activity, when PRC1 is absent. We show that in this condition Aurora B activity is critical for cytokinesis initiation, but it is unclear how Aurora B activates ECT2 at the equatorial cortex. Cytokinesis initiation in Aurora B inhibited cells is partially restored by expression of a phosphomimic mutant of an Aurora B site in MKLP1 (S708E). Since MKLP1 and RACGAP1 work in a heterotetrameric complex during anaphase (Mishima et al., 2002; Pavicic-Kaltenbrunner et al., 2007), we hypothesize that the phosphorylation of MKLP1 by Aurora B replaces the function of PLK1 in activating ECT2 via RACGAP1. The phosphorylation of S708 in MKLP1 by Aurora B disrupts the interaction between MKLP1 and 14-3-3 proteins, permitting centralspindlin oligomerization (Guse et al., 2005; Douglas et al., 2010; Basant et al., 2015). Oligomerization was shown to be important for centralspindlin localization and function on the spindle midzone in mammalian cells, and for RhoA activation at the equatorial cell membrane in one-cell C.elegans embryos (Basant et al., 2015; Hutterer et al., 2009). It is however not yet clear for human cells if it is in fact the oligomerization of centralspindlin that activates ECT2, or whether the phosphorylation of MKLP1 provides some sort of binding and activation site for ECT2, either directly or indirectly via the dissociation of 14-3-3 proteins. The most intuitive explanation is that there is already some affinity of ECT2 for RACGAP1 even without PLK1 phosphorylation and that the Aurora B induced oligomerization of centralspindlin catalyzes the activation of ECT2 (Basant and Glotzer, 2018; Wolfe et al., 2009; Burkard et al., 2009).

The MKLP1 T708E mutant accumulated in the equatorial cortex in Aurora B inhibited cells, suggesting that, similar to the situation in C. elegans embryos, centralspindlin clustering contributes to its cortical localization (Basant et al., 2015). Yet, the capacity to rescue furrow ingression in Aurora B inhibited cells was limited, most likely because other Aurora B substrates are not phosphorylated. Candidate substrates of Aurora B that may contribute to cytokinesis initiation are RACGAP1, vimentin, desmin, myosin II light chain and the PP1β/MYPT1 phosphatase (Goto et al., 2003; Yokoyama et al., 2005; Hengeveld et al.,

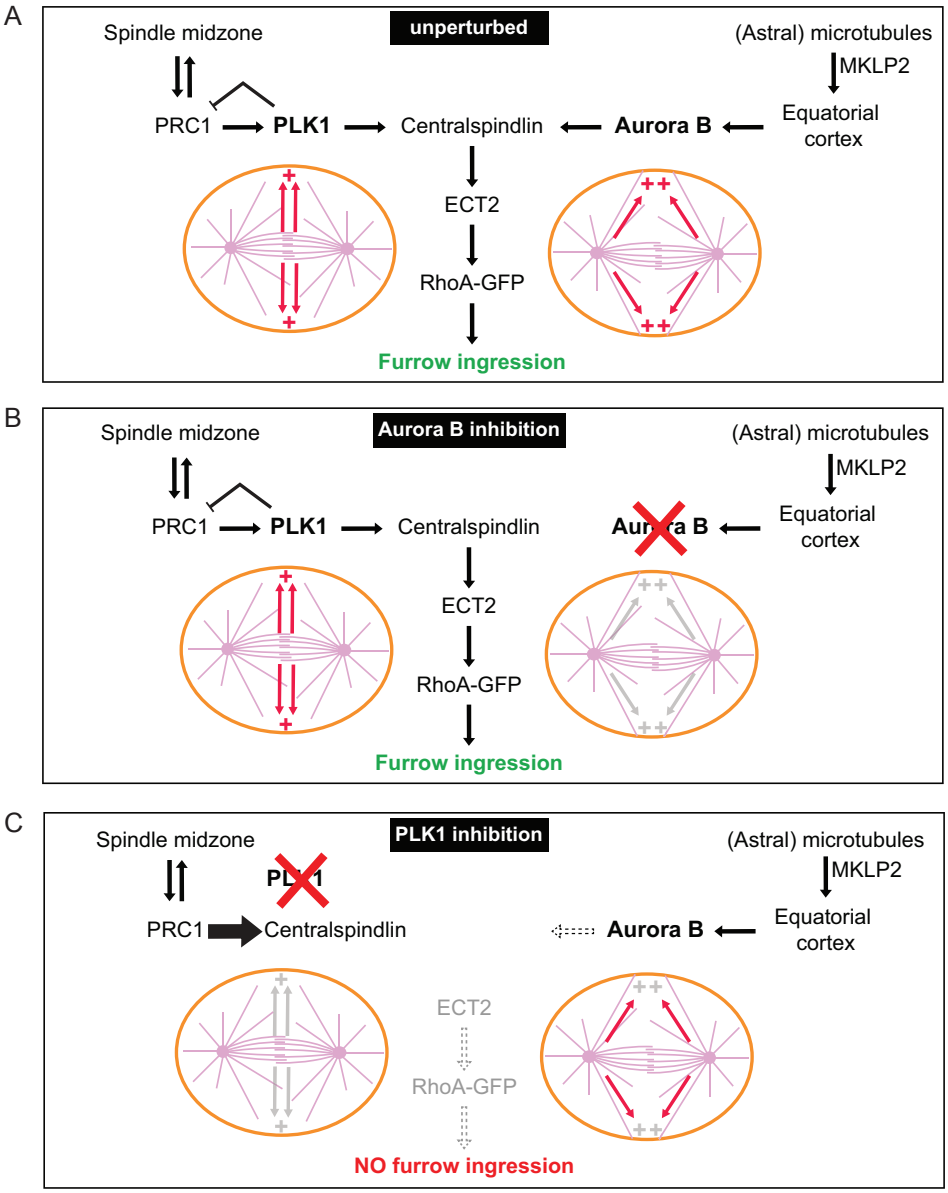

Figure 1: Scheme of the PLK1 and Aurora B dependent pathways that initiate furrow ingression
Summary of how PLK1 and Aurora B activate centralspindlin, ECT2 and RhoA and initiate furrow ingression. (A) PRC1 is required for formation of the spindle midzone and recruits PLK1 to the spindle midzone. Through phosphorylation of RACGAP1 in centralspindlin, PLK1 activates ECT2, and thereby RhoA. In a parallel pathway, Aurora B at the equatorial cortex phosphorylates MKLP1 in centralspindlin which induces its oligomerization and thereby activates ECT2. Aurora B is transported towards the equatorial cortex along (astral) microtubules by MKLP2. (B) In the absence of Aurora B activity, the spindle midzone and PLK1 pathway are sufficient to initiate cytokinesis. (C) Inhibition of PLK1 has two effects. RACGAP1 is not phosphorylated and because PLK1 acts as a brake on PRC1, in the absence of PLK1 activity, PRC1 (either directly or through hyperbundling of the spindle midzone microtubules) sequesters centralspindlin away

from the equatorial cortex. As a consequence, Aurora B at the equatorial cortex is unable to phosphorylate and therefore centralspindlin does not oligomerize and cytokinesis initiation fails.

2012; Minoshima et al., 2003; Kawajiri et al., 2003; Murata-Hori et al., 2000). We mutated the Aurora B phosphorylation sites of RACGAP1 and tested if furrow ingression was blocked when PRC1 was absent. However, the RACGAP1 phospho-dead mutant rescued furrow ingression (unpublished observations). This could mean that RACGAP1 phosphorylation by Aurora B is not relevant for cytokinesis initiation or that furrow ingression is only blocked when all Aurora B substrates are not phosphorylated. Vimentin and desmin are intermediate filaments that are part of the cytoskeleton. Aurora B phosphorylates vimentin and desmin at the equatorial cortex which is needed for their removal from the division site (Goto et al., 2003; Kawajiri et al., 2003). Clearly, myosin II light chain and the PP1β/MYPT1 phosphatase are important for contraction of the cytokinetic ring, and Aurora B seems to phosphorylate the same residues in myosin II light chain and the PP1β/MYPT1 phosphatase as ROCK1 (Yokoyama et al., 2005; Murata-Hori et al., 2000). Aurora B has many more targets, such as Septin1 and SHCBP1 (SHC binding and spindle associated 1), but these seem to be more important for the later stages of cytokinesis than for cytokinesis initiation (Qi et al., 2005; Asano et al., 2013). Moreover, more cytokinesis targets of Aurora B could still be out there. Phospho-proteomic screens using Aurora B inhibitors identified potential substrates such as several motor proteins (MCAK, KIF2A, KIF4A, KIF3A) and the RhoA guanine activating protein, ArhGAP12 (Hengeveld et al., 2012; Kettenbach et al., 2011; Hegemann et al., 2011). The role of these proteins in spindle midzone-independent cytokinesis initiation is of great interest.

Aurora B regulates several phases of cytokinesis

The work described in chapter 2 implies that in PRC1-proficient cells, PLK1 recruited to the spindle midzone by PRC1, is sufficient to initiate cytokinesis when Aurora B is inactive. This is based on the observation that when Aurora B is inhibited during metaphase or in very early anaphase, furrow ingression takes place. Thus, in the early phase of cytokinesis, Aurora B plays a more redundant role, while later on its function becomes non-redundant because the furrow regresses and cytokinesis fails when Aurora B is inhibited (Figure 2 and chapter 2). This is most likely caused by inhibition of the pool of Aurora B that is localized on the spindle midzone (Figure 1. MKLP1 is also an important Aurora B target on the spindle midzone (Guse et al., 2005; Neef et al., 2006). Phosphorylation of MKLP1 contributes to the bundling of midzone microtubules which is important for the stability of the spindle midzone and for formation of the midbody (Hutterer et al., 2009; Douglas et al., 2010). In fact, MKLP1 together with RACGAP1 helps to tether the ingressed cell membrane to the midbody (Hutterer et al., 2009; Lekomtsev et al., 2012), and failure to do so may explain why the furrow regresses when Aurora B is inactive (Guse et al., 2005; Ahonen et al., 2009; Steigemann and Gerlich, 2009; Adriaans et al., 2019). Interestingly, Aurora B inhibition during telophase, when cells have completed furrow ingression, leads to early abscission (Figure 2) (Steigemann and Gerlich, 2009), and it was recently demonstrated that the Aurora B-dependent phospho marks on MKLP1 need to be removed by the PP1β/MYPT1 phosphatase to facilitate microtubule disassembly at the midbody, which is critical for abscission (Capalbo et al., 2019). Together with the phosphorylation of several other substrates in the midbody, such as MKLP2 and the ESCRT III component CHMP4C

(Capalbo et al., 2019; Carlton et al., 2012; Fung et al., 2017) Aurora B activity controls abscission timing (Steigemann et al., 2009).

The redundant role of Aurora B during cytokinesis initiation contrasts earlier observations in cells where Aurora B or the non-enzymatic subunits of the CPC were knocked-down by siRNA, or where Aurora B kinase activity was inhibited when cells entered mitosis (Figure 2). In these conditions cytokinesis was hardly ever initiated (Kaitna et al., 2000; Adams et al., 2001; Giet and Glover, 2001; Kallio et al., 2002; Murata-Hori et al., 2002; Guse et al., 2005; Lens et al., 2003; Wheatley et al., 2004). This was explained by the fact that the lack of Aurora B activity during mitosis has dramatic consequence for chromosome biorientation and congression and hence in anaphase chromosomes massively mis-segregate and are not cleared from the midzone. This chromatin mass somehow physically hampers furrow ingression (Norden et al., 2006; Steigemann et al., 2009). However, if so, then why is furrow ingression not blocked when the mitotic checkpoint is silenced by for instance knock-down of MAD2 or inhibition the checkpoint kinase MPS1 (Santaguida et al., 2017; Tighe et al., 2008; Gorbsky et al., 1998; Meraldi et al., 2004)? In the absence of a functional mitotic checkpoint, cells do not delay anaphase onset until all chromosomes are connected to microtubules of the mitotic spindle (Corbett, 2017). Consequently, cells enter anaphase with many chromosomes lagging behind in the midzone, yet cytokinesis is initiated and completed, with the furrow cutting through the chromatin (Santaguida et al., 2017; Tighe et al., 2008; Gorbsky et al., 1998; Meraldi et al., 2004). We propose that the inhibition of Aurora B in early mitosis might lead to a malformed spindle midzone that is unable to localize PRC1 and PLK1, and that it thus cripples the spindle midzone-dependent route to furrow ingression. Hence, it mimics a state of Aurora B inhibition in the absence of PRC1.

MKLP2 takes the CPC where it needs to go

We show in chapter 2 that a pool of Aurora B, localized at the equatorial cortex, drives cytokinesis initiation when the spindle midzone is perturbed. Accumulation of Aurora B and the other members of the CPC at the equatorial cortex requires the presence of microtubules and of MKLP2, a member of the kinesin-6 subfamily of motor proteins. This has led to the hypothesis that the CPC is transported along microtubules by MKLP2 towards the equatorial cortex (Murata-Hori and Wang, 2002; Gruneberg et al., 2004; Hümmer and Mayer, 2009; Kitagawa et al., 2013). However, evidence supporting this model was lacking. In **chapter 3**, we used microscopy-based *in vitro* reconstitution assays with purified proteins, which allowed us to demonstrate that MKLP2 is a processive plus-end directed motor. Interestingly, we find that the presence of CPC proteins, increases the processivity of MKLP2. Whilst MKLP2 is a substrate of Aurora B (Fung et al., 2017), Aurora B kinase activity did not have an effect on MKLP2 motor capabilities, as CPC complexes with either active or inactive Aurora B had similar effects on kinesin velocity and processivity. This seems in line with the observation in cells, where the translocation of CPC from the centromeres in (pro)metaphase to the spindle midzone and equatorial cortex in anaphase does not rely on Aurora B kinase activity but does require ATPase activity of MKLP2 (Kitagawa et al., 2013; Gruneberg et al., 2004; Kitagawa et al., 2014; Adriaans et al., 2019; Tcherniuk et al., 2010; Guse et al., 2005). However, the relocation of the CPC seems to involve several steps: the dissociation of the protein complex from the

centromeres and chromatin, the binding to microtubules, and presumably motor-dependent microtubule-based transport towards the equatorial cortex and potentially towards the spindle midzone (chapter 3). The dissociation from the centromeres is most likely caused by the dephosphorylation of the histones that act as centromeric receptors for the CPC before anaphase (van der Horst et al., 2015). Yet, all the other steps involve MKLP2, even the dissociation from chromatin since the prime phenotype of MKLP2 knock-down or early inhibition of MKLP2 with paprotrain is, the retention of the CPC (and of MKLP2) on the anaphase chromosomes (Kitagawa et al., 2013; Gruneberg et al., 2004; Hümmer and Mayer, 2009; Kitagawa et al., 2014; Adriaans et al., 2019; Tcherniuk et al., 2010)). We deem it not very likely that chromatin retention is caused by a lack of microtubule-based transport but propose that chromatin removal of the CPC and MKLP2 might be another function of MKLP2 that requires its ATP-ase activity (Tcherniuk et al., 2010). To reveal MKLP2's microtubule-based transport function in cells, we attempted to inhibit MKLP2 after this chromatin removal step. Indeed, properly timed addition of paprotrain showed that after initial chromatin removal, MKLP2 kinesin activity is required for the localization of MKLP2 and the CPC towards the equatorial cortex and to a lesser extend to the spindle midzone. Combined with the observed directed movements of MKLP2 and the CPC scaffold protein INCENP in living cells, we propose that control of cytokinesis initiation by Aurora B requires its directional MKLP2-dependent transport towards the equatorial cortex.

Are MAP7 proteins the signs that lead the way?

In early anaphase cells, only a small fraction of MKLP2 and INCENP molecules showed directed motility indicative of motor transport. Most of MKLP2 and INCENP appeared stationary at the spindle midzone and in line with previous work from Landino *et al.* (Landino et al., 2017), we also observed diffusive behavior. What makes only some MKLP2/CPC complexes move along microtubules whilst others attach stably to the spindle midzone? We hypothesized that certain Microtubule Associated Proteins (MAPs) could either influence MKLP2 kinesin activity or specify microtubule populations on which MKLP2 could walk. In **chapter 4**, we aimed to identify MKLP2-interacting proteins using mass spectrometry and confirmed the Microtubule Associated Protein 7 (MAP7/Ensconsin) and MAP7 Domain-containing protein 2 (MAP7D2) as binding partners of MKLP2. Moreover, also MAP7D1 and MAP7D3 weakly interacted with MKLP2. Although MAP7D2 appeared to bind MKLP2 with high affinity, it is only expressed in neuronal tissue and in some cell lines such as HEK293T (Niida and Yachie, 2011; Lin et al., 2014), and we therefore directed our functional analysis to the other three MAP7 proteins. In the absence of MAP7 and more dramatically in the combined absence of MAP7, MAP7D1 and MAP7D3, the distribution of MKLP2 and the CPC was altered in HeLa cell anaphases. MKLP2 and the CPC no longer localized to the antiparallel microtubule overlaps of the spindle midzone, but appeared as foci that were distributed between the segregating chromosomes. The appearance of the MKLP2/CPC foci resembled liquid-liquid phase separation, but whether MKLP2 and the CPC truly phase separate in anaphase in the absence of MAP7 proteins requires further investigation. Irrespective of the biophysical properties of the foci, our findings suggest an involvement of MAP7 proteins in the anchoring of MKLP2 and the CPC to the antiparallel microtubule overlaps of the spindle midzone. Although cytokinesis is executed successfully in the absence of MAP7 proteins, this does not exclude a role for the MAP7 proteins in anaphase spindle

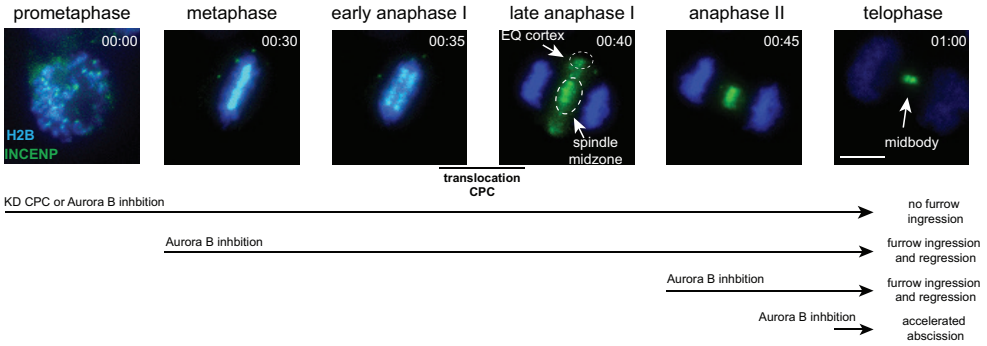

Figure 2: Consequences of a crippled CPC on cytokinesis
Stills of U2OS cells stably expressing H2B::mCherry and INCENP::GFP and going through mitosis and cytokinesis. CPC pools at the spindle midzone, equatorial cortex (EQ) and midbody are indicated with a white arrow. Note that the translocation of the CPC occurs after an initial separation of the sister chromatids. The consequence of CPC knockdown (KD) or Aurora B inhibition at different timepoints during mitosis and cytokinesis are indicated. Scale bar = 10 μm. Time is indicated in upper right corner (hours:minutes).

stability and/or elongation, and needs to be studied.

Moreover, in future *in vitro* microtubule tracking experiments, we would like to test the effect of all four MAP7 proteins on motility and microtubule binding of MKLP2. We find that MAP7 does not affect microtubule binding, velocity and processivity of MKLP2 (chapter 4), yet preliminary experiments suggest that MAP7D3 may have a strong inhibitory effect on MKLP2's interaction with microtubules (data not shown). This implies that highly similar proteins may have very different effects on MKLP2 function. Interestingly, MAP7D3 was identified as an Aurora B substrate and MAP7 and MAP7D1 as Aurora A substrates (Kettenbach et al., 2011). Although we show that Aurora B kinase activity does not influence MKLP2 motor function *in vitro*, in cells it might do so indirectly through phosphorylation of MAP7 proteins.

Overall conclusion

Overall, the work described in this thesis highlights the robustness and plasticity of cytokinesis in mammalian cells, and provides novel insights into the regulation of cytokinesis. In short, we have uncovered a PLK1-independent route to cytokinesis initiation that depends on a cortical-associated pool of Aurora B. Moreover, we provide the first demonstration that MKLP2 is a motile kinesin that can transport Aurora B and its associated CPC members along microtubules towards the equatorial cortex. And finally, we show that MAP7 proteins interact with MKLP2 and play a role in anchoring MKLP2 and the CPC to the antiparallel microtubule overlaps of the spindle midzone.

Addenda

References

Nederlandse samenvatting

Curriculum vitae

References

Adams, R.R., H. Maiato, W.C. Earnshaw, and M. Carmena. 2001. Essential roles of Drosophila inner centromere protein (INCENP) and aurora B in histone H3 phosphorylation, metaphase chromosome alignment, kinetochore disjunction, and chromosome segregation. *J. Cell Biol.* 153:865–80.

Adriaans, I.E., A. Basant, B. Ponsioen, M. Glotzer, and S.M.A. Lens. 2019. PLK1 plays dual roles in centralspindlin regulation during cytokinesis. *J. Cell Biol.* 218:1250–1264.

Ahonen, L.J., A.M. Kukkonen, J. Pouwels, M.A. Bolton, C.D. Jingle, P.T. Stukenberg, and M.J. Kallio. 2009. Perturbation of Incenp function impedes anaphase chromatid movements and chromosomal passenger protein flux at centromeres. *Chromosoma*. 118:71–84.

Ainsztein, A.M., S.E. Kandels-Lewis, A.M. Mackay, and W.C. Earnshaw. 1998. INCENP centromere and spindle targeting: identification of essential conserved motifs and involvement of heterochromatin protein HP1. *J. Cell Biol.* 143:1763–74.

Akhmanova, A., and J.A. Hammer. 2010. Linking molecular motors to membrane cargo. *Curr. Opin. Cell Biol*.

Alberti, S., A. Gladfelter, and T. Mittag. 2019. Considerations and Challenges in Studying Liquid-Liquid Phase Separation and Biomolecular Condensates. *Cell*.

Amano, M., M. Ito, K. Kimura, Y. Fukata, K. Chihara, T. Nakano, Y. Matsuura, and K. Kaibuchi. 1996. Phosphorylation and activation of myosin by Rho-associated kinase (Rho- kinase). *J. Biol. Chem*. 271:20246–20249.

Amano, M., M. Nakayama, and K. Kaibuchi. 2010. Rho-kinase/ROCK: A key regulator of the cytoskeleton and cell polarity. *Cytoskeleton (Hoboken)*. 67:545–54.

Andreassen, P.R., O.D. Lohez, F.B. Lacroix, and R.L. Margolis. 2001. Tetraploid State Induces p53-dependent Arrest of Nontransformed Mammalian Cells in G1. *Mol. Biol. Cell*. 12:1315–1328.

Asano, E., H. Hasegawa, T. Hyodo, S. Ito, M. Maeda, M. Takahashi, M. Hamaguchi, and T. Senga. 2013. The Aurora-B-mediated phosphorylation of SHCBP1 regulates cytokinetic furrow ingression. *J. Cell Sci.* 126:3263–70.

Asbury, C.L. 2017. Anaphase a: Disassembling microtubules move chromosomes toward spindle poles. *Biology (Basel)*.

Atherton, J., I.-M. Yu, A. Cook, J.M. Muretta, A. Joseph, J. Major, Y. Sourigues, J. Clause, M. Topf, S.S. Rosenfeld, A. Houdusse, and C.A. Moores. 2017. The divergent mitotic kinesin MKLP2 exhibits atypical structure and mechanochemistry. *Elife*. 6:e27793.

Ban, R., Y. Irino, K. Fukami, and H. Tanaka. 2004. Human Mitotic Spindle-associated Protein PRC1 Inhibits MgcRacGAP Activity toward Cdc42 during the Metaphase. *J. Biol. Chem.* 279:16394–16402.

Barlan, K., and V.I. Gelfand. 2017. Microtubule-based transport and the distribution, tethering, and organization of organelles. *Cold Spring Harb. Perspect. Biol.*

Barlan, K., W. Lu, and V.I. Gelfand. 2013. The microtubule-binding protein ensconsin is an essential cofactor of kinesin-1. *Curr. Biol.* 23:317–322.

Basant, A., and M. Glotzer. 2018. Spatiotemporal Regulation of RhoA during Cytokinesis. *Curr. Biol.* 28:R570–R580.

Basant, A., S. Lekomtsev, Y.C. Tse, D. Zhang, K.M. Longhini, M. Petronczki, and M. Glotzer. 2015.

Aurora B Kinase Promotes Cytokinesis by Inducing Centralspindlin Oligomers that Associate with the Plasma Membrane. *Dev. Cell*. 33:204–215.

Bastos, R.N., S.R. Gandhi, R.D. Baron, U. Gruneberg, E.A. Nigg, and F.A. Barr. 2013. Aurora B suppresses microtubule dynamics and limits central spindle size by locally activating KIF4A. *J. Cell Biol.* 202:605–621.

Bianconi, E., A. Piovesan, F. Facchin, A. Beraudi, R. Casadei, F. Frabetti, L. Vitale, M.C. Pelleri, S. Tassani, F. Piva, S. Perez-Amodio, P. Strippoli, and S. Canaider. 2013. An estimation of the number of cells in the human body. *Ann. Hum. Biol.* 40:463–471.

Bieling, P., L. Laan, H. Schek, E.L. Munteanu, L. Sandblad, M. Dogterom, D. Brunner, and T. Surrey. 2007. Reconstitution of a microtubule plus-end tracking system in vitro. *Nature*. 450:1100–1105.

Bieling, P., I.A. Telley, and T. Surrey. 2010. A minimal midzone protein module controls formation and length of antiparallel microtubule overlaps. *Cell*. 142:420–432.

Blethrow, J.D., J.S. Glavy, D.O. Morgan, and K.M. Shokat. 2008. Covalent capture of kinase-specific phosphopeptides reveals Cdk1-cyclin B substrates. *Proc. Natl. Acad. Sci. U. S. A.* 105:1442–7.

Brennan, I.M., U. Peters, T.M. Kapoor, and A.F. Straight. 2007. Polo-like kinase controls vertebrate spindle elongation and cytokinesis. *PLoS One*. 2:e409.

Breznau, E.B., M. Murt, T.L. Blasius, K.J. Verhey, and A.L. Miller. 2017. The MgcRacGAP SxIP motif tethers Centralspindlin to microtubule plus ends in *Xenopus laevis*. *J. Cell Sci.* 130:1809–1821.

Budnar, S., K.B. Husain, G.A. Gomez, M. Naghibosadat, A. Varma, S. Verma, N.A. Hamilton, R.G. Morris, and A.S. Yap. 2019. Anillin Promotes Cell Contractility by Cyclic Resetting of RhoA Residence Kinetics. *Dev. Cell*. 49:894-906.e12.

Bulinski, J.C., and A. Bossler. 1994. Purification and characterization of ensconsin, a novel microtubule stabilizing protein. *J. Cell Sci.* 107.

Burkard, M.E., J. Maciejowski, V. Rodriguez-Bravo, M. Repka, D.M. Lowery, K.R. Clauser, C. Zhang, K.M. Shokat, S.A. Carr, M.B. Yaffe, and P. V Jallepalli. 2009. Plk1 self-organization and priming phosphorylation of HsCYK-4 at the spindle midzone regulate the onset of division in human cells. *PLoS Biol.* 7.

Canman, J.C., L.A. Cameron, P.S. Maddox, A. Straight, J.S. Tirnauer, T.J. Mitchison, G. Fang, T.M. Kapoor, and E.D. Salmon. 2003. Determining the position of the cell division plane. *Nature*. 424:1074–1078.

Canman, J.C., D.B. Hoffman, and E.D. Salmon. 2000. The role of pre- and post-anaphase microtubules in the cytokinesis phase of the cell cycle. *Curr. Biol.*

Cao, L.G., and Y.L. Wang. 1996. Signals from the spindle midzone are required for the stimulation of cytokinesis in cultured epithelial cells. *Mol. Biol. Cell*. 7:225–32.

Capalbo, L., Z.I. Bassi, M. Geymonat, S. Todesca, L. Copoiu, A.J. Enright, G. Callaini, M.G. Riparbelli, L. Yu, J.S. Choudhary, E. Ferrero, S. Wheatley, M.E. Douglas, M. Mishima, and P.P. D'Avino. 2019. The midbody interactome reveals unexpected roles for PP1 phosphatases in cytokinesis. *Nat. Commun.*

Carlton, J.G., A. Caballe, M. Agromayor, M. Kloc, and J. Martin-Serrano. 2012. ESCRT-III Governs the Aurora B-Mediated Abscission Checkpoint Through CHMP4C. *Science (80-.).* 336:220–225.

Cesario, J.M., J.K. Jang, B. Redding, N. Shah, T. Rahman, and K.S. McKim. 2006. Kinesin 6 family

member Subito participates in mitotic spindle assembly and interacts with mitotic regulators. *J. Cell Sci.* 119:4770–4780.

Chang, J.-L., T.-H. Chen, C.-F. Wang, Y.-H. Chiang, Y.-L. Huang, F.-H. Wong, C.-K. Chou, and C.-M. Chen. 2006. Borealin/Dasra B is a cell cycle-regulated chromosomal passenger protein and its nuclear accumulation is linked to poor prognosis for human gastric cancer. *Exp. Cell Res.* 312:962–973.

Chen, A., P.D. Arora, C.A. McCulloch, and A. Wilde. 2017. Cytokinesis requires localized β-actin filament production by an actin isoform specific nucleator. *Nat. Commun.* 8:1530.

Corbett, K.D. 2017. Molecular Mechanisms of Spindle Assembly Checkpoint Activation and Silencing. Springer, Cham. 429–455.

Coudreuse, D., and P. Nurse. 2010. Driving the cell cycle with a minimal CDK control network. *Nature*. 468:1074–1079.

D'Avino, P.P., and L. Capalbo. 2016. Regulation of midbody formation and function by mitotic kinases. *Semin. Cell Dev. Biol.* 53:57–63.

DAN, J.C. 1948. On the mechanism of astral cleavage. *Physiol. Zool.*

Davies, T., S.N. Jordan, V. Chand, J.A. Sees, K. Laband, A.X. Carvalho, M. Shirasu-Hiza, D.R. Kovar, J. Dumont, and J.C. Canman. 2014. High-Resolution Temporal Analysis Reveals a Functional Timeline for the Molecular Regulation of Cytokinesis. *Dev. Cell*. 30:209–223.

Dean, S.O., and J.A. Spudich. 2006. Rho Kinase's role in Myosin recruitment to the equatorial cortex of mitotic Drosophila S2 cells is for Myosin regulatory light chain phosphorylation. *PLoS One*.

DeBonis, S., D.A. Skoufias, L. Lebeau, R. Lopez, G. Robin, R.L. Margolis, R.H. Wade, and F. Kozielski. 2004. In vitro screening for inhibitors of the human mitotic kinesin Eg5 with antimitotic and antitumor activities. *Mol. Cancer Ther.* 3:1079–90.

Dechant, R., and M. Glotzer. 2003. Centrosome separation and central spindle assembly act in redundant pathways that regulate microtubule density and trigger cleavage furrow formation. *Dev. Cell*. 4:333–344.

Devore, J.J., G.W. Conrad, and R. Rappaport. 1989. A model for astral stimulation of cytokinesis in animal cells. *J. Cell Biol.* 109:2225–2232.

Douglas, M.E., T. Davies, N. Joseph, and M. Mishima. 2010. Aurora B and 14-3-3 Coordinately Regulate Clustering of Centralspindlin during Cytokinesis. *Curr. Biol.* 20:927–933.

Duijf, P.H.G., N. Schultz, and R. Benezra. 2013. Cancer cells preferentially lose small chromosomes. *Int. J. Cancer*. 132:2316–2326.

Dull, T., R. Zufferey, M. Kelly, R.J. Mandel, M. Nguyen, D. Trono, and L. Naldini. 1998. A third-generation lentivirus vector with a conditional packaging system. *J. Virol*. 72:8463–71.

Earnshaw, W.C., and C. a Cooke. 1991. Analysis of the distribution of the INCENPs throughout mitosis reveals the existence of a pathway of structural changes in the chromosomes during metaphase and early events in cleavage furrow formation. *J. Cell Sci.* 98 (Pt 4):443–461.

Echard, A., F. Jollivet, O. Martinez, J.J. Lacapère, A. Rousselet, I. Janoueix-Lerosey, and B. Goud. 1998. Interaction of a Golgi-associated kinesin-like protein with Rab6. *Science*. 279:580–5.

Ferenz, N.P., A. Gable, and P. Wadsworth. 2010. Mitotic functions of kinesin-5. *Semin. Cell Dev. Biol.* 21:255–259.

Foe, V.E., and G. Von Dassow. 2008. Stable and dynamic microtubules coordinately shape the myosin activation zone during cytokinetic furrow formation. *J. Cell Biol.* 183:457–470.

Fu, M. meng, and E.L.F. Holzbaur. 2014. Integrated regulation of motor-driven organelle transport by scaffolding proteins. *Trends Cell Biol.*

Fuller, B.G., M.A. Lampson, E.A. Foley, S. Rosasco-Nitcher, K. V Le, P. Tobelmann, D.L. Brautigan, P.T. Stukenberg, and T.M. Kapoor. 2008. Midzone activation of aurora B in anaphase produces an intracellular phosphorylation gradient. *Nature*. 453:1132–1136.

Fung, S.Y.S., M. Kitagawa, P.-J. Liao, J. Wong, and S.H. Lee. 2017. Opposing Activities of Aurora B Kinase and B56-PP2A Phosphatase on MKlp2 Determine Abscission Timing. *Curr. Biol.* 13:1954–62.

Galipeau, P.C., D.S. Cowan, C.A. Sanchez, M.T. Barrett, M.J. Emond, D.S. Levine, P.S. Rabinovitch, and B.J. Reid. 1996. 17p (p53) allelic losses, 4N (G2/tetraploid) populations, and progression to aneuploidy in Barrett's esophagus. *Proc. Natl. Acad. Sci. U. S. A.* 93:7081–4.

Gallaud, E., R. Caous, A. Pascal, F. Bazile, J.P. Gagné, S. Huet, G.G. Poirier, D. Chrétien, L. Richard-Parpaillon, and R. Giet. 2014. Ensconsin/map7 promotes microtubule growth and centrosome separation in Drosophila neural stem cells. *J. Cell Biol.* 204:1111–1121.

Ganem, N.J., H. Cornils, S.-Y. Chiu, K.P. O'Rourke, J. Arnaud, D. Yimlamai, M. Théry, F.D. Camargo, and D. Pellman. 2014. Cytokinesis Failure Triggers Hippo Tumor Suppressor Pathway Activation. *Cell*. 158:833–848.

Ganem, N.J., S.A. Godinho, and D. Pellman. 2009. A mechanism linking extra centrosomes to chromosomal instability. *Nature*. 460:278–282.

Ganem, N.J., Z. Storchova, and D. Pellman. 2007. Tetraploidy, aneuploidy and cancer. *Curr. Opin. Genet. Dev.* 17:157–162.

Giet, R., and D.M. Glover. 2001. Drosophila Aurora B Kinase Is Required for Histone H3 Phosphorylation and Condensin Recruitment during Chromosome Condensation and to Organize the Central Spindle during Cytokinesis. 152. 669–681 pp.

Glotzer, M. 2009. The 3Ms of central spindle assembly: Microtubules, motors and MAPs. *Nat. Rev. Mol. Cell Biol.* 10:9–20.

Gorbsky, G.J., R.H. Chen, and A.W. Murray. 1998. Microinjection of antibody to Mad2 protein into mammalian cells in mitosis induces premature anaphase. *J. Cell Biol.* 141:1193–205.

Goto, H., Y. Yasui, A. Kawajiri, E.A. Nigg, Y. Terada, M. Tatsuka, K. ichi Nagata, and M. Inagaki. 2003. Aurora-B regulates the cleavage furrow-specific vimentin phosphorylation in the cytokinetic process. *J. Biol. Chem.* 278:8526–8530.

Green, R.A., E. Paluch, and K. Oegema. 2012. Cytokinesis in Animal Cells. *Annu. Rev. Cell Dev. Biol.* 28:29–58.

Gruneberg, U., R. Neef, R. Honda, E.A. Nigg, and F.A. Barr. 2004. Relocation of Aurora B from centromeres to the central spindle at the metaphase to anaphase transition requires MKlp2. *J. Cell Biol.* 166.

Guse, A., M. Mishima, and M. Glotzer. 2005. Phosphorylation of ZEN-4/MKLP1 by Aurora B Regulates Completion of Cytokinesis. 15. 778–786 pp.

Hannabuss, J., M. Lera-Ramirez, N.I. Cade, F.J. Fourniol, F. Nédélec, and T. Surrey. 2019. Self-

Organization of Minimal Anaphase Spindle Midzone Bundles. *Curr. Biol.*

Harper, J.W., S.J. Elledge, K. Keyomarsi, B. Dynlacht, L.H. Tsai, P. Zhang, S. Dobrowolski, C. Bai, L. Connell-Crowley, E. Swindell, M.P. Fox, and N. Wei. 1995. Inhibition of cyclin-dependent kinases by p21. *Mol. Biol. Cell*. 6:387–400.

Hegemann, B., J.R.A. Hutchins, O. Hudecz, M. Novatchkova, J. Rameseder, M.M. Sykora, S. Liu, M. Mazanek, P. Lénárt, J.K. Hériché, I. Poser, N. Kraut, A.A. Hyman, M.B. Yaffe, K. Mechtler, and J.M. Peters. 2011. Systematic phosphorylation analysis of human mitotic protein complexes. *Sci. Signal.*

Hengeveld, R.C.C., N.T. Hertz, M.J.M. Vromans, C. Zhang, A.L. Burlingame, K.M. Shokat, and S.M.A. Lens. 2012. Development of a chemical genetic approach for human aurora B kinase identifies novel substrates of the chromosomal passenger complex. *In* Molecular and Cellular Proteomics. 47–59.

Hickson, G.R.X., and P.H. O'Farrell. 2008. Rho-dependent control of anillin behavior during cytokinesis. *J. Cell Biol.* 180:285–94.

Hill, E., M. Clarke, and F.A. Barr. 2000. The Rab6-binding kinesin, Rab6-KIFL, is required for cytokinesis. *EMBO J.* 19:5711–9.

Hiramoto, Y. 1971. Analysis of cleavage stimulus by means of micromanipulation of sea urchin eggs. *Exp. Cell Res.* 68:291–298.

Honda, R., R. Körner, and E.A. Nigg. 2003. Exploring the functional interactions between Aurora B, INCENP, and survivin in mitosis. *Mol. Biol. Cell*. 14:3325–41.

Hooikaas, P.J., M. Martin, T. Mühlethaler, G.J. Kuijntjes, C.A.E. Peeters, E.A. Katrukha, L. Ferrari, R. Stucchi, D.G.F. Verhagen, W.E. Van Riel, I. Grigoriev, A.F.M. Altelaar, C.C. Hoogenraad, S.G.D. Rüdiger, M.O. Steinmetz, L.C. Kapitein, and A. Akhmanova. 2019. MAP7 family proteins regulate kinesin-1 recruitment and activation. *J. Cell Biol.* 218:1298–1318.

Van Der Horst, A., and S.M.A. Lens. 2014. Cell division: Control of the chromosomal passenger complex in time and space. *Chromosoma*.

van der Horst, A., M.J.M. Vromans, K. Bouwman, M.S. van der Waal, M.A. Hadders, and S.M.A. Lens. 2015. Inter-domain Cooperation in INCENP Promotes Aurora B Relocation from Centromeres to Microtubules. *Cell Rep.* 12:380–387.

Hu, C.-K., M. Coughlin, C.M. Field, and T.J. Mitchison. 2008. Cell polarization during monopolar cytokinesis. *J. Cell Biol.* 181:195–202.

Hu, C.-K., M. Coughlin, C.M. Field, and T.J. Mitchison. 2011. KIF4 regulates midzone length during cytokinesis. *Curr. Biol.* 21:815–24.

Hu, C.-K., M. Coughlin, and T.J. Mitchison. 2012a. Midbody assembly and its regulation during cytokinesis. *Mol. Biol. Cell*. 23:1024–1034.

Hu, C.-K.K., N. Ozlu, M. Coughlin, J.J. Steen, and T.J. Mitchison. 2012b. Plk1 negatively regulates PRC1 to prevent premature midzone formation before cytokinesis. *Mol. Biol. Cell*. 23:2702–2711.

Hümmer, S., and T.U. Mayer. 2009. Cdk1 Negatively Regulates Midzone Localization of the Mitotic Kinesin Mklp2 and the Chromosomal Passenger Complex. *Curr. Biol.* 19:607–612.

Hutterer, A., M. Glotzer, and M. Mishima. 2009. Clustering of Centralspindlin Is Essential for Its Accumulation to the Central Spindle and the Midbody. *Curr. Biol.* 19:2043–2049.

Hyman, A.A., C.A. Weber, and F. Jülicher. 2014. Liquid-Liquid Phase Separation in Biology. *Annu. Rev.*

Cell Dev. Biol.

Jain, A., and R.D. Vale. 2017. RNA phase transitions in repeat expansion disorders. *Nature*. 546:243–247.

Jaiswal, M., L. Gremer, R. Dvorsky, L.C. Haeusler, I.C. Cirstea, K. Uhlenbrock, and M.R. Ahmadian. 2011. Mechanistic Insights into Specificity, Activity, and Regulatory Elements of the Regulator of G-protein Signaling (RGS)-containing Rho-specific Guanine Nucleotide Exchange Factors (GEFs) p115, PDZ-RhoGEF (PRG), and Leukemia-associated RhoGEF (LARG). *J. Biol. Chem.* 286:18202–18212.

Janssen, A., M. Van Der Burg, K. Szuhai, G.J.P.L. Kops, and R.H. Medema. 2011. Chromosome segregation errors as a cause of DNA damage and structural chromosome aberrations. *Science (80-.).* 333:1895–1898.

Jeyaprakash, A.A., U.R. Klein, D. Lindner, J. Ebert, E.A. Nigg, and E. Conti. 2007. Structure of a Survivin-Borealin-INCENP Core Complex Reveals How Chromosomal Passengers Travel Together. *Cell*. 131:271–285.

Jiang, W., G. Jimenez, N.J. Wells, T.J. Hope, G.M. Wahl, T. Hunter, and R. Fukunaga. 1998. PRC1: a human mitotic spindle-associated CDK substrate protein required for cytokinesis. *Mol. Cell*. 2:877–85.

Joseph, N., A. Hutterer, I. Poser, and M. Mishima. 2012. ARF6 GTPase protects the post-mitotic midbody from 14-3-3-mediated disintegration. *EMBO J.*

Kaitna, S., M. Mendoza, V. Jantsch-Plunger, and M. Glotzer. 2000. Incenp and an Aurora-like kinase form a complex essential for chromosome segregation and efficient completion of cytokinesis. *Curr. Biol.* 10:1172–1181.

Kallio, M.J., M.L. McCleland, P.T. Stukenberg, and G.J. Gorbsky. 2002. Inhibition of Aurora B Kinase Blocks Chromosome Segregation, Overrides the Spindle Checkpoint, and Perturbs Microtubule Dynamics in Mitosis. *Curr. Biol.* 12:900–905.

Kamath, R.S., A.G. Fraser, Y. Dong, G. Poulin, R. Durbin, M. Gotta, A. Kanapin, N. Le Bot, S. Moreno, M. Sohrmann, D.P. Welchman, P. Zipperlen, and J. Ahringer. 2003. Systematic functional analysis of the Caenorhabditis elegans genome using RNAi. *Nature*. 421:231–237.

Kamijo, K., N. Ohara, M. Abe, T. Uchimura, H. Hosoya, J.-S. Lee, and T. Miki. 2006. Dissecting the Role of Rho-mediated Signaling in Contractile Ring Formation. *Mol. Biol. Cell*. 17:43–55.

Kawajiri, A., Y. Yasui, H. Goto, M. Tatsuka, M. Takahashi, K. ichi Nagata, and M. Inagaki. 2003. Functional significance of the specific sites phosphorylated in desmin at cleavage furrow: Aurora-B may phosphorylate and regulate type III intermediate filaments during cytokinesis coordinatedly with Rho-kinase. *Mol. Biol. Cell*.

Kawamura, K. 1977. Microdissection studies on the dividing neuroblast of the grasshopper, with special reference to the mechanism of unequal cytokinesis. *Exp. Cell Res.* 106:127–137.

Kettenbach, A.N., D.K. Schweppe, B.K. Faherty, D. Pechenick, A.A. Pletnev, and S.A. Gerber. 2011. Quantitative phosphoproteomics identifies substrates and functional modules of Aurora and Polo-like kinase activities in mitotic cells. *Sci. Signal.*

Kimura, K., M. Ito, M. Amano, K. Chihara, Y. Fukata, M. Nakafuku, B. Yamamori, J. Feng, T. Nakano, K. Okawa, A. Iwamatsu, and K. Kaibuchi. 1996. Regulation of myosin phosphatase by Rho and Rho-associated kinase (Rho- kinase). *Science (80-.).* 273:245–248.

Kimura, M., C. Uchida, Y. Takano, M. Kitagawa, and Y. Okano. 2004. Cell cycle-dependent regulation of

the human aurora B promoter. *Biochem. Biophys. Res. Commun.* 316:930–936.

Kitagawa, M., S.Y.S. Fung, U.F.S. Hameed, H. Goto, M. Inagaki, and S.H. Lee. 2014. Cdk1 Coordinates Timely Activation of MKlp2 Kinesin with Relocation of the Chromosome Passenger Complex for Cytokinesis. *Cell Rep.* 7:166–179.

Kitagawa, M., S.Y.S. Fung, N. Onishi, H. Saya, and S.H. Lee. 2013. Targeting Aurora B to the Equatorial Cortex by MKlp2 Is Required for Cytokinesis. *PLoS One*. 8:e64826.

Klein, U.R., E.A. Nigg, and U. Gruneberg. 2006. Centromere Targeting of the Chromosomal Passenger Complex Requires a Ternary Subcomplex of Borealin, Survivin, and the N-Terminal Domain of INCENP. *Mol. Biol. Cell*. 17:2547.

Koizumi, H., H. Fujioka, K. Togashi, J. Thompson, J.R. Yates, J.G. Gleeson, and K. Emoto. 2017. DCLK1 phosphorylates the microtubule-associated protein MAP7D1 to promote axon elongation in cortical neurons. *Dev. Neurobiol.* 77:493–510.

Kosako, H., T. Yoshida, F. Matsumura, T. Ishizaki, S. Narumiya, and M. Inagaki. 2000. Rho-kinase/ROCK is involved in cytokinesis through the phosphorylation of myosin light chain and not ezrin/radixin/moesin proteins at the cleavage furrow. *Oncogene*. 19:6059–6064.

Kotýnková, K., K.-C. Su, S.C. West, and M. Petronczki. 2016. Plasma Membrane Association but Not Midzone Recruitment of RhoGEF ECT2 Is Essential for Cytokinesis. *Cell Rep.* 17:2672–2686.

Kovar, D.R., E.S. Harris, R. Mahaffy, H.N. Higgs, and T.D. Pollard. 2006. Control of the assembly of ATP- and ADP-actin by formins and profilin. *Cell*.

Kühn, S., and M. Geyer. 2014. Formins as effector proteins of Rho GTPases. *Small GTPases*. 5:e29513.

Kurasawa, Y., W.C. Earnshaw, Y. Mochizuki, N. Dohmae, and K. Todokoro. 2004. Essential roles of KIF4 and its binding partner PRC1 in organized central spindle midzone formation. *EMBO J.* 23:3237–48.

Kwon, H.J., J.E. Park, H. Song, and C.Y. Jang. 2016. DDA3 and Mdp3 modulate Kif2a recruitment onto the mitotic spindle to control minus-end spindle dynamics. *J. Cell Sci.* 129:2719–2725.

Lammers, M., S. Meyer, D. Kühlmann, and A. Wittinghofer. 2008. Specificity of interactions between mDia isoforms and Rho proteins. *J. Biol. Chem.*

Landino, J., S.R. Norris, M. Li, E.R. Ballister, M.A. Lampson, and R. Ohi. 2017. Two mechanisms coordinate the recruitment of the chromosomal passenger complex to the plane of cell division. *Mol. Biol. Cell*. 28:3634–3646.

Lawrence, C.J., R.K. Dawe, K.R. Christie, D.W. Cleveland, S.C. Dawson, S.A. Endow, L.S.B. Goldstein, H. V Goodson, N. Hirokawa, J. Howard, R.L. Malmberg, J.R. Mcintosh, H. Miki, T.J. Mitchison, Y. Okada, A.S.N. Reddy, W.M. Saxton, M. Schliwa, J.M. Scholey, R.D. Vale, C.E. Walczak, and L. Wordeman. 2004. A standardized kinesin nomenclature. *J. Cell Biol.* 167:19–22.

Lee, K.Y., B. Esmaeili, B. Zealley, and M. Mishima. 2015. Direct interaction between centralspindlin and PRC1 reinforces mechanical resilience of the central spindle. *Nat. Commun.* 6.

Lee, S.H., F. McCormick, and H. Saya. 2010. Mad2 inhibits the mitotic kinesin MKlp2. *J. Cell Biol.* 191:1069–1077.

Leite, J., D.S. Osorio, A.F. Sobral, A.M. Silva, and A.X. Carvalho. 2019. Network Contractility During Cytokinesis-from Molecular to Global Views. *Biomolecules*.

Lekomtsev, S., K.C. Su, V.E. Pye, K. Blight, S. Sundaramoorthy, T. Takaki, L.M. Collinson, P. Cherepanov,

N. Divecha, and M. Petronczki. 2012. Centralspindlin links the mitotic spindle to the plasma membrane during cytokinesis. *Nature*. 492:276–279.

Lens, S.M.A., and R.H. Medema. 2019. Cytokinesis defects and cancer. *Nat. Rev. Cancer*. 19:32–45.

Lens, S.M.A., R.M.F. Wolthuis, R. Klompmaker, J. Kauw, R. Agami, T. Brummelkamp, G. Kops, and R.H. Medema. 2003. Survivin is required for a sustained spindle checkpoint arrest in response to lack of tension. *EMBO J.* 22:2934–2947.

Li, F., G. Ambrosini, E.Y. Chu, J. Plescia, S. Tognin, P.C. Marchisio, and D.C. Altieri. 1998. Control of apoptosis and mitotic spindle checkpoint by survivin. *Nature*. 396:580–584.

Li, J., M. Dallmayer, T. Kirchner, J. Musa, and T.G.P. Grünewald. 2018. PRC1: Linking Cytokinesis, Chromosomal Instability, and Cancer Evolution. *Trends in Cancer*. 4:59–73.

Li, J., J. Wang, H. Jiao, J. Liao, and X. Xu. 2010. Cytokinesis and cancer: Polo loves ROCK'n' Rho(A). *J. Genet. Genomics*. 37:159–172.

Li, M., and P. Zhang. 2009. Spindle assembly checkpoint, aneuploidy and tumorigenesis. *Cell Cycle*.

Lin, Y.C., M. Boone, L. Meuris, I. Lemmens, N. Van Roy, A. Soete, J. Reumers, M. Moisse, S. Plaisance, R. Drmanac, J. Chen, F. Speleman, D. Lambrechts, Y. Van De Peer, J. Tavernier, and N. Callewaert. 2014. Genome dynamics of the human embryonic kidney 293 lineage in response to cell biology manipulations. *Nat. Commun.*

Lubischer, J.L. 2007. The Cell Cycle, Principles of Control. David O. Morgan. 47. New Science Press. 794–795 pp.

Ma, H., L.-C. Tu, A. Naseri, M. Huisman, S. Zhang, D. Grunwald, and T. Pederson. 2016. Multiplexed labeling of genomic loci with dCas9 and engineered sgRNAs using CRISPRainbow. *Nat. Biotechnol.* 34:528–530.

Ma, X., M. Kovaćs, M.A. Conti, A. Wang, Y. Zhang, J.R. Sellers, and R.S. Adelstein. 2012. Nonmuscle myosin II exerts tension but does not translocate actin in vertebrate cytokinesis. *Proc. Natl. Acad. Sci. U. S. A.* 109:4509–4514.

Mackay, A.M., D.M. Eckley, C. Chue, and W.C. Earnshaw. 1993. Molecular analysis of the INCENPs (inner centromere proteins): separate domains are required for association with microtubules during interphase and with the central spindle during anaphase. *J. Cell Biol.* 123:373–85.

Makyio, H., M. Ohgi, T. Takei, S. Takahashi, H. Takatsu, Y. Katoh, A. Hanai, T. Ueda, Y. Kanaho, Y. Xie, H.W. Shin, H. Kamikubo, M. Kataoka, M. Kawasaki, R. Kato, S. Wakatsuki, and K. Nakayama. 2012. Structural basis for Arf6-MKLP1 complex formation on the Flemming body responsible for cytokinesis. *EMBO J.*

Mangal, S., J. Sacher, T. Kim, D.S. Osório, F. Motegi, A.X. Carvalho, K. Oegema, and E. Zanin. 2018. TPXL-1 activates Aurora A to clear contractile ring components from the polar cortex during cytokinesis. *J. Cell Biol.* 217:837–848.

Mangione, M.C., and K.L. Gould. 2019. Molecular form and function of the cytokinetic ring. *J. Cell Sci.* 132:jcs226928.

Manukyan, A., K. Ludwig, S. Sanchez-Manchinelly, S.J. Parsons, and P. Todd Stukenberg. 2015. A complex of p190RhoGAP-A and anillin modulates RhoA-GTP and the cytokinetic furrow in human cells. *J. Cell Sci.* 128:50–60.

Margolis, R.L., O.D. Lohez, and P.R. Andreassen. 2003. G1 tetraploidy checkpoint and the suppression of tumorigenesis. *J. Cell. Biochem.* 88:673–683.

Matsumura, F. 2005. Regulation of myosin II during cytokinesis in higher eukaryotes. *Trends Cell Biol.* 15:371–377.

Meadows, J.C., and J.B.A. Millar. 2015. Sharpening the anaphase switch. *Biochem. Soc. Trans.* 43:19–22.

Mendenhall, M.D., and A.E. Hodge. 1998. Regulation of Cdc28 Cyclin-Dependent Protein Kinase Activity during the Cell Cycle of the Yeast Saccharomyces cerevisiae. 62. 1191–1243 pp.

Mendes Pinto, I., B. Rubinstein, A. Kucharavy, J.R. Unruh, and R. Li. 2012. Actin Depolymerization Drives Actomyosin Ring Contraction during Budding Yeast Cytokinesis. *Dev. Cell*.

Meraldi, P., V.M. Draviam, and P.K. Sorger. 2004. Timing and Checkpoints in the Regulation of Mitotic Progression. *Dev. Cell*. 7:45–60.

Meraldi, P., and E.. Nigg. 2002. The centrosome cycle. *FEBS Lett.* 521:9–13.

Métivier, M., B.Y. Monroy, E. Gallaud, R. Caous, A. Pascal, L. Richard-Parpaillon, A. Guichet, K.M. Ori-McKenney, and R. Giet. 2018. Mechanisms of Kinesin-1 activation by Ensconsin/MAP7 in vivo. *bioRxiv*. 325035.

Metzger, T., V. Gache, M. Xu, B. Cadot, E.S. Folker, B.E. Richardson, E.R. Gomes, and M.K. Baylies. 2012. MAP and kinesin-dependent nuclear positioning is required for skeletal muscle function. *Nature*. 484:120–124.

Mierzwa, B., and D.W. Gerlich. 2014. Cytokinetic Abscission: Molecular Mechanisms and Temporal Control. *Dev. Cell*. 31:525–538.

Minoshima, Y., T. Kawashima, K. Hirose, Y. Tonozuka, A. Kawajiri, Y.C. Bao, X. Deng, M. Tatsuka, S. Narumiya, W.S. May, T. Nosaka, K. Semba, T. Inoue, T. Satoh, M. Inagaki, and T. Kitamura. 2003. Phosphorylation by Aurora B converts MgcRacGAP to a RhoGAP during cytokinesis. *Dev. Cell*.

Mishima, M. 2016. Centralspindlin in Rappaport's cleavage signaling. *Semin. Cell Dev. Biol.* 53:45–56.

Mishima, M., S. Kaitna, and M. Glotzer. 2002. Central spindle assembly and cytokinesis require a kinesin-like protein/RhoGAP complex with microtubule bundling activity. *Dev. Cell*. 2:41–54.

Mohan, R., E.A. Katrukha, H. Doodhi, I. Smal, E. Meijering, L.C. Kapitein, M.O. Steinmetz, and A. Akhmanova. 2013. End-binding proteins sensitize microtubules to the action of microtubule-targeting agents. *Proc. Natl. Acad. Sci. U. S. A.* 110:8900–5.

Mollinari, C., J.-P. Kleman, W. Jiang, G. Schoehn, T. Hunter, and R.L. Margolis. 2002. PRC1 is a microtubule binding and bundling protein essential to maintain the mitotic spindle midzone. *J. Cell Biol.* 157:1175–86.

Mollinari, C., J.-P. Kleman, Y. Saoudi, S.A. Jablonski, J. Perard, T.J. Yen, and R.L. Margolis. 2005. Ablation of PRC1 by Small Interfering RNA Demonstrates that Cytokinetic Abscission Requires a Central Spindle Bundle in Mammalian Cells, whereas Completion of Furrowing Does Not. *Mol. Biol. Cell*. 16:1043–1055.

Monroy, B.Y., D.L. Sawyer, B.E. Ackermann, M.M. Borden, T.C. Tan, and K.M. Ori-Mckenney. 2018. Competition between microtubule-associated proteins directs motor transport. *Nat. Commun.* 9:1487.

Montenegro Gouveia, S., K. Leslie, L.C. Kapitein, R.M. Buey, I. Grigoriev, M. Wagenbach, I. Smal,

E. Meijering, C.C. Hoogenraad, L. Wordeman, M.O. Steinmetz, and A. Akhmanova. 2010. In Vitro Reconstitution of the Functional Interplay between MCAK and EB3 at Microtubule Plus Ends. *Curr. Biol.* 20:1717–1722.

Morgan, D.O. 1995. Principles of CDK regulation. *Nature*. 374:131–134.

Morgan, D.O. 1997. CYCLIN-DEPENDENT KINASES: Engines, Clocks, and Microprocessors. *Annu. Rev. Cell Dev. Biol.*

Morin, X., and Y. Bellaïche. 2011. Mitotic Spindle Orientation in Asymmetric and Symmetric Cell Divisions during Animal Development. *Dev. Cell*. 21:102–119.

Motegi, F., N. V. Velarde, F. Piano, and A. Sugimoto. 2006. Two phases of astral microtubule activity during cytokinesis in C. elegans embryos. *Dev. Cell*. 10:509–520.

Murata-Hori, M., K. Fumoto, Y. Fukuta, T. Iwasaki, A. Kikuchi, M. Tatsuka, and H. Hosoya. 2000. Myosin II Regulatory Light Chain as a Novel Substrate for AIM-1, an Aurora/Ipl1p-related Kinase from Rat. *J. Biochem.* 128:903–907.

Murata-Hori, M., M. Tatsuka, and Y.-L. Wang. 2002. Probing the dynamics and functions of aurora B kinase in living cells during mitosis and cytokinesis. *Mol. Biol. Cell*. 13:1099–108.

Murata-Hori, M., and Y.L. Wang. 2002. Both midzone and astral microtubules are involved in the delivery of cytokinesis signals: Insights from the mobility of aurora B. *J. Cell Biol.* 159:45–53.

Murthy, K., and P. Wadsworth. 2008. Dual role for microtubules in regulating cortical contractility during cytokinesis. *J. Cell Sci.* 121:2350–2359.

Nasmyth, K. 2011. Cohesin: a catenase with separate entry and exit gates? *Nat. Cell Biol.* 13:1170–1177.

Neef, R., U. Grüneberg, and F.A. Barr. 2005. Assay and functional properties of Rabkinesin-6/Rab6-KIFL/MKlp2 in cytokinesis. *Methods Enzymol.* 403:618–628.

Neef, R., U. Gruneberg, R. Kopajtich, X. Li, E.A. Nigg, H. Sillje, and F.A. Barr. 2007. Choice of Plk1 docking partners during mitosis and cytokinesis is controlled by the activation state of Cdk1. *Nat. Cell Biol.* 9:436–444.

Neef, R., U.R. Klein, R. Kopajtich, and F.A. Barr. 2006. Cooperation between Mitotic Kinesins Controls the Late Stages of Cytokinesis. *Curr. Biol.* 16:301–307.

Neef, R., C. Preisinger, J. Sutcliffe, R. Kopajtich, E.A. Nigg, T.U. Mayer, and F.A. Barr. 2003. Phosphorylation of mitotic kinesin-like protein 2 by polo-like kinase 1 is required for cytokinesis. *J. Cell Biol.* 162:863–875.

Nguyen, P.A., A.C. Groen, M. Loose, K. Ishihara, M. Wühr, C.M. Field, and T.J. Mitchison. 2014. Spatial organization of cytokinesis signaling reconstituted in a cell-free system. *Science (80-.).* 346:244–247.

Niida, Y., and A. Yachie. 2011. MAP7D2 is a brain expressing X-linked maternal imprinted gene in humans. *Nat. Preced.* 1–1.

Nishimura, Y. 2006. Centralspindlin regulates ECT2 and RhoA accumulation at the equatorial cortex during cytokinesis. *J. Cell Sci.* 119:104–114.

Norden, C., M. Mendoza, J. Dobbelaere, C. V. Kotwaliwale, S. Biggins, and Y. Barral. 2006. The NoCut Pathway Links Completion of Cytokinesis to Spindle Midzone Function to Prevent Chromosome Breakage. *Cell*.

O'Connell, C.B., and Y. Wang. 2000. Mammalian Spindle Orientation and Position Respond to Changes

in Cell Shape in a Dynein-dependent Fashion. *Mol. Biol. Cell*. 11:1765–1774.

Otomo, T., C. Otomo, D.R. Tomchick, M. Machius, and M.K. Rosen. 2005. Structural basis of Rho GTPase-mediated activation of the formin mDia1. *Mol. Cell*. 18:273–281.

Özlü, N., F. Monigatti, B.Y. Renard, C.M. Field, H. Steen, T.J. Mitchison, and J.J. Steen. 2010. Binding partner switching on microtubules and Aurora-B in the mitosis to cytokinesis transition. *Mol. Cell. Proteomics*. 9:336–350.

Pamula, M.C., L. Carlini, S. Forth, P. Verma, S. Suresh, W.R. Legant, A. Khodjakov, E. Betzig, and T.M. Kapoor. 2019. High-resolution imaging reveals how the spindle midzone impacts chromosome movement. *J. Cell Biol.* jcb.201904169.

Pan, X., Y. Cao, R. Stucchi, P.J. Hooikaas, S. Portegies, L. Will, M. Martin, A. Akhmanova, M. Harterink, and C.C. Hoogenraad. 2019. MAP7D2 Localizes to the Proximal Axon and Locally Promotes Kinesin-1-Mediated Cargo Transport into the Axon. *Cell Rep.* 26:1988-1999.e6.

Pavicic-Kaltenbrunner, V., M. Mishima, and M. Glotzer. 2007. Cooperative assembly of CYK-4/MgcRacGAP and ZEN-4/MKLP1 to form the centralspindlin complex. *Mol. Biol. Cell*.

Perez-Riverol, Y., A. Csordas, J. Bai, M. Bernal-Llinares, S. Hewapathirana, D.J. Kundu, A. Inuganti, J. Griss, G. Mayer, M. Eisenacher, E. Pérez, J. Uszkoreit, J. Pfeuffer, T. Sachsenberg, Ş. Yilmaz, S. Tiwary, J. Cox, E. Audain, M. Walzer, A.F. Jarnuczak, T. Ternent, A. Brazma, and J.A. Vizcaíno. 2019. The PRIDE database and related tools and resources in 2019: Improving support for quantification data. *Nucleic Acids Res.* 47:D442–D450.

Peters, J.M., A. Tedeschi, and J. Schmitz. 2008. The cohesin complex and its roles in chromosome biology. *Genes Dev.* 22:3089–3114.

Petronczki, M., M. Glotzer, N. Kraut, and J.M. Peters. 2007. Polo-like Kinase 1 Triggers the Initiation of Cytokinesis in Human Cells by Promoting Recruitment of the RhoGEF Ect2 to the Central Spindle. *Dev. Cell*. 12:713–725.

Piekny, A., M. Werner, and M. Glotzer. 2005. Cytokinesis: Welcome to the Rho zone. *Trends Cell Biol.* 15:651–658.

Piekny, A.J., and M. Glotzer. 2008. Anillin Is a Scaffold Protein That Links RhoA, Actin, and Myosin during Cytokinesis. *Curr. Biol.* 18:30–36.

Piekny, A.J., and A.S. Maddox. 2010. The myriad roles of Anillin during cytokinesis. *Semin. Cell Dev. Biol.* 21:881–891.

Potapova, T., and G.J. Gorbsky. 2017. The Consequences of Chromosome Segregation Errors in Mitosis and Meiosis. *Biology (Basel).* 6.

Primorac, I., and A. Musacchio. 2013. Panta rhei: The APC/C at steady state. *J. Cell Biol.*

Prosser, S.L., and L. Pelletier. 2017. Mitotic spindle assembly in animal cells: A fine balancing act. *Nat. Rev. Mol. Cell Biol.* 18:187–201.

Qi, M., W. Yu, S. Liu, H. Jia, L. Tang, M. Shen, X. Yan, H. Saiyin, Q. Lang, B. Wan, S. Zhao, and L. Yu. 2005. Septin1, a new interaction partner for human serine/threonine kinase aurora-B. *Biochem. Biophys. Res. Commun.*

Raaijmakers, J.A., R.G.H.P. Van Heesbeen, J.L. Meaders, E.F. Geers, B. Fernandez-Garcia, R.H. Medema, and M.E. Tanenbaum. 2012. Nuclear envelope-associated dynein drives prophase centrosome

separation and enables Eg5-independent bipolar spindle formation. *EMBO J.* 31:4179–4190.

Ran, F.A., P.D. Hsu, J. Wright, V. Agarwala, D.A. Scott, and F. Zhang. 2013. Genome engineering using the CRIPR-Cas9 system. *Nature*.

Rappaport, R. 1961. Experiments concerning the cleavage stimulus in sand dollar eggs. *J. Exp. Zool.* 148:81–89.

Rappaport, R. 1971. Cytokinesis in Animal Cells. *Int. Rev. Cytol.* 31:169–214.

Rappaport, R. 1996. Cytokinesis in Animal Cells. Cambridge University Press. 404 pp.

Rappaport, R., and B.N. Rappaport. 1974. Establishment of cleavage furrows by the mitotic spindle. *J. Exp. Zool.* 189:189–196.

Rappsilber, J., M. Mann, and Y. Ishihama. 2007. Protocol for micro-purification, enrichment, pre-fractionation and storage of peptides for proteomics using StageTips. *Nat. Protoc.* 2:1896–1906.

van Riel, W.E., A. Rai, S. Bianchi, E.A. Katrukha, Q. Liu, A.J. Heck, C.C. Hoogenraad, M.O. Steinmetz, L.C. Kapitein, and A. Akhmanova. 2017. Kinesin-4 KIF21B is a potent microtubule pausing factor. *Elife*. 6.

Rodrigues, N.T.L., S. Lekomtsev, S. Jananji, J. Kriston-Vizi, G.R.X. Hickson, and B. Baum. 2015. Kinetochore-localized PP1-Sds22 couples chromosome segregation to polar relaxation. *Nature*. 524:489–492.

Romero, S., C. Le Clainche, D. Didry, C. Egile, D. Pantaloni, and M.F. Carlier. 2004. Formin is a processive motor that requires profilin to accelerate actin assembly and associated ATP hydrolysis. *Cell*.

Salimian, K.J., E.R. Ballister, E.M. Smoak, S. Wood, T. Panchenko, M.A. Lampson, and B.E. Black. 2011. Feedback Control in Sensing Chromosome Biorientation by the Aurora B Kinase. *Curr. Biol.* 21:1158–1165.

Samejima, K., M. Platani, M. Wolny, H. Ogawa, G. Vargiu, P.J. Knight, M. Peckham, and W.C. Earnshaw. 2015. The Inner Centromere Protein (INCENP) Coil Is a Single α-Helix (SAH) Domain That Binds Directly to Microtubules and Is Important for Chromosome Passenger Complex (CPC) Localization and Function in Mitosis. *J. Biol. Chem.* 290:21460–72.

Santagata, S., T.J. Boggon, C.L. Baird, C.A. Gomez, J. Zhao, Wei Song Shan, D.G. Myszka, and L. Shapiro. 2001. G-protein signaling through tubby proteins. *Science (80-.).* 292:2041–2050.

Santaguida, S., A. Richardson, D.R. Iyer, O. M'Saad, L. Zasadil, K.A. Knouse, Y.L. Wong, N. Rhind, A. Desai, and A. Amon. 2017. Chromosome Mis-segregation Generates Cell-Cycle-Arrested Cells with Complex Karyotypes that Are Eliminated by the Immune System. *Dev. Cell*. 41:638-651.e5.

Santamaria, A., R. Neef, U. Eberspächer, K. Eis, M. Husemann, D. Mumberg, S. Prechtl, V. Schulze, G. Siemeister, L. Wortmann, F.A. Barr, and E.A. Nigg. 2007. Use of the novel Plk1 inhibitor ZK-thiazolidinone to elucidate functions of Plk1 in early and late stages of mitosis. *Mol. Biol. Cell*. 18:4024–36.

Saxton, W.M., and J.R. McIntosh. 1987. Interzone microtubule behavior in late anaphase and telophase spindles. *J. Cell Biol.*

Sessa, F., M. Mapelli, C. Ciferri, C. Tarricone, L.B. Areces, T.R. Schneider, P.T. Stukenberg, and A. Musacchio. 2005. Mechanism of Aurora B Activation by INCENP and Inhibition by Hesperadin. *Mol. Cell*. 18:379–391.

Shackney, S.E., C.A. Smith, B.W. Miller, D.R. Burholt, K. Murtha, H.R. Giles, D.M. Ketterer, and A.A.

Pollice. 1989. Model for the genetic evolution of human solid tumors. *Cancer Res.* 49:3344–54.

Sherr, C.J., and J.M. Roberts. 1999. CDK inhibitors: Positive and negative regulators of G1-phase progression. *Genes Dev.*

Shlevkov, E., H. Basu, M.-A. Bray, A.E. Carpenter, R.J. Kleiman, and T.L. Schwarz Correspondence. 2019. A High-Content Screen Identifies TPP1 and Aurora B as Regulators of Axonal Mitochondrial Transport Graphical Abstract Highlights d High-content imaging and object tracking enables a screen for mitochondrial motility d Aurora Kinase B or TPP1 inhibition or. *CellReports*. 28:3224-3237.e5.

Shutova, M.S., and T.M. Svitkina. 2018. Common and Specific Functions of Nonmuscle Myosin II Paralogs in Cells HHS Public Access. *Biochem.* 83:1459–1468.

Silkworth, W.T., I.K. Nardi, L.M. Scholl, and D. Cimini. 2009. Multipolar spindle pole coalescence is a major source of kinetochore mis-attachment and chromosome mis-segregation in cancer cells. *PLoS One*. 4:e6564.

Skop, A.R., H. Liu, J. Yates, B.J. Meyer, and R. Heald. 2004. Dissection of the mammalian midbody proteome reveals conserved cytokinesis mechanisms. *Science (80-.).*

Somers, W.G., and R. Saint. 2003. A RhoGEF and Rho family GTPase-activating protein complex links the contractile ring to cortical microtubules at the onset of cytokinesis. *Dev. Cell*. 4:29–39.

Spira, F., S. Cuylen-Haering, S. Mehta, M. Samwer, A. Reversat, A. Verma, R. Oldenbourg, M. Sixt, and D.W. Gerlich. 2017. Cytokinesis in vertebrate cells initiates by contraction of an equatorial actomyosin network composed of randomly oriented filaments. *Elife*. 6.

Steegmaier, M., M. Hoffmann, A. Baum, P. Lénárt, M. Petronczki, M. Krššák, U. Gürtler, P. Garin-Chesa, S. Lieb, J. Quant, M. Grauert, G.R. Adolf, N. Kraut, J.M. Peters, and W.J. Rettig. 2007. BI 2536, a Potent and Selective Inhibitor of Polo-like Kinase 1, Inhibits Tumor Growth In Vivo. *Curr. Biol.* 17:316–322.

Steigemann, P., and D.W. Gerlich. 2009. Cytokinetic abscission: cellular dynamics at the midbody. *Trends Cell Biol.* 19:606–616.

Steigemann, P., C. Wurzenberger, M.H.A. Schmitz, M. Held, J. Guizetti, S. Maar, and D.W. Gerlich. 2009. Aurora B-Mediated Abscission Checkpoint Protects against Tetraploidization. *Cell*.

Storchova, Z., and C. Kuffer. 2008. The consequences of tetraploidy and aneuploidy. *J. Cell Sci.* 121:3859–3866.

Storchova, Z., and D. Pellman. 2004. From polyploidy to aneuploidy, genome instability and cancer. *Nat. Rev. Mol. Cell Biol.* 5:45–54.

Straight, A.F., C.M. Field, and T.J. Mitchison. 2005. Anillin binds nonmuscle myosin II and regulates the contractile ring. *Mol. Biol. Cell*. 16:193–201.

Su, K.-C., W.M. Bement, M. Petronczki, and G. von Dassow. 2014. An astral simulacrum of the central spindle accounts for normal, spindle-less, and anucleate cytokinesis in echinoderm embryos. *Mol. Biol. Cell*. 25:4049–4062.

Subramanian, R., S.-C. Ti, L. Tan, S.A. Darst, and T.M. Kapoor. 2013. Marking and measuring single microtubules by PRC1 and kinesin-4. *Cell*. 154:377–90.

Subramanian, R., E.M. Wilson-Kubalek, C.P. Arthur, M.J. Bick, E.A. Campbell, S.A. Darst, R.A. Milligan, and T.M. Kapoor. 2010. Insights into antiparallel microtubule crosslinking by PRC1, a conserved nonmotor microtubule binding protein. *Cell*. 142:433–443.

Sun, X., X. Shi, M. Liu, D. Li, L. Zhang, X. Liu, and J. Zhou. 2011. Mdp3 is a novel microtubule-binding protein that regulates microtubule assembly and stability. *Cell Cycle*.

Sung, H.-H., I.A. Telley, P. Papadaki, A. Ephrussi, T. Surrey, and P. Rørth. 2008. Drosophila Ensconsin Promotes Productive Recruitment of Kinesin-1 to Microtubules. *Dev. Cell*. 15:866–876.

Szentpetery, Z., A. Balla, Y. Kim, M.A. Lemmon, and T. Balla. 2009. Live cell imaging with protein domains capable of recognizing phosphatidylinositol 4,5-bisphosphate; a comparative study. *BMC Cell Biol.* 10:67.

Tame, M.A., J.A. Raaijmakers, B. van den Broek, A. Lindqvist, K. Jalink, and R.H. Medema. 2014. Astral microtubules control redistribution of dynein at the cell cortex to facilitate spindle positioning. *Cell Cycle*. 13:1162–70.

Tanaka, H., H. Goto, A. Inoko, H. Makihara, A. Enomoto, K. Horimoto, M. Matsuyama, K. Kurita, I. Izawa, and M. Inagaki. 2015. Cytokinetic failure-induced tetraploidy develops into aneuploidy, triggering skin aging in phosphovimentin-deficient mice. *J. Biol. Chem.* 290:12984–12998.

Tanaka, T.U. 2005. Chromosome bi-orientation on the mitotic spindle. *In* Philosophical Transactions of the Royal Society B: Biological Sciences. 581–589.

Taylor, A.M., J. Shih, G. Ha, G.F. Gao, X. Zhang, A.C. Berger, S.E. Schumacher, C. Wang, H. Hu, J. Liu, A.J. Lazar, A.D. Cherniack, R. Beroukhim, M. Meyerson, S.J. Caesar-Johnson, J.A. Demchok, I. Felau, M. Kasapi, M.L. Ferguson, C.M. Hutter, H.J. Sofia, R. Tarnuzzer, Z. Wang, L. Yang, J.C. Zenklusen, J. (Julia) Zhang, S. Chudamani, J. Liu, L. Lolla, R. Naresh, T. Pihl, Q. Sun, Y. Wan, Y. Wu, J. Cho, T. DeFreitas, S. Frazer, N. Gehlenborg, G. Getz, D.I. Heiman, J. Kim, M.S. Lawrence, P. Lin, S. Meier, M.S. Noble, G. Saksena, D. Voet, H. Zhang, B. Bernard, N. Chambwe, V. Dhankani, T. Knijnenburg, R. Kramer, K. Leinonen, Y. Liu, M. Miller, S. Reynolds, I. Shmulevich, V. Thorsson, W. Zhang, R. Akbani, B.M. Broom, A.M. Hegde, Z. Ju, R.S. Kanchi, A. Korkut, J. Li, H. Liang, S. Ling, W. Liu, Y. Lu, G.B. Mills, K.-S. Ng, A. Rao, M. Ryan, J. Wang, J.N. Weinstein, J. Zhang, A. Abeshouse, J. Armenia, D. Chakravarty, W.K. Chatila, I. de Bruijn, J. Gao, B.E. Gross, Z.J. Heins, R. Kundra, K. La, M. Ladanyi, A. Luna, M.G. Nissan, A. Ochoa, S.M. Phillips, E. Reznik, F. Sanchez-Vega, C. Sander, N. Schultz, R. Sheridan, et al. 2018. Genomic and Functional Approaches to Understanding Cancer Aneuploidy. *Cancer Cell*. 33:676-689.e3.

Tcherniuk, S., D.A. Skoufias, C. Labriere, O. Rath, F. Gueritte, C. Guillou, and F. Kozielski. 2010. Relocation of aurora B and survivin from centromeres to the central spindle impaired by a kinesin-specific MKLP-2 inhibitor. *Angew. Chemie - Int. Ed.* 49:8228–8231.

Théry, M., V. Racine, A. Pépin, M. Piel, Y. Chen, J.-B. Sibarita, and M. Bornens. 2005. The extracellular matrix guides the orientation of the cell division axis. *Nat. Cell Biol.* 7:947–953.

Tighe, A., O. Staples, and S. Taylor. 2008. Mps1 kinase activity restrains anaphase during an unperturbed mitosis and targets Mad2 to kinetochores. *J. Cell Biol.* 181:893–901.

Timmons, L., and A. Fire. 1998. Specific interference by ingested dsRNA [10]. *Nature*. 395:854.

Totsukawa, G., Y. Yamakita, S. Yamashiro, D.J. Hartshorne, Y. Sasaki, and F. Matsumura. 2000. Distinct roles of ROCK (Rho-kinase) and MLCK in spatial regulation of MLC phosphorylation for assembly of stress fibers and focal adhesions in 3T3 fibroblasts. *J. Cell Biol.* 150:797–806.

Trivedi, P., F. Palomba, E. Niedzialkowska, M.A. Digman, E. Gratton, and P.T. Stukenberg. 2019a. The

inner centromere is a biomolecular condensate scaffolded by the chromosomal passenger complex. *Nat. Cell Biol*. 21:1127–1137.

Trivedi, P., A. V. Zaytsev, M. Godzi, F.I. Ataullakhanov, E.L. Grishchuk, and P.T. Stukenberg. 2019b. The binding of Borealin to microtubules underlies a tension independent kinetochore-microtubule error correction pathway. *Nat. Commun.* 10:682.

Tse, Y.C., A. Piekny, and M. Glotzer. 2011. Anillin promotes astral microtubule-directed cortical myosin polarization. *Mol. Biol. Cell*. 22:3165–3175.

Tseng, B.S., L. Tan, T.M. Kapoor, and H. Funabiki. 2010. Dual Detection of Chromosomes and Microtubules by the Chromosomal Passenger Complex Drives Spindle Assembly. *Dev. Cell*. 18:903–912.

Tymanskyj, S.R., B.H. Yang, K.J. Verhey, and L. Ma. 2018. MAP7 regulates axon morphogenesis by recruiting kinesin-1 to microtubules and modulating organelle transport. *Elife*. 7.

Uetake, Y., and G. Sluder. 2004. Cell cycle progression after cleavage failure: Mammalian somatic cells do not possess a “tetraploidy checkpoint.” *J. Cell Biol.* 165:609–615.

Vader, G., C.W.A. Cruijsen, T. Van Harn, M.J.M. Vromans, R.H. Medema, and S.M.A. Lens. 2007. The chromosomal passenger complex controls spindle checkpoint function independent from its role in correcting microtubule-kinetochore interactions. *Mol. Biol. Cell*. 18:4553–4564.

Vader, G., J.J.W. Kauw, R.H. Medema, and S.M.A. Lens. 2006. Survivin mediates targeting of the chromosomal passenger complex to the centromere and midbody. *EMBO Rep.* 7:85–92.

Vale, R.D., J.A. Spudich, and E.R. Griffis. 2009. Dynamics of myosin, microtubules, and Kinesin-6 at the cortex during cytokinesis in Drosophila S2 cells. *J. Cell Biol.* 186.

van der Vaart, B., W.E. van Riel, H. Doodhi, J.T. Kevenaar, E.A. Katrukha, L. Gumy, B.P. Bouchet, I. Grigoriev, S.A. Spangler, K.L. Yu, P.S. Wulf, J. Wu, G. Lansbergen, E.Y. van Battum, R.J. Pasterkamp, Y. Mimori-Kiyosue, J. Demmers, N. Olieric, I.V. Maly, C.C. Hoogenraad, and A. Akhmanova. 2013. CFEOM1-Associated Kinesin KIF21A Is a Cortical Microtubule Growth Inhibitor. *Dev. Cell*. 27:145–160.

Verbrugghe, K.J.C., and J.G. White. 2004. SPD-1 Is Required for the Formation of the Spindle Midzone but Is Not Essential for the Completion of Cytokinesis in C. elegans Embryos. *Curr. Biol.* 14:1755–1760.

Verhey, K.J., and J.W. Hammond. 2009. Traffic control: Regulation of kinesin motors. *Nat. Rev. Mol. Cell Biol.*

Verma, V., and T.J. Maresca. 2019. Microtubule plus-ends act as physical signaling hubs to activate RhoA during cytokinesis. *Elife*. 8.

Wagner, E., and M. Glotzer. 2016. Local RhoA activation induces cytokinetic furrows independent of spindle position and cell cycle stage. *J. Cell Biol.* 213:641–649.

Watanabe, S., Y. Ando, S. Yasuda, H. Hosoya, N. Watanabe, T. Ishizaki, and S. Narumiya. 2008. mDia2 Induces the Actin Scaffold for the Contractile Ring and Stabilizes Its Position during Cytokinesis in NIH 3T3 Cells. *Mol. Biol. Cell*. 19:2328–2338.

Watanabe, S., K. Okawa, T. Miki, S. Sakamoto, T. Morinaga, K. Segawa, T. Arakawa, M. Kinoshita, T. Ishizaki, and S. Narumiya. 2010. Rho and anillin-dependent control of mDia2 localization and function in cytokinesis. *Mol. Biol. Cell*.

Weaver, B.A., and D.W. Cleveland. 2006. Does aneuploidy cause cancer? *Curr. Opin. Cell Biol.* 18:658–

667.

Werner, M., E. Munro, and M. Glotzer. 2007. Astral Signals Spatially Bias Cortical Myosin Recruitment to Break Symmetry and Promote Cytokinesis. *Curr. Biol.* 17:1286–1297.

Wheatley, S.P., A.J. Henzing, H. Dodson, W. Khaled, and W.C. Earnshaw. 2004. Aurora-B Phosphorylation in Vitro Identifies a Residue of Survivin That Is Essential for Its Localization and Binding to Inner Centromere Protein (INCENP) in Vivo. *J. Biol. Chem.* 279:5655–5660.

Wheatley, S.P., S.E. Kandels-Lewis, R.R. Adams, A.M. Ainsztein, and W.C. Earnshaw. 2001. INCENP Binds Directly to Tubulin and Requires Dynamic Microtubules to Target to the Cleavage Furrow. *Exp. Cell Res.* 262:122–127.

White, E.A., and M. Glotzer. 2012. Centralspindlin: At the heart of cytokinesis. *Cytoskeleton*. 69:882–892.

Wiggan, O., A.E. Shaw, J.G. DeLuca, and J.R. Bamburg. 2012. ADF/Cofilin Regulates Actomyosin Assembly through Competitive Inhibition of Myosin II Binding to F-Actin. *Dev. Cell*.

Wijeratne, S., and R. Subramanian. 2018. Geometry of antiparallel microtubule bundles regulates relative sliding and stalling by PRC1 and Kif4A. *Elife*. 7.

Wolfe, B.A., T. Takaki, M. Petronczki, and M. Glotzer. 2009. Polo-like kinase 1 directs assembly of the HsCyk-4 RhoGAP/Ect2 RhoGEF complex to initiate cleavage furrow formation. *PLoS Biol.* 7.

Wollert, T., C. Wunder, J. Lippincott-Schwartz, and J.H. Hurley. 2009. Membrane scission by the ESCRT-III complex. *Nature*.

Wühr, M., E.S. Tan, S.K. Parker, H.W. Detrich, T.J. Mitchison, and T.J. Mitchison. 2010. A model for cleavage plane determination in early amphibian and fish embryos. *Curr. Biol.* 20:2040–5.

Wurzenberger, C., M. Held, M.A. Lampson, I. Poser, A.A. Hyman, and D.W. Gerlich. 2012. Sds22 and Repo-Man stabilize chromosome segregation by counteracting Aurora B on anaphase kinetochores. *J. Cell Biol.* 198:173–83.

Xiong, Y., G.J. Hannon, H. Zhang, D. Casso, R. Kobayashi, and D. Beach. 1993. p21 is a universal inhibitor of cyclin kinases. *Nature*. 366:701–704.

Xue, Z., and A.M. Sokac. 2016. Back-to-back mechanisms drive actomyosin ring closure during drosophila embryo cleavage. *J. Cell Biol.*

Yadav, S., P.J. Verma, and D. Panda. 2014. C-Terminal Region of MAP7 Domain Containing Protein 3 (MAP7D3) Promotes Microtubule Polymerization by Binding at the C-Terminal Tail of Tubulin. *PLoS One*. 9:e99539.

Yau, K.W., S.F.B. van Beuningen, I. Cunha-Ferreira, B.M.C. Cloin, E.Y. van Battum, L. Will, P. Schätzle, R.P. Tas, J. van Krugten, E.A. Katrukha, K. Jiang, P.S. Wulf, M. Mikhaylova, M. Harterink, R.J. Pasterkamp, A. Akhmanova, L.C. Kapitein, and C.C. Hoogenraad. 2014. Microtubule minus-end binding protein CAMSAP2 controls axon specification and dendrite development. *Neuron*. 82:1058–73.

Yokoyama, T., H. Goto, I. Izawa, H. Mizutani, and M. Inagaki. 2005. Aurora-B and Rho-kinase/ROCK, the two cleavage furrow kinases, independently regulate the progression of cytokinesis: Possible existence of a novel cleavage furrow kinase phosphorylates ezrin/radizin/moesin (ERM). *Genes to Cells*. 10:127–137.

Yu, M., M. Yuan, and H. Ren. 2006. Visualization of actin cytoskeletal dynamics during the cell cycle in tobacco (Nicotiana tabacum L. cv Bright Yellow) cells. *Biol. Cell*. 98:295–306.

Yüce, Ö., A. Piekny, and M. Glotzer. 2005. An ECT2-centralspindlin complex regulates the localization and function of RhoA. *J. Cell Biol.* 170:571–582.

Yue, Y., T.L. Blasius, S. Zhang, S. Jariwala, B. Walker, B.J. Grant, J.C. Cochran, and K.J. Verhey. 2018. Altered chemomechanical coupling causes impaired motility of the kinesin-4 motors KIF27 and KIF7. *J. Cell Biol.* 217:1319–1334.

Zhang, D., and M. Glotzer. 2015. The RhoGAP activity of CYK-4/MgcRacGAP functions non-canonically by promoting RhoA activation during cytokinesis. *Elife*. 4.

Zhao, W., and G. Fang. 2005. MgcRacGAP controls the assembly of the contractile ring and the initiation of cytokinesis. *Proc. Natl. Acad. Sci. U. S. A.* 102:13158–63.

Zhu, C., and W. Jiang. 2004. Cell cycle-dependent translocation of PRC1 on the spindle by Kif4 is essential for midzone formation and cytokinesis. *Proc. Natl. Acad. Sci.* 102:343–348.

Zhu, C., E. Lau, R. Schwarzenbacher, E. Bossy-Wetzel, and W. Jiang. 2006. Spatiotemporal control of spindle midzone formation by PRC1 in human cells. *Proc. Natl. Acad. Sci.* 103:6196–6201.

Zou, Y., Z. Shao, J. Peng, F. Li, D. Gong, C. Wang, X. Zuo, Z. Zhang, J. Wu, Y. Shi, and Q. Gong. 2014. Crystal structure of triple-BRCT-domain of ECT2 and insights into the binding characteristics to CYK-4. *FEBS Lett.* 588:2911–2920.

Nederlandse samenvatting

Het menselijk lichaam bestaat uit biljoenen cellen die zijn ontstaan door de celdeling van één bevruchte eicel. Ook in een volwassen persoon vindt nog steeds celdeling plaats om weefsels te onderhouden en te repareren, en voor het in standhouden van het immuunsysteem. Celdeling kan worden waargenomen door een lichtmicroscoop als een enkele cel die zich splitst in twee. Wat men ziet als celdeling is eigenlijk de laatste fase van celdeling, cytokinese.

Celdeling vindt plaats aan het einde van de celcyclus. De celcyclus is onderverdeeld in een aantal fases, waaronder de S-fase, waarin het DNA wordt gekopieerd, en de M-fase, waarin de cel daadwerkelijk in tweeën deelt. De M-fase bestaat weer uit de deling van de celkern, genaamd mitose, en uit de deling van het cytoplasma (alles behalve de celkern), genaamd cytokinese.

Tijdens mitose wordt het DNA, dat onderverdeelt is in chromosomen, in het midden van de cel gepositioneerd en dan verdeelt over twee helften van de cel. Dit resulteert erin dat elke cel een complete set chromosomen krijgt. Cytokinese start tijdens de mitose, op het moment dat de chromosomen beginnen te scheiden en terwijl deze zich in tegenovergestelde richting bewegen. Cytokinese start met de vorming van een ringvormige structuur bestaande uit actomyosine. Door contractie van deze ring vormt zich een insnoering die steeds dieper wordt totdat er twee nieuwe cellen gevormd zijn die alleen nog maar aan elkaar vastzitten door middel van een dunne intracellulaire brug. De laatste stap in cytokinese is het doorsnijden van deze brug, een proces dat abscissie wordt genoemd. Dit resulteert in twee nieuwe dochtercellen.

De regulatie van celdeling is zeer belangrijk voor de gezondheid van het organisme waarvan de cel deel uit maakt. Misregulatie kan leiden tot het ontstaan van kanker of, als het voortplantingscellen betreft, leiden tot miskramen en aandoeningen zoals Downsyndroom. Tijdens de laatste fase van celdeling vindt de deling van de celkern tegelijk samen met de deling van het cytoplasma. Deze processen moeten nauwkeurig gecoördineerd worden in tijd en ruimte zodat de cel pas deelt na de celkern. Zo wordt het gekopieerde DNA dat zich in de celkern bevindt netjes verdeeld over de twee nieuwe cellen. Als de laatste fase van celdeling faalt resulteert dit een cel die tweemaal de hoeveelheid chromosomen heeft, wat problemen geeft tijdens de volgende deling.

Een belangrijk eiwitcomplex dat meerdere rollen heeft tijdens de celdeling is het Chromosomale Passagiers Complex (CPC). Het complex bestaat uit vier eiwitten, namelijk Survivin, Borealin, INCENP en het enzym Aurora B kinase. Het CPC is betrokken bij verscheidene processen tijdens mitosis. Tijdens de start van cytokinese verplaatst het complex naar twee specifieke plekken in de cel. De eerste plek, is een structuur in het midden van de cel dat de spindel midzone of centrale spindel heet. De spindel midzone bestaat uit microtubuli, een soort kabels, en eiwitten die deze kabels samenbundelen. De tweede plek, is de equatoriale cortex van de cel waar zich de actomyosine ring vormt. De spindel midzone en de equatoriale cortex zijn twee cruciale structuren voor succesvolle cytokinese. De functie van het CPC op deze

plekken tijdens cytokinese is niet duidelijk.

In hoofdstuk 2 van dit proefschrift wordt onderzocht wat de functie is van het CPC tijdens cytokinese. Door het bestaan van parallelle signaleringsroutes die beide cytokinese kunnen initiëren, is het moeilijk functies van eiwitten in afzonderlijke signaleringsroutes te bestuderen. De ene signaleringsroute is afhankelijk van de spindel midzone, en de andere niet. De CPC lokaliseert naar de equatoriale cortex, maar het is niet duidelijk of het hier een belangrijke functie heeft. Door het platleggen van één van de twee signaleringsroutes, namelijk die plaatsvindt bij de spindel midzone, kan de functie van het CPC bestudeerd worden in de andere signaleringsroute. Deze methode liet zien dat het CPC cruciaal is voor cytokinese initiatie als de spindel midzone niet gevormd wordt. Als de spindel midzone er wel was, is cytokinese initiatie afhankelijk van de functie van PLK1 (Polo-like kinase 1). Tevens werd een nieuwe rol van PLK1 duidelijk, namelijk het reguleren van de lokalisatie van belangrijke cytokinese eiwitten naar de spindel midzone en de equatoriale cortex.
In hoofdstuk 3 wordt onderzocht hoe het CPC lokaliseert naar de spindel midzone en de equatoriale cortex. Het is bekend dat het CPC een interactie vormt met het motor eiwit MKLP2, en dat deze interactie belangrijk is voor de lokalisatie van het CPC en van MKLP2 tijdens cytokinese. In hoofdstuk 3 wordt duidelijk hoe het CPC en MKLP2 interacteren met elkaar. Daarnaast laten wij zien dat MKLP2 een echt motor eiwit is dat het CPC kan transporteren langs microtubuli. Met name het CPC dat gevonden wordt op de equatoriale cortex is afhankelijk van MKLP2. In tegenstelling is de lokalisatie van het CPC naar de spindel midzone grotendeels onafhankelijk van de motorcapaciteit van MKLP2 maar wel van MKLP2 zelf.
In hoofdstuk 4 identificeren we met behulp van massaspectrometrie een interactie tussen MKLP2 en MAP7 eiwitten. Wij laten zien dat MAP7 de lokalisatie van het CPC en MKLP2 beïnvloedt tijdens cytokinese op zowel de spindel midzone als de equatoriale cortex. In afwezigheid van MAP7, lokaliseert het CPC en MKLP2 in druppelvormige structuren verdeelt over de midden van de cel. Vooralsnog is het onduidelijk hoe deze structuren tot stand komen en wat de gevolgen zijn voor cytokinese.
In hoofdstuk 5 worden alle bevindingen nogmaals samengevat en bediscussieerd aan de hand van de huidige literatuur

Curriculum Vitae

Ingrid Elisabeth Adriaans was born on September the 24th, 1984 in Dordrecht, the Netherlands. In 2005 she graduated from the Stebo in Utrecht. In 2005, she started with the Bachelor's program Biomedical Sciences at Utrecht University. In 2010, she obtained her Bachelor degree and entered the Master's program Biology of Disease at the Utrecht University. During her master she performed an internship in the lab of Prof. dr. P.J. van Diest under the supervision of dr. P. van der Groep, and a second internship in the lab of Prof. dr. W. Stoorvogel en Prof. dr. H.C. Korswagen under the supervision of Dr. C. Zijlstra and K. Okihara. In 2012, she obtained her Master of Science degree. In 2013, she started as a PhD student in de lab of Prof. dr. S.M.A. Lens where she studied the role of the Chromosomal Passenger Complex during cytokinesis. This work is described in this thesis.